

**Development of Dual-Electrode Amperometric Detectors for Liquid Chromatography and  
Capillary Electrophoresis**

By

Megan K. Dorris

B.S. University of Colorado at Colorado Springs

Colorado Springs, CO

Submitted to the graduate degree program in Chemistry and the Graduate Faculty of the University of  
Kansas in partial fulfillment of the requirements for the degree of Doctor of Philosophy.

---

Craig Lunte (Chairperson)

---

Susan Lunte

---

Mario Rivera

---

Michael Johnson

---

Emily Scott

Date Defended: December 11<sup>th</sup> 2012

Development of Dual-Electrode Systems for Evaluation of Redox Status

---

Chairperson: Dr. Craig E. Lunte

Date Approved: February 5, 2013

## Abstract

The body of this research was focused on the use and development dual-electrode detection schemes for liquid chromatography and capillary electrophoresis. These detection schemes were developed to investigate redox chemistries for endogenous and exogenous antioxidants that play key roles in maintaining tissue redox homeostasis under oxidative stress conditions. A parallel adjacent dual electrode detector was first proposed for liquid chromatography in which redox cycling was hypothesized to occur between the electrodes resulting in signal enhancement. Flow rates for these systems were too high ( $\geq 1.0$  mL) to obtain redox cycling and subsequently no signal enhancement was observed for these systems. Flow rates in capillary electrophoresis are significantly lower compared to liquid chromatography. Therefore, a parallel dual-electrode was developed for capillary electrophoresis in this work. The dual-electrode was investigated using reduced phenolic acids, which were chemically reversible, semi-reversible and non-reversible compounds allowing all potential electrochemistry's to be investigated. Redox cycling and signal enhancement was observed with the developed dual-electrode. Furthermore, the parallel dual-electrode could be operated in either a redox cycling mode or dual-potential mode, where either chemical reversibility or voltammetry could be used as a means to confirm migration based peak identification, respectively. The same design was then applied for a dual Au/Hg electrode for capillary electrophoresis, in which thiols and disulfides were investigated *in vivo*. With the developed dual Au/Hg electrode redox changes were observed as a result of chemically induced oxidative stress.

To my Grandma R. you were a  
woman ahead of your time and such an inspiration.

I miss you every day.

## Acknowledgements

In high school my chemistry professor Roger Rogers (he signed his name R<sup>2</sup>) suggested that I take the advanced chemistry course. At the time this seemed completely off base from what I wanted to go on to study in college (sports psychology) that I decided not to take the course. Obviously, psychology was not the path I ultimately chose. At the beginning of my sophomore year of college I took a general chemistry course taught by Dr. David Weiss. Dr. Weiss was a bioanalytical chemist whose research focused on developing biosensors to monitor biomarkers associated with various diseases. I began research in his group the following semester and became interested in using instrumentation to improve detection of biomarkers for diseases and detection of disease states. Wanting to pursue this research further, I joined Dr. Lunte's lab. Without these three, I would not be where I am today. Thank you. Most of all thank you Craig for sticking with me and for always pushing me to strive for more in my research.

I would also like to thank my parents for their support throughout this process and always. Your encouragement and unconditional love are so much appreciated...I will never be able to repay you. Although, Dad, I hope you feel that you have gotten a good return on your investment (i.e. my education).

To the rest of my family your support throughout this process has been tremendous. Aunt Carol, thanks for your words of wisdom, patience and willingness to listen. Uncle Jim, I love our conversations about science. Your curiosity and insatiable appetite for knowledge are truly inspirational. Uncle Paul, Aunt Marilyn and Aunt Nan, thanks for always encouraging me to explore all options and inspiring ambition in everything I do. Last, but not least, my cousin Josh.

You have always been the big brother I have never had. I will never forget when you attempted to “drowned” me in the pool in Branson, MO...I was so mad at you, but who else was going to give me a hard time? Or the time when you held me upside down in front of a turtle and told me he went inside his shell because I was so ugly. Most of all thanks for encouraging me to not be afraid to push myself in life and in my choice of career. I don’t think I would be where I am if it wasn’t for all of our little chats. You constantly strive for more and I admire all you do more than you know.

I think one of the things that I will always remember about my time here at KU will be all of the wonderful friends I have made. I don’t think I would have made it through this experience without any of you. Phil Livanec, Maggie Livanec, Amanda Glass, Drew Vartia, Joe Jarvis, Rachel Meyers, John Meyers, Dan Clark, Tom Linz, Cassie Ward, Sara Thomas, Jen Settle, Heath and Emily Huckabay, Matt and Megen Culpepper, Natalie Ciaccio...I think that’s everyone? We have shared amazing times and some not so great ones! Amanda thanks for all of the “therapy Friday breakfast” sessions, you are truly a great friend and I know we will always be in touch no matter where we are. To Phil and Maggie Livanec, you guys are amazing. Mags thanks for keeping me sane with our constant emailing.

Finally, to my best friend (Justin) Carl Cooley. I still remember the first day we meant in orientation. You introduced yourself as “Justin, but we could call you Carl”. What?!? In a short time you showed yourself to be an amazing person and friend and maybe it wasn’t so strange to call you Carl. You have been by my side through thick and thin. I cannot imagine my life without you. I look forward to sharing my life with you. I can’t wait to see what is in store for us!

## Table of Contents

<b>Chapter 1: Introduction</b> .....	1
1.1 Oxidative Stress.....	1
1.1.2 Mitochondrial Dysfunction.....	2
1.2 Current Approaches for Treatment of Neurological Disorders.....	6
1.2.1 Alternative Therapeutic Approaches.....	6
1.3 Electrochemistry in Dynamic Systems.....	10
1.3.1 Faradaic Processes.....	10
1.3.2 Electrode Double Layer.....	12
1.3.3 Hydrodynamic Amperometry.....	15
1.4 Applications to Liquid Chromatography and Capillary Electrophoresis Systems.....	19
1.4.1 Thin-layer Cell Development.....	19
1.4.2 Integration of Electrochemical Detection with Capillary Electrophoresis.....	27
1.5 Overview of Research.....	31
1.6 References.....	32
<b>Chapter 2: Development of a Dual Electrode Liquid Chromatography Method for the Determination of Co-enzyme Q<sub>10</sub> in Plasma</b> .....	37
2.0 Background and Significance.....	37
2.1 Introduction.....	37
2.1.1 Ubiquinone-10 Role in Regulation of Oxidative Stress Response.....	37
2.1.2 Previous Detection Schemes for Determination of Ubiquinone-10.....	41
2.1.3 Specific Aims.....	44

2.2 Methods.....	44
2.2.1 Chemicals and Reagents.....	44
2.2.2 Instrumentation and Conditions.....	47
2.2.2.1 Method Conditions.....	47
2.2.2.2 Sample Preparation.....	50
2.3 Results and Discussion.....	50
2.3.1 Investigation of Series and Parallel Electrode Configurations.....	50
2.3.1.1 Establishing Chemical Mechanism of Ubiquinone-10 in Bulk Solution.....	50
2.3.1.2 Establishing Optimal Working Potentials using Hydrodynamic Amperometry....	52
2.3.1.3 Series Dual Electrode Configuration.....	54
2.3.1.4 Parallel Dual Electrode Configuration.....	56
2.3.2 Validation of Analytical Method.....	59
2.3.2.1 Plasma Sample Analysis.....	60
2.4 Conclusions.....	65
2.5 References.....	66
<b>Chapter 3: Development of a Parallel Dual Electrode for Capillary Electrophoresis.....</b>	<b>69</b>
3.0 Background and Significance.....	69
3.1 Introduction.....	70
3.1.1 Dual Electrode Detection.....	70
3.1.2 Phenolic Acids.....	71
3.1.3 Specific Aims.....	71
3.2 Methods.....	73
3.2.2 Instrumentation.....	73
3.2.2.1 Capillary Electrophoresis.....	73

3.2.2.2 Initial Approaches to Integration of Dual Electrode Detection with Capillary Electrophoresis.....	77
3.2.2.2.1 Cellulose Acetate Decoupler.....	77
3.2.2.2.2 Wireless Isolated Potentiostat and End Column Detection on PDMS Microchips.....	81
3.2.2.3 Instrumental Conditions.....	85
3.2.3 Dual Electrode Fabrication.....	85
3.2.4 Experimental Conditions.....	86
3.3 Results and Discussion.....	88
3.3.1 Optimization of Working Potentials.....	88
3.3.2 Redox Cycling Mode.....	90
3.3.3 Dual-Potential Mode.....	97
3.3.3.1 Whiskey Analysis.....	97
3.4 Conclusions.....	105
3.5 References.....	106

**Chapter 4: Development of a Dual Au/Hg Electrode Capillary Electrophoresis Method**

<b>for the Determination of Thiols and Disulfides.....</b>	<b>109</b>
4.0 Background and Significance.....	109
4.1 Introduction.....	109
4.1.1 Endogenous Antioxidants.....	111

4.1.2 Analysis of Thiols and Disulfides.....	115
4.1.2.1 Liquid Chromatography (LC).....	115
4.1.2.2 Capillary Electrophoresis (CE).....	119
4.1.3 Specific Aims.....	125
4.2 Methods.....	125
4.2.1 Chemicals and Reagents.....	125
4.2.2 Dual Au/Hg Electrode Fabrication.....	126
4.2.3 Instrumentation and Separation Conditions.....	127
4.2.3.1 Micellar Electrokinetic Chromatography.....	127
4.2.3.2 Separation Conditions and Electrode Pretreatment.....	128
4.2.4 Standard and Sample Preparation.....	129
4.3 Results and Discussion.....	130
4.3.1 Method Development.....	130
4.3.1.1 Normal Polarity.....	130
4.3.1.2 MEKC Approach using Normal Polarity.....	131
4.3.1.3 Reversed Polarity.....	135
4.3.2 Dual Au/Hg Electrode.....	140
4.3.2.1 Mechanism of Response for Dual Au/Hg Electrode.....	145
4.3.3 Monitoring Redox Status <i>In Vivo</i> .....	148
4.4 Conclusions.....	152
4.5 References.....	154
<b>Chapter 5: Conclusions and Future Directions.....</b>	<b>158</b>
5.1 Conclusions.....	158

5.1.1 Chapter 2.....	158
5.1.2 Chapter 3.....	159
5.1.3 Chapter 4.....	160
5.2 Future Directions.....	162
5.2.1 Mitigation of Oxidative Stress in Neurodegenerative Diseases via Antioxidant Therapies.....	162
5.2.1.2 Dietary Co-enzyme Q <sub>10</sub> .....	162
5.2.1.3 Application for Dual Carbon Fiber Electrode.....	164
5.2.1.4 Thiols and Disulfides.....	166
5.3 Development of a Robust Decoupler for CEEC.....	167
5.4 References.....	172

## Table of Contents for Figures

### Chapter 1

Figure 1.1.....	3
Figure 1.2.....	5
Figure 1.3.....	8
Figure 1.4.....	13
Figure 1.5.....	14
Figure 1.6.....	16
Figure 1.7.....	17
Figure 1.8.....	20
Figure 1.9.....	23
Figure 1.10.....	24
Figure 1.11.....	26
Figure 1.12.....	28

### Chapter 2

Figure 2.1.....	39
Figure 2.2.....	42
Figure 2.3.....	46
Figure 2.4.....	51
Figure 2.5.....	53
Figure 2.6.....	55
Figure 2.7.....	57

Figure 2.8.....	58
Figure 2.9.....	61
Figure 2.10.....	64

### Chapter 3

Figure 3.1.....	72
Figure 3.2.....	75
Figure 3.3.....	78
Figure 3.4.....	82
Figure 3.5.....	84
Figure 3.6.....	87
Figure 3.7.....	89
Figure 3.8.....	91
Figure 3.9.....	92
Figure 3.10.....	98
Figure 3.11.....	101
Figure 3.12.....	102
Figure 3.13.....	103

### Chapter 4

Figure 4.1.....	110
Figure 4.2.....	112
Figure 4.3.....	114
Figure 4.4.....	117
Figure 4.5.....	121

Figure 4.6.....	123
Figure 4.7.....	124
Figure 4.8.....	134
Figure 4.9.....	136
Figure 4.10.....	139
Figure 4.11.....	140
Figure 4.12.....	142
Figure 4.13.....	144
Figure 4.14.....	146
Figure 4.15.....	149
Figure 4.16.....	151
Figure 4.17.....	153
Chapter 5	
Figure 5.1.....	163
Figure 5.2.....	169
Figure 5.3.....	170

## Table of Contents for Tables

### Chapter 2

Table 2.1.....	63
----------------	----

### Chapter 3

Table 3.1.....	80
----------------	----

Table 3.2.....	94
----------------	----

Table 3.3.....	96
----------------	----

Table 3.4.....	100
----------------	-----

### Chapter 4

Table 4.1.....	132
----------------	-----

Table 4.2.....	143
----------------	-----

### Chapter 5

Table 5.1.....	165
----------------	-----

## Chapter 1

### 1.0 Introduction

Oxidative stress is defined as an imbalance between pro-oxidant and antioxidant homeostasis as a result of overactive or unregulated production of free radical species.<sup>1-3</sup> The disruption in homeostasis can result in the development of numerous diseases including: Parkinson's, Alzheimer's, cancer, cardiovascular, cataracts, diabetes and epilepsy.<sup>1-4</sup> The ability to assess redox states requires the development of sensitive and selective analytical methods and instrumentation. Hydrodynamic amperometry coupled with liquid chromatography (LC) or capillary electrophoresis (CE) offers a sensitive and selective means by which electrochemically active compounds can be detected. As redox chemistry is involved in the chemical processes that transfer electrons and protons, compounds involved in these routes are inherently electroactive. Therefore analysis with electrochemical detection offers the most direct approach to analysis with no additional sample preparation. Furthermore, detection schemes can be manipulated and easily miniaturized with no loss in limits of detection (LOD) due to surface area to sample volume ratios.

### 1.1 Oxidative Stress

The susceptibility of the brain to oxidative stress and subsequently the onset or progression of a number of the aforementioned neurological disorders makes the need to investigate the pathways associated with the progression of these diseases important. The brain is highly susceptible to oxidative stress for several key reasons: 1) it utilizes the largest amount of oxygen compared with other major organs in the body, 2) it contains a large number of polyunsaturated fatty acids that can easily undergo lipid peroxidation and 3) it is rich in iron, which catalyzes hydroxyl radical formation.

Under oxidative stress conditions, a portion of tissue is deprived of molecular oxygen due to an interruption in blood supply. At the cellular level, ATP production is decreased, electrolyte balance is disturbed causing cell membranes to lose their shape, with a resultant accumulation in lactic acid. Figure 1.1 shows a proposed mechanism of oxidative stress in relation to the development of epileptogenesis in more detail. Glutamate is the main excitatory neurotransmitter in the brain with multiple receptor sites on the cell membrane including; N-methyl-D-aspartate (NMDA),  $\alpha$ -amino-3-hydroxy-5-methyl-4-isoxazolepropionic acid receptor (AMPA) and kainite receptors (KA).<sup>9</sup> Depending on the extent of seizure activity or prolonged surge of glutamate, membrane depolarization will occur. The increase in extracellular glutamate will overstimulate NMDA receptors, causing an increase in intracellular  $\text{Ca}^{2+}$ . This then results in a loss of neuronal  $\text{Ca}^{2+}$  homeostasis. The excess intracellular  $\text{Ca}^{2+}$  loading increases conductance within the mitochondrial membrane, reducing the mitochondrial membrane potential and leading to mitochondrial dysfunction; thereby diminishing the production of cellular ATP. Due to the change in pH, lysosomal enzymes begin to digest cellular contents causing irreversible damage. Although oxidative stress itself can cause severe and irreversible damage to the affected tissue, the surge of molecular oxygen reaching the tissue after the events described above have been noted as being the most damaging process. This molecular oxygen is converted to reactive oxygen species (ROS) through a variety of proposed mechanisms. Free radicals produced through these processes go on to attack DNA, lipids, and proteins, causing irreversible oxidative damage.

### 1.1.2 Mitochondrial Dysfunction

Maintenance of mitochondrial function has been recently scrutinized as being the key player in both cell death and cell survival.<sup>2,9</sup>

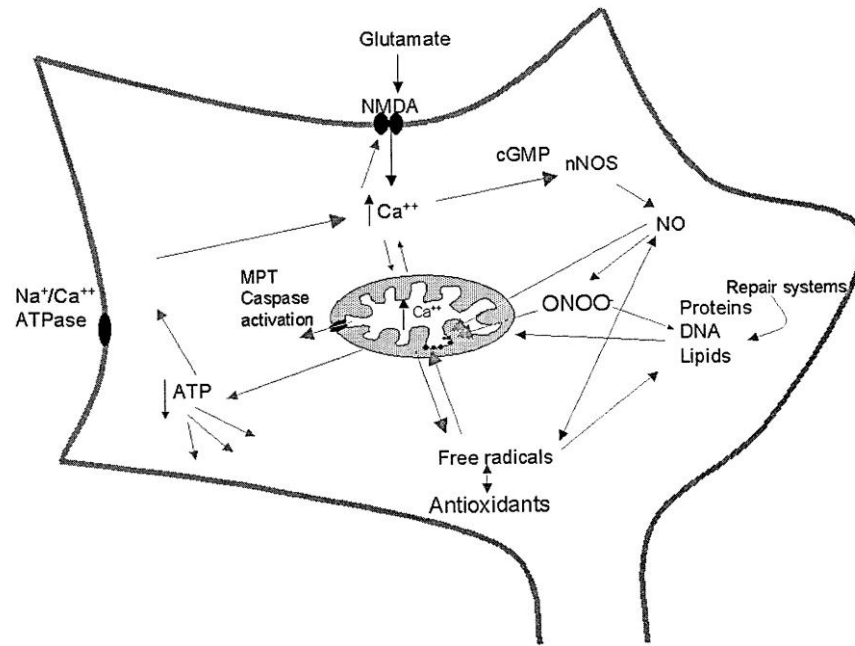


Figure 1.1: Oxidative stress at the cellular level. Changes in membrane potential from influx of  $\text{Ca}^{2+}$  result in depolarization leading activation of nitric oxide synthesis and production of ROS, with permission.<sup>8</sup>

As mitochondria are the main producers of ROS this organelle has gained significant attention for its key role in signaling cell death or maintaining cell survival. Endogenous sources of free radicals include the mitochondrial electron transport chain and lipid peroxidation. It is estimated that 1 to 5 percent of the oxygen undergoing metabolism escapes as free radical intermediates. As shown in Figure 1.2, the intracellular matrix of mitochondria contain fatty acid  $\beta$ -oxidation systems and Krebs's cycle enzymes, which are used to breakdown foods and convert them into fuels for the body. Electrons from these systems are passed to the mitochondrial respiratory chain. Electrons are transported via enzymatic complexes that result in the production of ATP.<sup>8</sup> Electron transport via these enzymatic complexes is important in maintaining ionic homeostasis (*i.e.*  $\text{Ca}^{2+}$  and  $\text{Na}^+$  regulation), repair systems, and proper maintenance of action potentials.<sup>8</sup> Imbalance within these systems results in the formation of ROS, leading to oxidative stress and several types of damage to biological components, such as oxidative DNA damage, strand breakage, mutation and cell death<sup>10-14</sup>. Additionally, these ROS can undergo toxic secondary reactions; the most significant being the production of peroxynitrite from nitric oxide and superoxide radicals.<sup>8</sup> Although the aforementioned information would lead to the conclusion that mitochondria are perhaps the organelle in the cell most responsible for contributing to and signaling cell death, they also play a key role in maintaining homeostasis under normal physiological conditions.<sup>8</sup> Mitochondria are the basis for numerous antioxidant systems, such as superoxide dismutase and glutathione peroxidase. Both of these defense systems primarily function to scavenge free radicals and actively convert  $\text{H}_2\text{O}_2$  to  $\text{H}_2\text{O}$ . These two steps protect DNA from oxidation and prevent downstream lipid peroxidation. However, under stressful conditions these systems are overwhelmed by the surge in free radical production, failing to prevent the cell from signaling apoptosis.

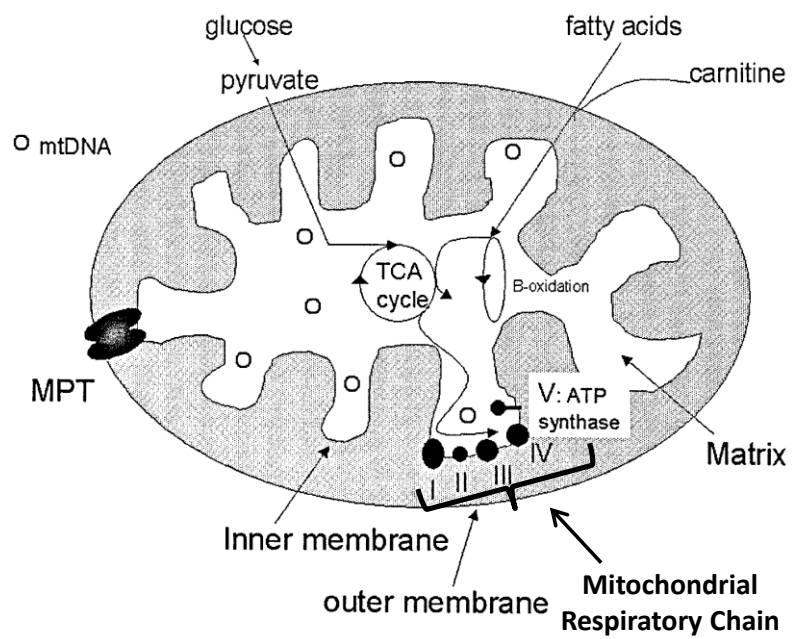


Figure 1.2: Mitochondrial components and mechanisms of action, adapted from Cock, with permission.<sup>8</sup> Numerals I-IV enzymatic complexes within the mitochondrial respiratory chain.

Currently the mechanism behind the onset of several neurological disorders with regard to the role oxidative stress is not clear. Is the role of oxidative stress in the development of neurological disorders caused by 1) extracellular glutamate triggering the over activation of  $Ca^{2+}$  or 2) an intracellular mitochondrial event causing excess production of free radicals?<sup>2, 4</sup>

## 1.2 Current Approaches to Treatments for Neurological Disorders

Current treatments for several neurological disorders aim to suppress certain physical traits associated with diseases. For example, treatments for epilepsy involve diminishing seizure events or the severity of the seizure by treating symptoms associated with epilepsy.<sup>9</sup> More severe forms of treatment involve removal of portions of the brain that have been damaged from seizures as a means to stop seizure activity in general or minimize the effect on surrounding tissues. However, very few of these treatments do much to deter or stabilize the underlying chemical pathways associated with the proliferation of these diseases. In some instances current treatments, for example anti-epileptic drugs, aid in oxidative stress and subsequently cell death.<sup>9</sup>

### 1.2.1 Alternative Therapeutic Approaches

It has been reported that epileptic patients have low levels of endogenous antioxidants. In particular vitamins A, E and C are consistently lower in these patients versus normal patients of similar sex and demographic backgrounds.<sup>15-17</sup> In addition, low levels of reduced glutathione (GSH) have also been reported in conjunction with increased levels of oxidized glutathione (GSSG).<sup>16</sup> The decreased amounts of these endogenous antioxidants in epileptic patients makes them more vulnerable to increased or unregulated production of ROS, resulting in increasing frequency and intensity of seizures. In addition, anti-epileptic drugs can be metabolized to generate reactive metabolites that can covalently bind to

macromolecules resulting in increased cellular toxicity.<sup>15</sup> There is also evidence that patients receiving phenobarbital who did not experience seizures after 1 year of treatment showed increased levels of vitamin E and C when compared to levels prior to treatment, suggesting that some of these treatments do have neuroprotective effects. However, the study did not follow patients who received phenobarbital, but still experienced seizures within the year after treatment.

As stated previously, uncontrolled production of ROS results in disruption of tissue homeostasis causing oxidative stress and cell death. More recently alternative therapeutic approaches, such as the kinetic diet have gained more attention. This diet is high in fats and low in carbohydrates. It has been reported that epileptics on this diet experience fewer epileptic events and a decrease in seizure intensity.<sup>2,3</sup> These effects have been proposed to occur through two mechanisms 1) increased fat in diet increases cellular fatty acid oxidation which decreases the frequency of neuronal firing in conjunction with a reduction in resting membrane potential or 2) mitochondrial antioxidant capacity is improved through either an increase in lipoic acid, reducing coenzyme A levels, or glutamate cysteine ligase levels are increased enabling production of GSH to be maintained.<sup>2,3,9,18</sup>

Another approach is through dietary intake of endogenous antioxidants, for example vitamins E and C. Figure 1.3 shows the chemical structures of several dietary antioxidants that have been associated with free radical scavenging or mitigation of other pathways associated with oxidative stress. Vitamin E has received much attention due to its ability to scavenge free radicals in the brain, as well as its function in preventing radical chain reactions within lipid layers of biological membranes, protecting the integrity of the blood brain barrier.<sup>19</sup> Vitamin C has also been reported to effectively scavenge free radicals including molecular oxygen, nitrogen radicals and chlorine radicals. Vitamin C is more easily oxidized compared to species like Vitamin E or other tocopherols making its sustained therapeutic benefit not as significant.<sup>19</sup> In addition, Co-enzyme Q<sub>10</sub> (Co-Q<sub>10</sub>) has also received significant attention for its ability to help maintain

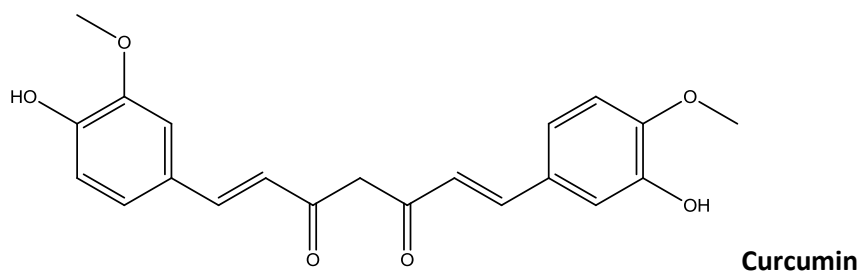
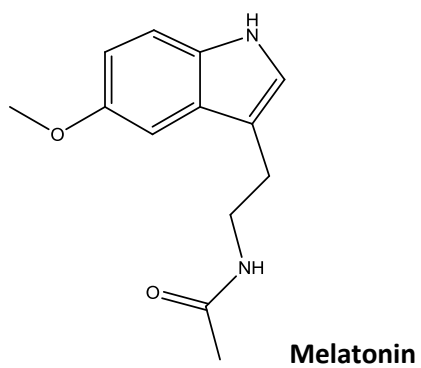
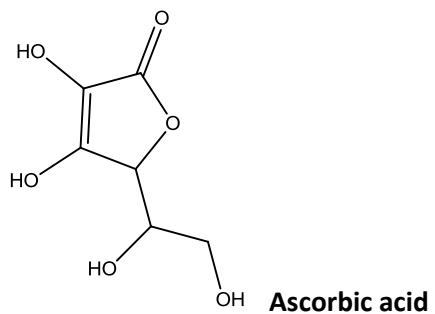
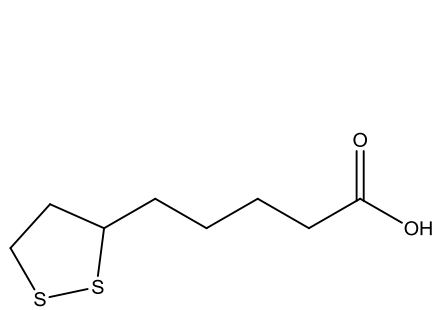
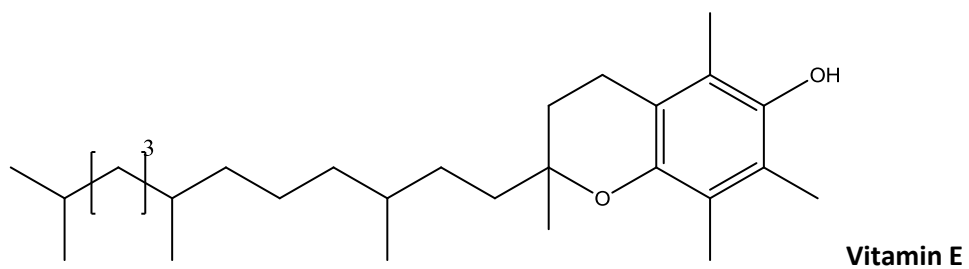


Figure 1.3 Structures of some of the most common antioxidants used to mitigate oxidative stress processes.

tissue redox homeostasis through free radical scavenging, as well as regeneration of other critical endogenous antioxidants, such as vitamin E and glutathione.<sup>19</sup>

Melatonin has been used extensively to regulate mood, sleep, sexual-behavior and circadian rhythms. It has also received attention for its ability to scavenge free radicals (ROS and RNS), protect DNA and lipid oxidation, and help maintain electron transport along the mitochondrial respiratory chain through upregulation of GSH.<sup>19</sup>

Lipoic acid is a naturally occurring disulfide which has been shown to be an essential cofactor in regulation of mitochondrial enzymes and lipid metabolism once reduced to dihydrolipoic acid.<sup>19</sup> It has also been shown to chelate transition metals and scavenge hydroxyl radicals and nitric oxide radicals. Furthermore, it regenerates other endogenous antioxidants, such as vitamin E indirectly by first regenerating ascorbate from dehydroascorbate. Ascorbate is then free to reduce the free radical form of vitamin E back to its reduced form.<sup>2, 19-21</sup>

Curcumin is an extract from turmeric and has been used in traditional medicines to treat gastrointestinal and hepatic disorders.<sup>22</sup> Its exact mechanism of action is not well understood, but it has been shown to inhibit arachadonic acid metabolism via inhibition of cPLA phosphorylation and COX-1 activity, *in vitro*.<sup>22</sup> In addition it has also been shown to up regulate levels of GSH via activation of hemeoxygenase-1.<sup>23</sup>

While each of these dietary antioxidants has shown some therapeutic advantage most of these studies have been conducted *in vitro* with large doses ( $\mu\text{M}$ - mM) that would not be biologically relevant. de Freitas *et al.* administered lipoic acid in conjunction with pilocarpine and observed reduction in seizure intensity and latency in seizure onset when compared to the control group given only pilocarpine.<sup>20</sup> In addition, administration of lipoic acid in this study was only given with pilocarpine (*i.e.* prior to seizure onset not after). The efficacy of these antioxidants needs to be determined as a means to regulate oxidative stress processes after the initial seizure, particularly in latency/chronic stages, as this is a

critical point in regulating the progression of neurological disorders such as epilepsy. Furthermore, mechanisms of action *in vivo* need to be better defined along with dosing.

Several of these endogenous antioxidant systems, which regulate oxidative stress and maintain tissue homeostasis, are electrochemically active. Therefore, the investigation of their *in vivo* mechanisms will be investigated using separations techniques in conjunction with hydrodynamic amperometry.

### 1.3 Electrochemistry in Dynamic Systems

Electrochemistry has broad applications that span several disciplines, from environmental analysis, to biology, as well as analysis in industrial settings aiding in quality control. Within the last three decades electrochemistry has become a more applicable technique for pharmaceutical industry. Electrochemistry exhibits low detection limits (LOD) (low nanomolar-picomolar) and a wide dynamic range, rivaling spectroscopic techniques, which are often used in industrial settings along with MS and NMR. In addition to having comparable LOD's, EC detection has good selectivity due to fewer electroactive interferants, which often plague spectroscopic detection schemes. Furthermore, electrochemical techniques require minimal sample volume ( $\leq 10$ s of microliters) making this type of detection amenable to biomedical analysis at the cellular level. Lastly in comparison, electrochemical detection is cost effective and easily miniaturized.

#### 1.3.1 Faradaic Processes

Faradaic processes are defined by a chemical reaction taking place at the electrode surface and as a result the current produced is directly proportional to the number of electrons transferred. More simply, if an analyte is reduced or oxidized at the electrode surface then a Faradaic process is being followed. However, when electrodes act in a capacitive sense, there is a buildup of charge at the electrode surface due to either adsorption or desorption resulting non-Faradaic currents.

Following faradaic processes there are three types of mass transport to the electrode surface: 1) diffusion, 2) migration and 3) convection. Diffusion is perhaps the most obvious means of transport, as it is based on the concentration gradient in solution. Molecules will transfer from areas of high concentration to low concentration. The second process, migration, involves electrostatic interactions between the surface charge of the electrode and molecules in solution. The last process, convection, involves mechanical perturbation of the solution forcing molecules to the surface of the electrode. In any of these mass transport mechanisms it is important to understand how these processes relate to the current produced. While diffusion is the primary mass transport mechanism for stationary systems, it does not describe the mechanism of transport in dynamic systems where solution flow is occurring. This is the case for hydrodynamic amperometry, discussed later in this chapter.

With any of these mass transport mechanisms there is a concentration gradient that exists from bulk solution to the electrode surface. The distribution of molecules as a function of distance from the electrode surface is termed flux.<sup>5,6</sup> Equation 1 or Fick's First Law describes this process.

$$J(x, t) = -D \frac{\partial C(x, t)}{\partial x} \quad (1)$$

Where J is flux, D is diffusion coefficient, C is concentration and x is the distance from the electrode. The response or current produced is therefore a function of the flux, as shown in equation 2.

$$i = nFA \left( \frac{\partial C(x, t)}{\partial x} \right) \quad (2)$$

Where n is the number of electrons transferred, F is Faraday's constant and A is the area of the electrode. While it is important to understand how current relates to the concentration gradient in solution, it should be noted that Fick's First Law does not directly relate concentration or distribution of molecules with time, which is generally an easier way to understand the solution dynamics. In order to relate the flux to time, an example laid out by Kissinger *et al* will be used.<sup>6</sup> A box with fixed walls of

distance ( $x_2 \pm \Delta x/2$ ) containing some concentration of material can be used, as shown in Figure 1.4.<sup>6</sup> If the flux at two different distances remains equivalent ( $J_{x-\Delta x/2} = J_{x+\Delta x/2}$ ) then the concentration of the material will remain constant as a function of time per unit area; however, this is not a realistic scenario. Material will move into the box shifting the equilibrium of the flux in one direction or another ( $J_{x-\Delta x/2} > J_{x+\Delta x/2}$ ) changing the concentration of material in the box. Since the flux can be defined by some unit area, in this case the area of the box, then a rate can be obtained by dividing the flux by the distance of the box. A relationship can now be drawn between concentration, time and flux defined by Fick's Second Law given in equation 3, below.

$$\frac{C(x,t)}{\quad} \quad (3)$$

While the flux describes movement of a species along the concentration gradient, it does not specifically address interactions from other molecules in solution.

### 1.3.2 Electrode Double Layer

One of the largest factors effecting mass transport of ions in solution to the electrode surface is the diffusion layer.<sup>5,6</sup> The diffusion layer is a part of the electric double layer. The electric double layer arises when a voltage is applied to an electrode and as a result a buildup of charge occurs at the electrode surface. This can be thought of as a capacitor, although in keeping with Faradiac processes charge will not continually build up at the surface, but instead ions will be transferred across solution. There are three components to the electric double layer: 1) the Inner Helholtz Plane, 2) the Outer Helmholtz Plane and 3) the diffuse layer. Figure 1.5 shows a diagram of the electric double layer. The Inner Helmholtz Plane (IHP) is composed of a layer of partially solvated molecules, as well as

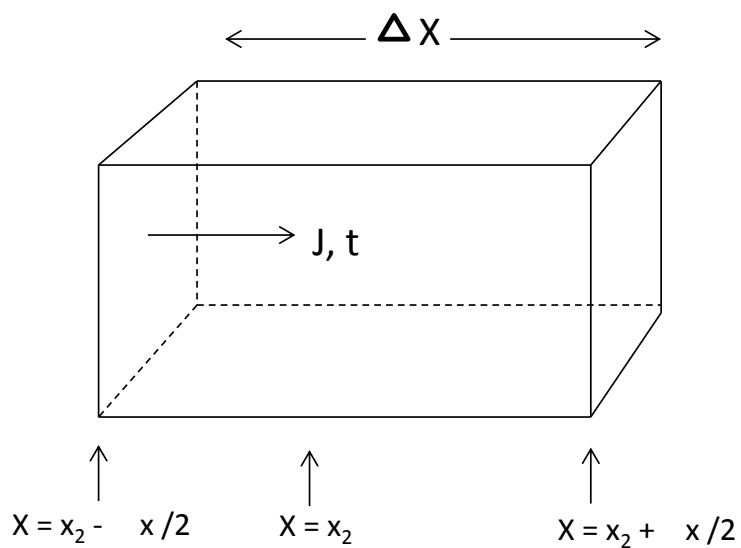


Figure 1.4: Cross-sectional area of solution, time is a function of molecule in solution at some distance  $x_2$  from the electrode surface, adapted from Kissinger with permission<sup>6</sup>.

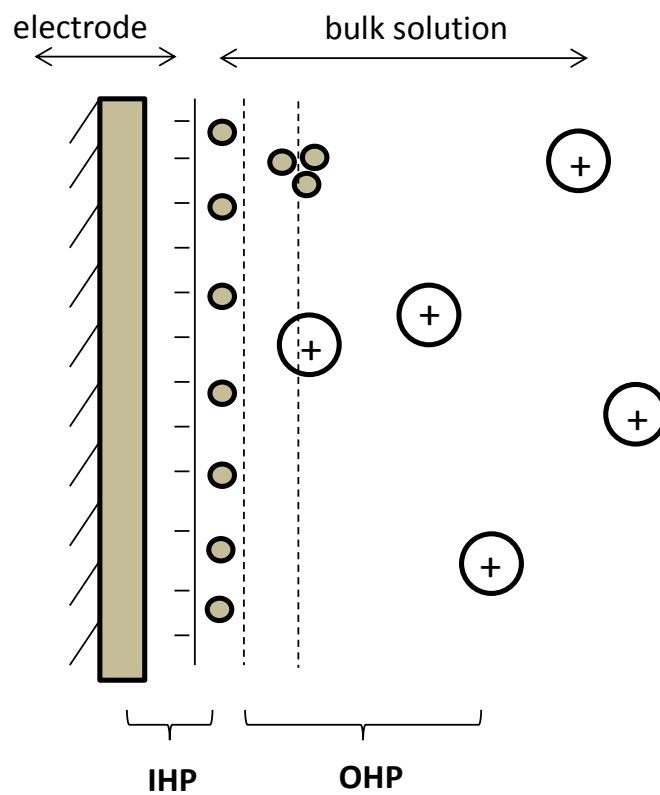


Figure 1.5: Electric Double-Layer, adapted from Bard<sup>5</sup>. IHP, inner Helmholtz plane. OHP, outer Helmholtz plane.

charged particles that are in close proximity or adsorbed to the electrode surface.<sup>6</sup> The Outer Helmholtz Plane (OHP) is made up of solvated molecules that are attracted through electrostatic forces. Then on the outside barrier of the OHP is the diffusion layer. This layer consists of scattered ions extending from the OHP out into bulk solution. In this instance there are no ordering forces present, instead thermal motion dictates the balance of ions in solution.<sup>6</sup>

### 1.3.3 Hydrodynamic Amperometry

In hydrodynamic amperometry the geometry of the cell limits diffusion and the flow of the solution across the electrode surface creates a steady state. Hydrodynamic amperometry arose from chronoamperometry. A potential step experiment can be used to describe chronoamperometry by the chemical conversion of O to R. In this technique an initial potential is applied to the working electrode, which is not sufficient to reduce O to R at the electrode surface. The potential is then stepped up to a second potential ( $E_2$ ) that is sufficient to reduce O to R and held for some amount of time ( $\tau$ ). It can then either be stepped back down, as shown in Figure 1.6 to a final potential ( $E_f$ ) or held at  $E_2$ <sup>5, 6</sup>. In either scenario, current is being monitored as a function of time. In hydrodynamic amperometry the excitation waveform changes slightly. In this technique the voltage at which the chemical conversion occurs is applied to the electrode and held constant over time, producing the current trace as indicated by the dashed line in Figure 1.7. Furthermore, this experiment, unlike chronoamperometry is not carried out in quiescent solution, but instead solution is flowed across the electrode surface by either pressure (LC) or electroosmotic flow (CE). For this technique species are brought to the electrode surface(s) by convective mass transport, as a result the plot of current vs. time, shown in Figure 1.7 changes. Instead of the current approaching zero over time, the current plateaus due to constant flow of solution over the electrode surface(s).

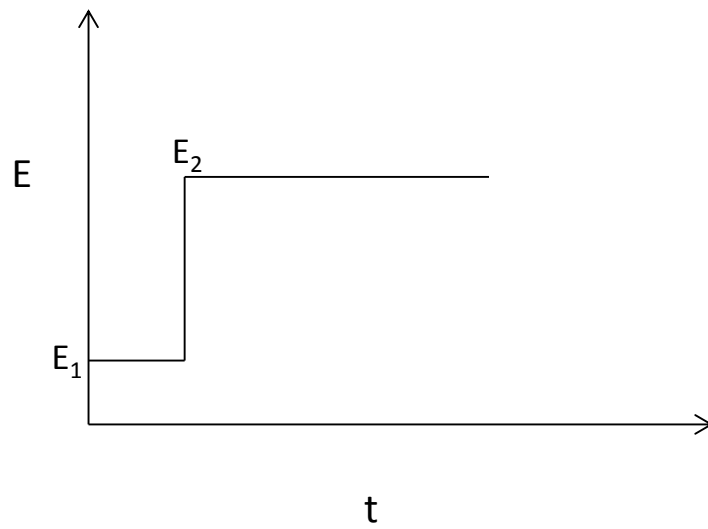


Figure 1.6: Waveform for potential step, where  $t$  is time and  $E$  is potential applied to the electrode.

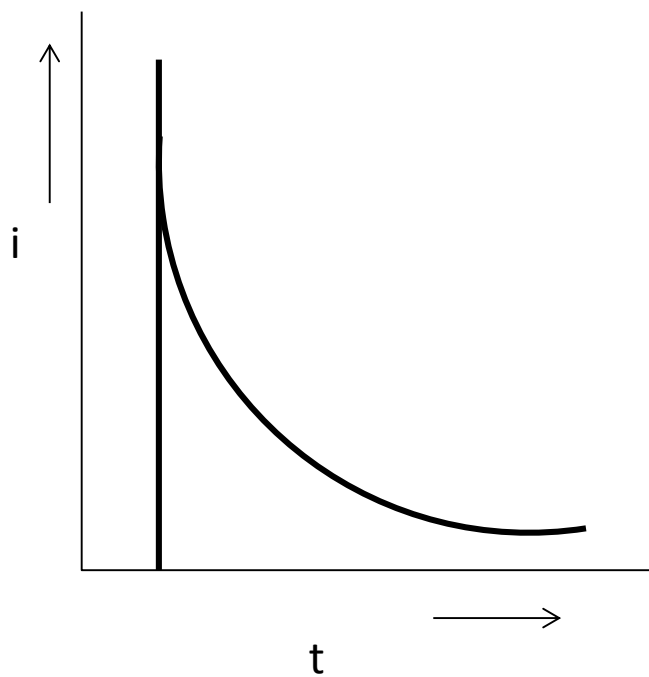


Figure 1.7: Current ( $i$ ) vs time ( $t$ ) plot for amperometric detection. Current instantaneously increases as potential is applied at the electrode surface due to charge build up from the double layer. Current dissipates over time as charge from the double layer diminishes, but does not reach zero as convection or flow of solution is governing mass transport to the electrode surface.

As shown in Figure 1.7 when the potential is stepped from  $E_1$  to  $E_2$  the current instantaneously increases at the electrode surface as a result of the reduction of O to R. The intensity of the current is directly related to the amount of material converted at the electrode-solution interface.<sup>6, 24-27</sup> The rate at which this occurs is proportional to the current. The current is a result of charge moving through solution, where charge ( $Q$ ) is proportional to the number of moles of electrons ( $n$ ) times Faraday's constant ( $F$ ), as shown in equation 4.

$$(4)$$

Initially, though there is some contribution to the current as a result of the charge build up on the electrode surface, described by the double layer capacitive current, this ultimately does not contribute to the overall signal observed as steady state is quickly reached. Because of the convective mass transport to the electrode surface, current in these systems are not described in terms of diffusion, but instead as a rate of conversion of charge as a function of time. As, a species O is being converted to R, Faraday's Law, equation (4), becomes:

Where,  $N$  is the number of moles of species O or R converted at the electrode surface and  $n$  is the number of moles of electrons per mole of analyte transferred. Taking the derivative of this equation with respect to time, results in an instantaneous rate or the current produced, as shown in equation (5).

$$i = nF \left( \frac{dN}{dt} \right) \quad (5)$$

If the number of moles of electrons is known for the given redox reaction then charge is directly related to concentration of analyte. From equation 5, current is a function of charge per unit time allowing for current to also be a quantitative measure of analyte concentration.

## 1.4 Application to LC and CE systems

Electrochemical detection was initially implemented with LC for the detection of catecholamines. The analytical requirements often necessary to analyze biological samples are: low limits of detection (nM-pM), small sample volumes (> 20 $\mu$ l) and good selectivity in complex matrices.<sup>7</sup> Compared to other detection modes, such as fluorescence and UV, electrochemical detection has inherent selectivity, sensitivity, can be easily miniaturized and is relatively inexpensive. The main type of electrochemical detection coupled with dynamic systems, such as LC and CE, has been hydrodynamic amperometric detection. It should be noted that there are other types of electrochemical detection often coupled with these separation techniques, namely potentiometric detection and conductivity detection. Potentiometric detection is used to assess potential differences in solution across lipophilic membranes, while conductivity detection measures the “conductivity of a volume of solution between two electrodes”, which is applicable to any species carrying a charge and not dependent upon an analyte having a redox reaction.<sup>27, 28</sup>

### 1.4.1 Thin-layer cell development

Detection using hydrodynamic amperometry is based on the transfer of electrons to or from an electroactive compound typically at a solid electrode (exception hanging Hg drop electrode) with a constant potential applied to the electrode surface. The current produced is a function of the redox reaction occurring at the surface of the electrode and is proportional to chemical conversion at the electrode surface.<sup>28</sup>

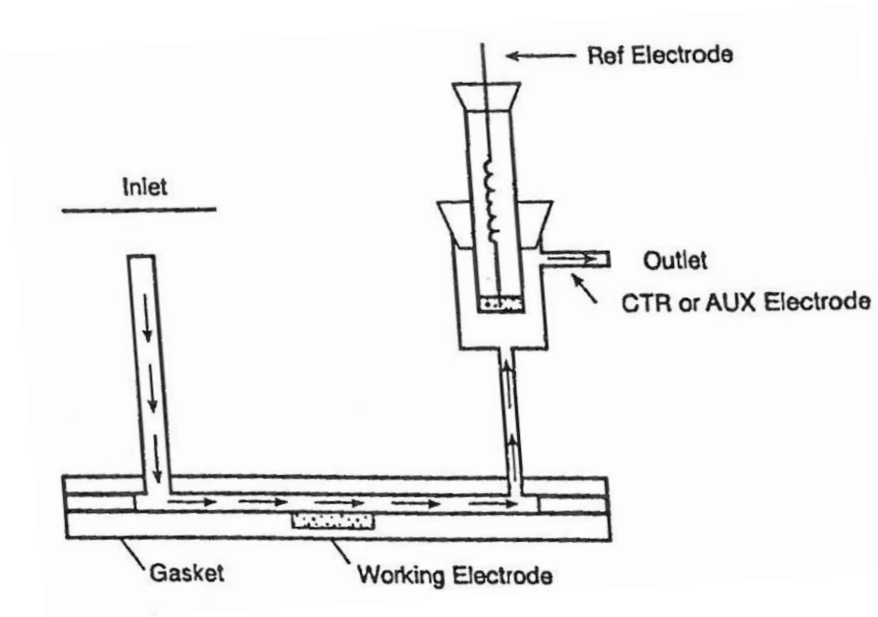


Figure 1.8: Initial thin-layer cell for HPLC. (with permission).<sup>7</sup>

Two types of detection schemes compete frequently in literature, the thin layer cell and the “so-called” coulometric detector or packed bed electrodes. The first thin layer cell design for LC was reported by Adams and co-workers.<sup>25</sup> It incorporated the use of a carbon paste electrode imbedded in teflon, as shown in Figure 1.8. Flow was parallel to the electrode surface and incorporated significant dead volume from the column to the electrode.<sup>7, 24-27</sup> While it was sufficient for the detection of some catecholamines, the dead volume contributed to significant band broadening and the placement of the working electrode in relation to the reference electrode resulted in significant iR drop. A reference electrode is added to the cell to maintain a constant potential difference at the working electrode. The most common reference electrodes used are Ag/AgCl or saturated calomel electrode. These electrodes are high impedance electrodes whose potential difference remains constant relative to the reaction occurring at the working electrode. The placement of the reference electrode and auxiliary electrode in relation to the working electrode in these cell designs is a key factor in minimizing iR drop in solution and subsequently decreasing overpotential required to maintain control at the working electrode.

The alternative is the use of “packed-bed” electrodes, sometimes referred to as coulometric detection. This detection scheme operates under the principle of 100% conversion efficiencies for species, as compared with thin-layer cells where roughly 30% conversion efficiencies are obtained.<sup>7, 29, 30</sup> Theoretically, if 100% of an analyte is being converted from O to R, then absolute measurements of each analyte that is resolved chromatographically could be determined. However, these types of detectors require large surface areas which increase dead volume and residence times. As the surface areas are increased to obtain higher conversion efficiencies the amount of product being converted is approximately proportional to the amount of background noise produced. As a result, the signal-to-noise ratio (S/N) is diminished and larger sample volumes are required to overcome the loss in and attain LODs comparable to those achieved with thin layer flow cells.<sup>6, 24, 26</sup> Additionally, these electrodes are typically used as generator electrodes. Generator electrodes are placed upstream of the detection cell

and are placed at potentials sufficient to oxidized or reduce everything in solution prior to the detection electrode. In this respect interferences can be minimized; however, these cells do not allow for peak confirmation analysis by voltammetry nor can simultaneous detection of redox couples be observed.

Although conversion efficiencies are lower for thin layer cells, less noise is produced due to decreased surface areas with proportionally larger signal produced from analyte conversion, thus improving signal-to-noise ratios. To improve upon this initial design several different electrode configurations were assessed in order to yield the best conversion efficiencies while still maintaining control over the working electrodes. Figure 1.9, as shown in "Laboratory Techniques in Electroanalytical Chemistry, 2<sup>nd</sup> Ed", shows the various electrode configurations tested. Figure 1.9a, is most similar to the initial design by Kissinger *et al*, where the reference and auxillary electrode are placed downstream from the working electrode, which results in significant iR drop across the working electrode. Figure 1.9b shows the working and auxillary electrode adjacent to one another with the reference electrode placed downstream. In this instance there is an even distribution of potential across the working electrode resulting in minimal iR drop. Additionally, no chemical interaction is observed, because diffusion occurring across the thin layer is larger/longer than the diffusion between the electrodes. Figure 1.9c is the same design as 9b with the addition of an ionically conducting membrane. The ionically conducting membrane was put in place to allow exchange of ions between the electrodes, but not bulk flow of the electrolyte. Figure 1.9d shows the reference electrode adjacent to the working electrode with the auxillary electrode downstream, resulting in uneven distribution of potential across the working electrode. Figure 1.9e is the most desirable configuration, because of the placement of the working electrode in relation to both the auxillary and reference electrodes; however, it was found to be difficult to fabricate and maintain.<sup>6</sup> The design of the thin layer dual-electrode cell most frequently used has the glassy carbon electrodes adjacent to the auxillary electrode with the reference electrode in a side

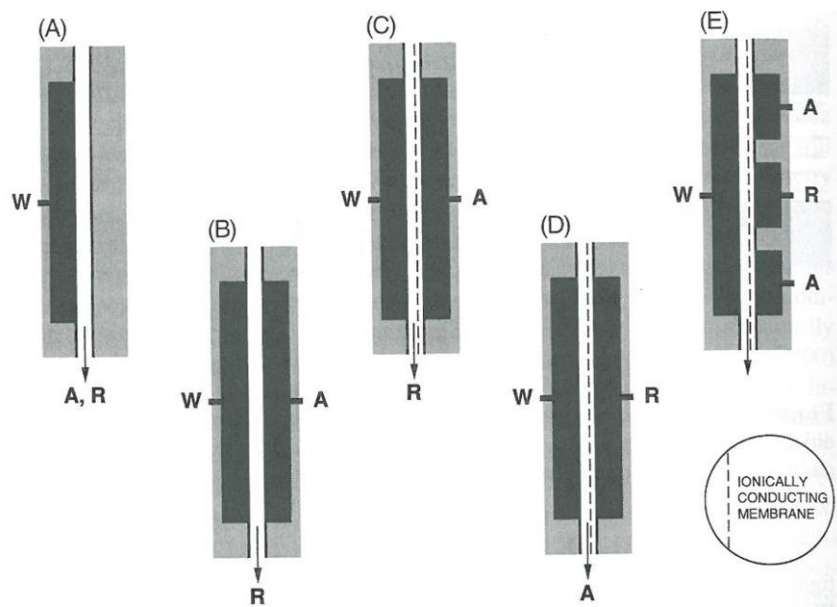


Figure 1.9: Evolution of electrode configurations for the development of thin layer cell, with permission.<sup>6</sup>

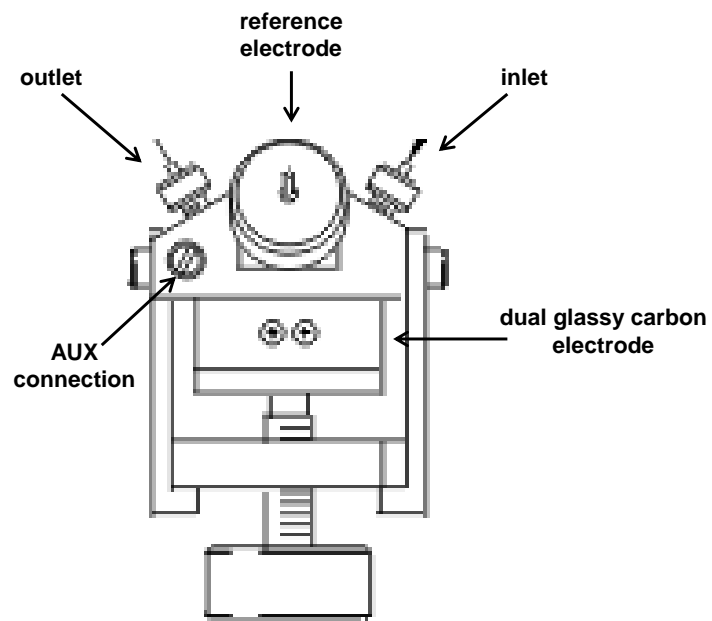


Figure 1.10: Thin layer flow cell for liquid chromatography. Reference electrode adjacent to working electrode minimizing  $iR$  drop, adapted from Kissinger, with permission<sup>6</sup>.

compartment adjacent to the working and auxiliary electrodes as shown in Figure 1.10. This was an evolution of the design shown in Figure 9b.

There are three different electrode configurations that can be used to elicit different chemical information with the thin layer dual-electrode cell. These configurations are shown in Figure 1.11. The first configuration shown in Figure 11a is the series configuration, in which flow runs across the surface of the electrodes, indicated by the black arrow. In this configuration analytes of interest are oxidized or reduced at the upstream electrode and re-reduced or re-oxidized at the downstream electrode. The ratio of the current response at the downstream electrode to that of upstream electrode can be used to obtain the collection efficiency. This is a good way to improve selectivity in complex matrix, namely because while it is likely that several species will have a significant response at the upstream electrode (due to the applied potential) the likelihood that the response or the magnitude of the response will be the same at the downstream electrode is slim.<sup>26</sup> More specifically, only chemically reversible compounds will respond at the downstream electrode, which is often at analytical favorable potential. The series mode can also be used in a “generator” mode. This is particularly useful for samples containing redox couples where both reduced and oxidized forms are present and are chemically reversible.<sup>31-37</sup> This has been used extensively for the detection of thiols and disulfides; disulfides are reduced at -1.0 V vs. Ag/AgCl, resulting in high background noise making quantitative detection nearly impossible.

Figure 1.11b shows the thin layer dual-electrode cell being used in a parallel-adjacent configuration, where flow occurs between the two electrodes. This configuration lends itself to a quantitative estimate of peak purity.<sup>26</sup> In this configuration two different oxidation or reduction potentials can be monitored simultaneously instantly producing a two point voltammogram. The current ratio obtained from the response at these two electrodes can be used in conjunction with migration times to confirm peak identity in complex matrices.

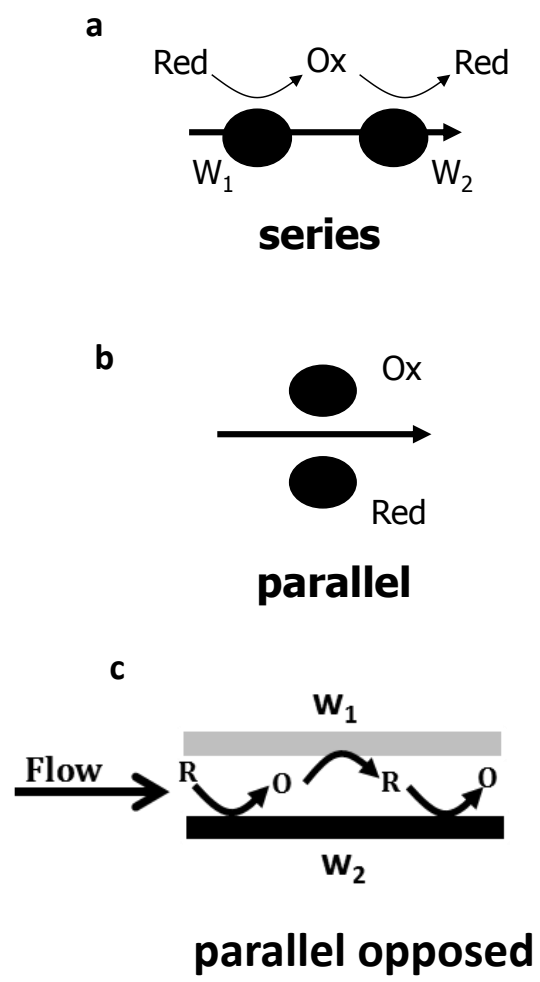


Figure 1.10: Dual-electrode configurations with electrochemical responses.

Additionally, this configuration can also be used to simultaneously monitor reducible and oxidizable species by holding one electrode at an oxidation potential and the other at a reduction potential. In this configuration, the two working electrodes are essentially independent of each other.

Lastly, a parallel-opposed configuration can also be integrated into the thin layer flow cell. The design would be modified so that two working electrodes are opposite each other, with flow between the electrodes, shown in Figure 1.11c. In this configuration redox cycling could potentially occur by holding one electrode at an oxidation potential and the second at a reduction potential. Molecules could diffuse between electrodes and subsequently be reoxidized at the first working electrode enhancing signal and improving detection limits. Several factors influence the enhancement that can be obtained including: velocity of the electrolyte, diffusion of the analyte, length of the electrodes, electrode spacing and chemical reversibility. This mode had not been successfully implemented with LC due to high flow rates, but with the advent of new capillary columns this configuration or variations of it, specifically interdigitated array microelectrodes (IDA) signal enhancement has been observed.<sup>26, 38-44</sup>

#### 1.4.2 Integration of Electrochemical Detection with CE

EC detection has also been integrated with CE. CE systems frequently employ microelectrodes. Microelectrodes are unique from planar electrodes used in thin layer flow cells in that there are two types of diffusion that contribute to the observed current, planar diffusion occurring perpendicular to the electrode surface and radial diffusion happening at the edges of the electrode. Radial diffusion increases mass transport at the electrode surface to the extent that the rate of diffusion is proportional to the material being brought to the surface of the electrode, achieving a steady state. As a result, charging currents are reduced and signal-to-noise ratios improve relative to larger ( $\geq 1.0$  mm) planar electrodes.<sup>45-50</sup> Microelectrodes can be used as part of single electrode detection or dual electrode detection systems. Dual electrode schemes have been incorporated and used in series configurations for

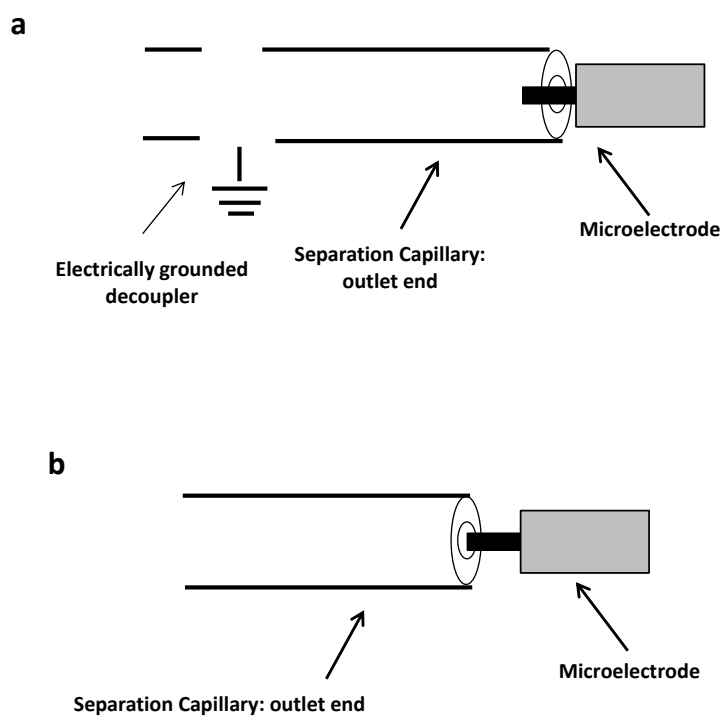


Figure 1.11: EC detection with CE demonstrated with single electrodes. a) on-capillary detection, b) end-capillary detection

sample clean up or for determination of thiols as Allison and Schoup reported for LC.<sup>31</sup> Single electrodes can also be used on-capillary and off-capillary systems. Both of these can be employed in capillary electrophoresis with electrochemical detection (CEEC).

On-capillary detection is generally described as the working electrode (WE) being on or inside the capillary, as shown in Figure 1.12a<sup>51</sup>. This mode of detection is desirable because there is minimal loss of analyte signal due to diffusion away from the electrode surface, thus providing greater sensitivity. Typically, this approach involves isolating the separation current from the current of the WE, which has most often been accomplished using an electric decoupler. One of the first decouplers was reported by Wallingford and Ewing, involved fracturing the capillary into two pieces, which were linked using a porous glass sleeve creating a joint.<sup>52</sup> This concept evolved into a bare fracture, whereby the capillary pieces are not joined by another material, but instead are immersed in run buffer and analytes are moved towards the detector by electroosmotic flow generated from the separation voltage.<sup>53</sup> The idea of the electric decoupler was carried out further with the addition of a Nafion polymer coating.<sup>54, 55</sup> In this case the polymer was used to maintain the structure of the capillary and minimize loss or exchange of analyte through this region, thus improving detection limits. Hu *et al.* used HF acid to create an etched joint in the capillary.<sup>56</sup> More recently, Osbourn *et al.* developed a decoupler using cellulose acetate polymer.<sup>57</sup> Instead of removing the polyamide coating and HF etching down the walls of the capillary as Hu *et al.* demonstrated, laser ablation was used to create holes in the capillary that were then covered using the previously mentioned polymer. Although these approaches eliminate challenges such as electrode alignment and reproducibility of electrode positioning, fabrication of decouplers pose challenges and their fragile nature decreases the robustness of the system. A more robust approach to on-capillary electrochemical detection, when compared to conventional CE systems, is through the use of microchips.<sup>36, 58-64</sup> The most commonly used approach for these systems is accomplished by placing a large palladium electrode upstream from the WE.<sup>36, 59, 65-70</sup> The palladium electrode absorbs and

dissipates hydrogen produced at the upstream electrophoretic cathode, decoupling the devices at field strengths up to 1200 V/cm.<sup>36</sup>

Conventionally, in end-column detection the electrode is placed outside the capillary and aligned with the outlet, as shown in Figure 1.12b.<sup>51</sup> This detection scheme is easily fabricated for CE, as it does not require an electric decoupler; however, reproducibility of electrode positioning is difficult and creates significant variability in response. Instead the current produced from the separation is dissipated to a degree from the WE by using capillaries with small inner diameters (5-25  $\mu\text{m}$ ).<sup>71-75</sup> Small inner diameters with long capillary lengths are adequate to prevent electrophoretic current produced from coming back through the ground for the detector, which can cause an increase in background noise. Alignment of the electrode with the outlet of the capillary results in band broadening due to diffusion of the analyte away from the electrode surface, resulting in decreased sensitivity. To improve end-column detection Ewing and co-workers employed HF etching, whereby the inner walls of the capillary are dissolved and the inner diameter of the capillary is opened sufficiently to insert a micro-WE.<sup>73</sup> While this leads to improved sensitivity, due to less diffusion of the analyte away from the surface of the electrode, the separation current is not completely shielded from the current of the WE resulting in shifts in apparent peak potentials.<sup>76, 77</sup> End-column detection has also been widely employed in microchip systems by placing the WE at the outlet of the capillary, typically in the waste reservoir.<sup>37, 78-82</sup> These systems experience the same issues as conventional systems employing end-column detection: reproducibility in electrode alignment and distance, diffusion of the analyte away from the electrode surface, and increased background noise at the detector (due to some residual field effects produced from the electrophoretic current produced upstream).

## 1.5 Overview of Research

The focus of this research has been on the development of new methodologies involved in the separation and detection of redox species that play roles in maintaining tissue homeostasis under stressful conditions. In addition to the methods developed to probe these biological interactions, a newly developed parallel dual-electrode for capillary electrophoresis was also developed. Using this dual-electrode design redox cycling was observed, which resulted in signal enhancement and improved detection limits over previously reported dual electrode schemes. In addition, this dual electrode could be used to enhance selectivity of migration based peak identification using voltammetry. Improving selectivity in complex matrices will be advantageous for microdialysis samples.

## 1.6 References

1. Patel, M. N., Oxidative stress, mitochondrial dysfunction, and epilepsy. *Free Radical Research* **2002**, *36* (11), 1139-1146.
2. Shin, E.-J.; Jeong, J.-H.; Chung, Y.-H.; Kim, W.-K.; Ko, K.-H.; Bach, J.-H.; Hong, J.-S.; Yoneda, Y.; Kim, H.-C., Role of oxidative stress in epileptic seizures. *Neurochemistry International* **2011**, *59* (2), 122-137.
3. Vicente, S. J. V.; Ishimoto, E. Y.; Cruz, R. J.; Pereira, C. D. S.; Torres, E. A. F. D. S., Increase of the Activity of Phase II Antioxidant Enzymes in Rats after a Single Dose of Coffee. *Journal of Agricultural and Food Chemistry* **2011**, *59* (20), 10887-10892.
4. Costello, D. J.; Delanty, N., Oxidative injury in epilepsy: Potential for antioxidant therapy? *Expert Review of Neurotherapeutics* **2004**, *4* (3), 541-553.
5. Bard, A. J., Faulkner, L.R., *Electrochemical Methods, Fundamentals and Applications, 2nd Ed.* John Wiley and Sons, Inc.: New York, NY, 2001.
6. Kissinger, P. T., Heineman, W.R., *Laboratory Techniques in Electroanalytical Chemistry, 2nd Ed.* Marcel Dekker Inc. : New York, NY, 1996.
7. Acworth, I. N.; Bowers, M., An introduction to HPLC-based electrochemical detection: from single electrode to multi-electrode arrays. *Progress in HPLC-HPCE* **1997**, *6* (Coulometric Electrode Array Detectors for HPLC), 3-50.
8. Cock, H. R., The role of mitochondria and oxidative stress in neuronal damage after brief and prolonged seizures. *Progress in Brain Research* **2002**, *135* (Do Seizures Damage the Brain), 187-196.
9. Hamed, S. A., The multimodal prospects for neuroprotection and disease modification in epilepsy: Relationship to its challenging neurobiology. *Restorative Neurology and Neuroscience* **2010**, *28* (3), 323-348.
10. Ames, B. N. S., Halliwell, M.K., Aruoma, B., *In DNA and Free Radicals.* Ellis Horwood Ltd: West Sussex, England, 1993.
11. Klaunig, J. E.; Xu, Y.; Han, C.; Kamendulis, L. M.; Chen, J.; Heiser, C.; Gordon, M. S.; Mohler, E. R., III, The effect of tea consumption on oxidative stress in smokers and nonsmokers. *Proceedings of the Society for Experimental Biology and Medicine* **1999**, *220* (4), 249-254.
12. Loft, S.; Fischer-Nielsen, A.; Jeding, I. B.; Vistisen, K.; Poulsen, H. E., 8-Hydroxydeoxyguanosine as a urinary biomarker of oxidative DNA damage. *Journal of Toxicology and Environmental Health* **1993**, *40* (2-3), 391-404.
13. Fleming, J. E.; Miquel, J.; Cottrell, S. F.; Yengoyan, L. S.; Economos, A. C., Is cell aging caused by respiration-dependent injury to the mitochondrial genome? *Gerontology* **1982**, *28* (1), 44-53.
14. Basu, A. K.; Marnett, L. J., Unequivocal demonstration that malondialdehyde is a mutagen. *Carcinogenesis* **1983**, *4* (3), 331-3.
15. Hamed, S. A.; Abdallah, M. M.; El-Melegy, N., Blood levels of trace elements, electrolytes, and oxidative stress/antioxidant systems in epileptic patients. *Journal of Pharmacological Sciences (Tokyo, Japan)* **2004**, *96* (4), 465-473.
16. Sudha, K.; Rao, A. V.; Rao, A., Oxidative stress and antioxidants in epilepsy. *Clinica Chimica Acta* **2001**, *303* (1-2), 19-24.
17. Varoglu, A. O.; Yildirim, A.; Aygul, R.; Gundogdu, O. L.; Sahin, Y. N., Effects of Valproate, Carbamazepine, and Levetiracetam on the Antioxidant and Oxidant Systems in Epileptic Patients and Their Clinical Importance. *Clinical Neuropharmacology* **2010**, *33* (3), 155-157.

18. Mattson, M. P., Excitotoxic and Excitoprotective Mechanisms, Abundant Targets for the Prevention and Treatment of Neurodegenerative Disorders. *Neuromolecular Medicine* **2003**, *3*.
19. Azam, F., *Therapeutic Potential of Free Radical Scavengers in Neurological Disorders*. Nova Science Publishers, Inc. : 2010.
20. de Freitas Rivelilson, M., Lipoic acid alters delta-aminolevulinic dehydratase, glutathione peroxidase and Na<sup>+</sup>,K<sup>+</sup>-ATPase activities and glutathione-reduced levels in rat hippocampus after pilocarpine-induced seizures. *Cellular and molecular neurobiology* **2010**, *30* (3), 381-7.
21. Packer, L.; Witt, E. H.; Tritschler, H. J., Alpha-lipoic acid as a biological antioxidant. *Free Radical Biology & Medicine* **1995**, *19* (2), 227-50.
22. Hong, J.; Bose, M.; Ju, J.; Ryu, J.-H.; Chen, X.; Sang, S.; Lee, M.-J.; Yang, C. S., Modulation of arachidonic acid metabolism by curcumin and related  $\beta$ -diketone derivatives: effects on cytosolic phospholipase A<sub>2</sub>, cyclooxygenases and 5-lipoxygenase. *Carcinogenesis* **2004**, *25* (9), 1671-1679.
23. Scapagnini, G.; Foresti, R.; Calabrese, V.; Giuffrida Stella, A. M.; Green, C. J.; Motterlini, R., Caffeic acid phenethyl ester and curcumin: a novel class of heme oxygenase-1 inducers. *Molecular Pharmacology* **2002**, *61* (3), 554-561.
24. Kissinger, P. T., Amperometric and coulometric detectors for high-performance liquid chromatography. *Analytical Chemistry* **1977**, *49* (4), 447A-448A, 450A, 452A, 454A, 456A.
25. Kissinger, P. T.; Refshauge, C.; Dreiling, R.; Adams, R. N., Electrochemical detector for liquid chromatography with picogram sensitivity. *Analytical Letters* **1973**, *6* (5), 465-77.
26. Roston, D. A.; Kissinger, P. T., Series dual-electrode detector for liquid chromatography/electrochemistry. *Analytical Chemistry* **1982**, *54* (3), 429-34.
27. Hulvey, M. K., Lunte, Susan M., Fischer, David, J., and Kuhnline, Courtney D., Electrochemical Detection Methods Following Liquid Chromatography, Capillary Electrophoresis, and Microchip Electrophoresis Separations. In *Encyclopedia of Analytical Chemistry*, Meyers, R. A., Ed. John Wiley & Sons, Inc.: 2010.
28. Landers, J. P., *Handbook of Capillary Electrophoresis, 2nd Ed.* CRC Press: Boca Raton, FL, 1997.
29. Hepler, B. R.; Weber, S. G.; Purdy, W. C., The amperometric detection of thyroid hormones following reverse-phase high-performance liquid chromatography. *Analytica Chimica Acta* **1980**, *113* (2), 269-76.
30. Schieffer, G. W., Dual coulometric-amperometric cells for increasing the selectivity of electrochemical detection in high-performance liquid chromatography. *Analytical Chemistry* **1980**, *52* (12), 1994-8.
31. Allison, L. A.; Shoup, R. E., Dual electrode liquid chromatography detector for thiols and disulfides. *Analytical Chemistry* **1983**, *55* (1), 8-12.
32. Allison, L. A.; Shoup, R. E., Determination of thiols by liquid chromatography/electrochemistry. *Clin. Liq. Chromatogr.* **1984**, *1*, 185-9.
33. Blank, C. L., Dual electrochemical detector for liquid chromatography. *Journal of Chromatography* **1976**, *117* (1), 35-46.
34. Lunte, C. E.; Kissinger, P. T.; Shoup, R. E., Difference mode detection with thin-layer dual-electrode liquid chromatography/electrochemistry. *Analytical Chemistry* **1985**, *57* (8), 1541-6.
35. McClintock, S. A.; Purdy, W. C., Dual working-electrode electrochemical detector for liquid chromatography. *Analytica Chimica Acta* **1983**, *148*, 127-33.
36. Mecker, L. C.; Martin, R. S., Use of micromolded carbon dual electrodes with a palladium decoupler for amperometric detection in microchip electrophoresis. *Electrophoresis* **2006**, *27* (24), 5032-5042.

37. Pumera, M.; Merkoci, A.; Alegret, S., Carbon nanotube detectors for microchip CE: comparative study of single-wall and multiwall carbon nanotube, and graphite powder films on glassy carbon, gold, and platinum electrode surfaces. *Electrophoresis* **2007**, *28* (8), 1274-1280.
38. Cullison, J. K.; Waraska, J.; Buttaro, D. J.; Acworth, I. N.; Bowers, M. L., Electrochemical detection of catecholamines at sub-5 fg levels by redox cycling. *Journal of Pharmaceutical and Biomedical Analysis* **1999**, *19* (1-2), 253-259.
39. Kim, S. K.; Hesketh, P. J.; Li, C.; Thomas, J. H.; Halsall, H. B.; Heineman, W. R., Fabrication of comb interdigitated electrodes array (IDA) for a microbead-based electrochemical assay system. *Biosensors & Bioelectronics* **2004**, *20* (4), 887-894.
40. Morita, M.; Niwa, O.; Horiuchi, T., Interdigitated array microelectrodes as electrochemical sensors. *Electrochimica Acta* **1997**, *42* (20-22), 3177-3183.
41. Niwa, O., Electroanalysis with interdigitated array microelectrodes. *Electroanalysis* **1995**, *7* (7), 606-13.
42. Niwa, O.; Tabei, H.; Solomon, B. P.; Xie, F.; Kissinger, P. T., Improved detection limit for catecholamines using liquid chromatography-electrochemistry with a carbon interdigitated array microelectrode. *Journal of Chromatography, B: Biomedical Applications* **1995**, *670* (1), 21-8.
43. Niwa, O.; Xu, Y.; Halsall, H. B.; Heineman, W. R., Small-volume voltammetric detection of 4-aminophenol with interdigitated array electrodes and its application to electrochemical enzyme immunoassay. *Analytical Chemistry* **1993**, *65* (11), 1559-63.
44. Kurita, R.; Tabei, H.; Liu, Z.; Horiuchi, T.; Niwa, O., Fabrication and electrochemical properties of an interdigitated array electrode in a microfabricated wall-jet cell. *Sensors and Actuators, B: Chemical* **2000**, *B71* (1-2), 82-89.
45. Bard, A. J.; Crayston, J. A.; Kittlesen, G. P.; Varco Shea, T.; Wrighton, M. S., Digital simulation of the measured electrochemical response of reversible redox couples at microelectrode arrays: consequences arising from closely spaced ultramicroelectrodes. *Analytical Chemistry* **1986**, *58* (11), 2321-31.
46. Galus, Z.; Schenk, J. O.; Adams, R. N., Electrochemical behavior of very small electrodes in solution. Double potential step, cyclic voltammetry and chronopotentiometry with current reversal. *J. Electroanal. Chem. Interfacial Electrochem.* **1982**, *135* (1), 1-11.
47. Ito, T.; Maruyama, K.; Sobue, K.; Ohya, S.; Niwa, O.; Suzuki, K., Electrochemical behavior of parallel opposed dual electrode in a microchannel. *Electroanalysis* **2004**, *16* (24), 2035-2041.
48. Kovach, P. M.; Caudill, W. L.; Peters, D. G.; Wightman, R. M., Faradaic electrochemistry at microcylinder, band, and tubular band electrodes. *J. Electroanal. Chem. Interfacial Electrochem.* **1985**, *185* (2), 285-95.
49. Oldham, K. B., Edge effects in semiinfinite diffusion. *J. Electroanal. Chem. Interfacial Electrochem.* **1981**, *122*, 1-17.
50. Wightman, R. M., Microvoltammetric electrodes. *Analytical Chemistry* **1981**, *53* (9), 1125A-1126, 1128A, 1130A, 1132A, 1134A.
51. Lunte, S. M.; Martin, R. S.; Lunte, C. E., Capillary electrophoresis/electrochemistry: Instrument design and bioanalytical applications. *Electroanalytical Methods for Biological Materials* **2002**, 461-490.
52. Wallingford, R. A.; Ewing, A. G., Capillary zone electrophoresis with electrochemical detection. *Analytical Chemistry* **1987**, *59* (14), 1762-6.
53. Linhares, M. C.; Kissinger, P. T., Use of an on-column fracture in capillary zone electrophoresis for sample introduction. *Analytical Chemistry* **1991**, *63* (18), 2076-8.

54. O'Shea, T. J.; Greenhagen, R. D.; Lunte, S. M.; Lunte, C. E.; Smyth, M. R.; Radzik, D. M.; Watanabe, N., Capillary electrophoresis with electrochemical detection employing an on-column Nafion joint. *Journal of Chromatography* **1992**, *593* (1-2), 305-12.
55. Park, S.; Lunte, S. M.; Lunte, C. E., A perfluorosulfonated ionomer joint for capillary electrophoresis with on-column electrochemical detection. *Analytical Chemistry* **1995**, *67* (5), 911-18.
56. Hu, S.; Wang, Z.-L.; Li, P.-b.; Cheng, J.-k., Amperometric Detection in Capillary Electrophoresis with an Etched Joint. *Analytical Chemistry* **1997**, *69* (2), 264-267.
57. Osbourn, D. M.; Lunte, C. E., Cellulose Acetate Decoupler for On-Column Electrochemical Detection in Capillary Electrophoresis. *Analytical Chemistry* **2001**, *73* (24), 5961-5964.
58. Castano-Alvarez, M.; Fernandez-Abedul, M. T.; Costa-Garcia, A., Amperometric detector designs for capillary electrophoresis microchips. *Journal of Chromatography, A* **2006**, *1109* (2), 291-299.
59. Lai, C.-C. J.; Chen, C.-h.; Ko, F.-H., In-channel dual-electrode amperometric detection in electrophoretic chips with a palladium film decoupler. *Journal of Chromatography, A* **2004**, *1023* (1), 143-150.
60. Chen, C.; Hahn, J. H., Dual-Channel Method for Interference-Free In-Channel Amperometric Detection in Microchip Capillary Electrophoresis. *Analytical Chemistry (Washington, DC, United States)* **2007**, *79* (18), 7182-7186.
61. Dawoud, A. A.; Kawaguchi, T.; Jankowiak, R., In-channel modification of electrochemical detector for the detection of bio-targets on microchip. *Electrochemistry Communications* **2007**, *9* (7), 1536-1541.
62. Gunasekara, D. B.; Hulvey, M. K.; Lunte, S. M., In-channel amperometric detection for microchip electrophoresis using a wireless isolated potentiostat. *Electrophoresis* **2011**, *32* (8), 832-837.
63. Guan, Q.; Henry, C. S., Improving MCE with electrochemical detection using a bubble cell and sample stacking techniques. *Electrophoresis* **2009**, *30* (19), 3339-3346.
64. Lacher, N. A.; Garrison, K. E.; Martin, R. S.; Lunte, S. M., Microchip capillary electrophoresis/electrochemistry. *Electrophoresis* **2001**, *22* (12), 2526-2536.
65. Antwi, C.; Johnson, A. S.; Selimovic, A.; Martin, R. S., Use of microchip electrophoresis and a palladium/mercury amalgam electrode for the separation and detection of thiols. *Analytical Methods* **2011**, *3* (5), 1072-1078.
66. Vickers, J. A., Henry, Charles. S., Simplified current decoupler for microchip capillary electrophoresis with electrochemical and pulsed amperometric detection. *Electrophoresis* **2005**, *26*, 4641-4647.
67. Fischer, D. J.; Vandaveer, W. R. I. V.; Grigsby, R. J.; Lunte, S. M., Pyrolyzed photoresist carbon electrodes for microchip electrophoresis with dual-electrode amperometric detection. *Electroanalysis* **2005**, *17* (13), 1153-1159.
68. Lacher, N. A.; Lunte, S. M.; Martin, R. S., Development of a microfabricated palladium decoupler/electrochemical detector for microchip capillary electrophoresis using a hybrid glass/poly(dimethylsiloxane) device. *Analytical Chemistry* **2004**, *76* (9), 2482-2491.
69. Martin, R. S., Gawron, Andrew J., Lunte, Susan M., Henry, Charles S., Dual-Electrode Electrochemical Detection for Poly(dimethylsiloxane)-Fabricated Capillary Electrophoresis Microchips. *Analytical Chemistry (Washington, DC, United States)* **2000**, *72*, 3196-3202.
70. Mecker, L. C., Filla, Laura A., Martin, R. Scott, Use of a Carbon-Ink Microelectrode Array for Signal Enhancement in Microchip Electrophoresis with Electrochemical Detection. *Electroanalysis* **2010**, *22* (19), 2141-2146.
71. Huang, X.; Zare, R. N.; Sloss, S.; Ewing, A. G., End-column detection for capillary zone electrophoresis. *Analytical Chemistry* **1991**, *63* (2), 189-92.

72. Sloss, S.; Ewing, A. G., Improved method for end-column amperometric detection for capillary electrophoresis. *Analytical Chemistry* **1993**, *65* (5), 577-81.
73. Powell, P. R.; Woods, L. A.; Ewing, A. G., Characterization of etched electrochemical detection for electrophoresis in micron inner diameter capillaries. *Journal of Separation Science* **2005**, *28* (18), 2540-2545.
74. Woods, L. A.; Ewing, A. G., Etched electrochemical detection for electrophoresis in nanometer inner diameter capillaries. *ChemPhysChem* **2003**, *4* (2), 207-211.
75. Qian, J.; Wu, Y.; Yang, H.; Michael, A. C., An integrated decoupler for capillary electrophoresis with electrochemical detection: Application to analysis of brain microdialyzate. *Analytical Chemistry* **1999**, *71* (20), 4486-4492.
76. Matysik, F.-M., Improved end-column amperometric detection for capillary electrophoresis. *Journal of Chromatography, A* **1996**, *742* (1+2), 229-234.
77. Wallenborg, S. R.; Nyholm, L.; Lunte, C. E., End-Column Amperometric Detection in Capillary Electrophoresis: Influence of Separation-Related Parameters on the Observed Half-Wave Potential for Dopamine and Catechol. *Analytical Chemistry* **1999**, *71* (3), 544-549.
78. Wu, Y.-Y.; Qu, F.; Lin, J.-M., Microchip capillary electrophoresis with an end-channel amperometric detector and its preliminary application. *Chinese Journal of Chemistry* **2005**, *23* (2), 155-159.
79. Wang, Y.; Chen, H.; He, Q.; Soper, S. A., A high-performance polycarbonate electrophoresis microchip with integrated three-electrode system for end-channel amperometric detection. *Electrophoresis* **2008**, *29* (9), 1881-1888.
80. Wu, Y.; Lin, J.-M.; Su, R.; Qu, F.; Cai, Z., An end-channel amperometric detector for microchip capillary electrophoresis. *Talanta* **2004**, *64* (2), 338-344.
81. Wang, J.; Pumera, M., Dual Conductivity/Amperometric Detection System for Microchip Capillary Electrophoresis. *Analytical Chemistry* **2002**, *74* (23), 5919-5923.
82. Vazquez, M.; Frankenfeld, C.; Coltro, W. K. T.; Carrilho, E.; Diamond, D.; Lunte, S. M., Dual contactless conductivity and amperometric detection on hybrid PDMS/glass electrophoresis microchips. *Analyst (Cambridge, United Kingdom)* **2010**, *135* (1), 96-103.

## Chapter 2: Development of a Dual Electrode Liquid Chromatography Method for the Determination of Co-enzyme Q<sub>10</sub> in Plasma

### 2.0 Background and Significance

Antioxidants, such as ubiquinone-10, also known as, Co-enzyme Q<sub>10</sub> (Co-Q<sub>10</sub>), have the ability to scavenge oxygen radicals and modulate energy use and production. Ubiquinone-10 has been reported to help patients who suffer from strokes by minimizing tissue damage as a result of oxidative stress. As discussed previously, oxidative stress plays a key role in the progression of numerous neurological diseases in which tissue redox hemostasis plays a central role in maintaining normal cell function or committing a cell to apoptosis. Therefore, it would be advantageous to assess the efficacy of dietary ubiquinone-10 regarding its ability to help scavenge free radicals and better maintain endogenous antioxidant systems as a result of a chemically induced seizure or stroke.

### 2.1 Introduction

#### 2.1.1 Ubiquinone-10 Role in Regulation of Oxidative Stress Response

Enzymatic and non-enzymatic antioxidants help guard against attack of free radicals on critical cellular components but may not be able to keep up with their formation. While ideally the repair rate should equal the rate of damage, oxidative stress will result if the products of damage accumulate. This buildup may lead to heart disease, cataracts, Parkinson's disease, Alzheimer's disease, cancer and arthritis<sup>1-10</sup>.

For several years ubiquinone-10 has been touted as an effective exogenous antioxidant that can be taken by patients suffering from heart disease as a preventative measure to protect membrane function and myocardial function during reperfusion. Ubiquinone-10 is a lipid-soluble benzoquinone that acts as an essential component for the transfer of electrons and protons from complex I (NADH dehydrogenase) and complex II (succinate dehydrogenase) to complex III (ubiquinol-cytochrome c reductase) within the mitochondrial membrane<sup>11</sup>. More specifically, electron transport through these complexes in the mitochondrial respiratory chain is coupled to the generation of a transmembrane chemiosmotic proton

gradient, driving cellular energy production <sup>12</sup>. Under oxidative stress conditions, elevated concentrations of NADH and glycerol-3-phosphate increase delivery of electrons to complexes of the respiratory chain in which ubiquinone-10 is a key intermediate, leading to the loss of electron transport to complex III<sup>12</sup>. The resultant breakdown between oxidative phosphorylation and electron transport results in a decrease in the production of ATP within the mitochondria<sup>12</sup>. The loss of electron transport from ubiquinone-10 to complex III results in an increased transfer of electrons to molecular oxygen, which then increases the production of ROS<sup>12</sup>. Ubiquinone-10 has also been shown to reduce depletion of ATP, reduce incidence of reperfusion arrhythmias, aid in the protection of membrane tissues, protect DNA and proteins against ROS, as well as limit the amount of lipid peroxidation and regenerate vitamin E ( $\alpha$ -tocopherol)<sup>13-16</sup>. The ability for ubiquinone-10 to aid in the regeneration of other endogenous antioxidants, as well as biologically regenerate itself through a series of one electron reductions makes it key in the prevention of lipid peroxidation and DNA damage. These aspects of ubiquinone-10 make it a powerful antioxidant. Figure 2.1 shows the mechanism by which the mitochondrial respiratory chain functions normally (2.1a) with ubiquinone-10 (Co-Q<sub>10</sub>) and the mechanism by which ROS are formed via the mitochondrial respiratory chain during oxidative stress (2.1b)<sup>12</sup>.

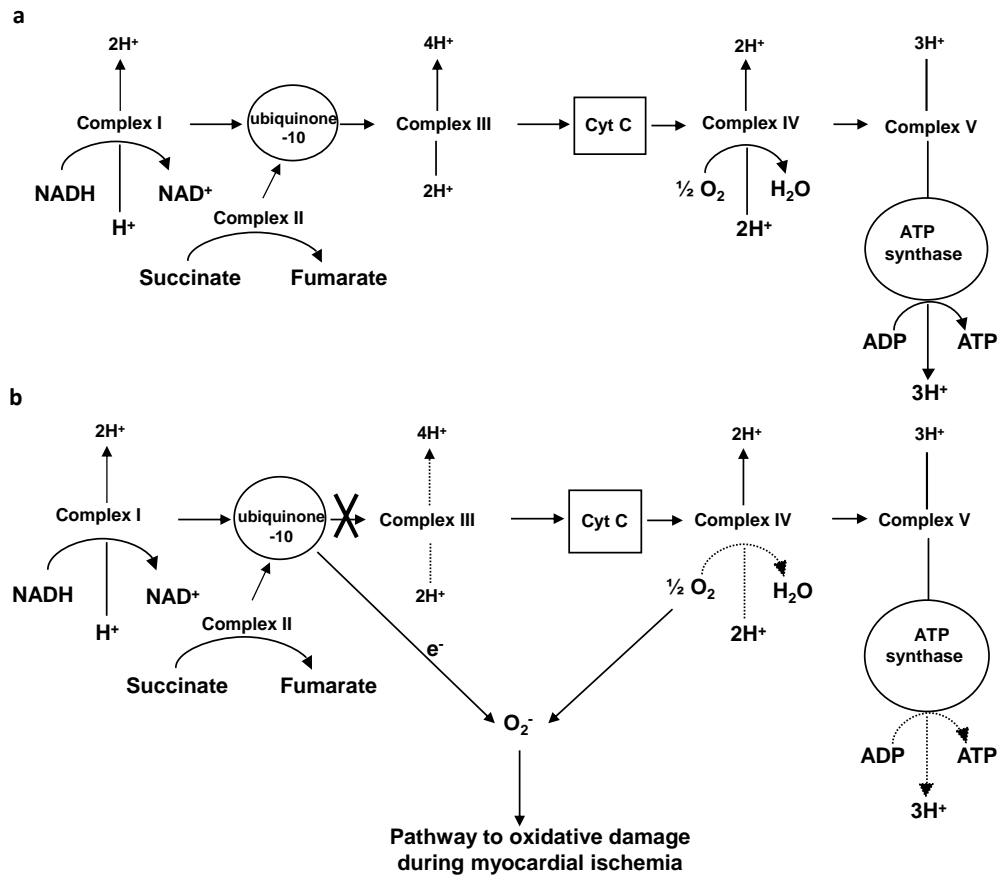


Figure 2.1: Mitochondrial respiratory chain under a) normal conditions and b) oxidative stress

Ubiquinone-10 is found in several tissues including the heart, liver, spleen and ovaries. A significant amount is found in the mitochondria, in which ubiquinone-10 functions together with other enzymes involved in respiration and ATP generation<sup>17</sup>. These facets make ubiquinone-10 an ideal supplement for antioxidant therapy for the treatment of various cardiovascular diseases.

Ischemic damage is a condition in which blood flow is restricted to part of the body resulting in cellular damage. Because ubiquinone-10 is a key component in the mitochondrial respiratory chain and therefore contributes to the synthesis of ATP, it is thought to be useful in preventing cellular damage. Ubiquinone-10 synthesis is known to decrease during ischemia-reperfusion<sup>17</sup>. Whitman et. al. showed ubiquinone-10 improved cardiac power in ischemic and re-perfused isolated rat hearts, using <sup>31</sup>P-NMR to quantify ATP and phosphocreatine. In addition, ubiquinone-10 was also used to monitor the formation oxygen radicals as a result of ischemia-reperfusion using Lucigenin Enhanced Chemiluminescence (LEC)<sup>18</sup>. Although, the results showed an apparent decrease in injury due to oxidative stress, the ability of superoxide to undergo cycles of reduction and oxidation has been shown to contribute to the formation of additional superoxide radicals<sup>19</sup>. Due to this increase, results using this method cannot be considered an accurate way to gauge oxidative damage.

In addition to these studies ubiquinone-10 has also been used to regulate both cardiomyopathy and hypertension<sup>17</sup>. It was reported in cases of cardiomyopathy that ubiquinone-10 was significantly deficient in myopic myocardial tissue. Since the mitochondrial respiratory chain directly controls cardiac metabolism this could affect the risk for abrupt cardiac mortality<sup>17</sup>. The results from the study showed an improvement in bio-energetic activity in patients dosed with ubiquinone-10<sup>17</sup>. Similarly, another study focusing on hypertension showed that administration of ubiquinone-10 improved systolic and diastolic pressures in hypertensive patients<sup>17</sup>. This improvement was thought to be due to improvement

in energy production and quenched toxic properties of peroxynitrite as a result of increased levels of endogenous ubiquinone-10<sup>17</sup>.

Time lines associated with the administration of ubiquinone-10 have been reported previously in order to correlate dosing with tissue damage due to ischemia-reperfusion. Birnbaum reported that ubiquinone-10 had no effect on decreasing infarct size in rats dosed with ubiquinone-10 either during or prior to inducing myocardial ischemia<sup>13</sup>; however, more recent literature has suggested that ubiquinone-10 is more efficacious if taken as a daily supplement. For example, Kalenikova reported a decrease in infarct size with chronic administration of ubiquinone-10 prior to inducing myocardial ischemia<sup>15</sup>.

In addition to studies related to cardiovascular disease, there have been other studies that have looked at the potential effects of ubiquinone-10 on treatments for diabetes resulting in oxidative stress<sup>11, 12</sup>, neurodegenerative disorders such as, Alzheimer's, Parkinson's and epilepsy<sup>20</sup>, as well as aging<sup>17</sup> and topical skin treatments<sup>21</sup>. Although, these potential applications have shown promise for the application of ubiquinone-10, they are beyond the scope of this current proposal, but should be developed further.

#### 2.1.2 Previous Detection Schemes for Determination of Ubiquinone-10

Figure 2.2 shows the mechanism for the reversible redox chemistry that occurs between ubiquinone-10 and ubiquinol-10<sup>22, 23</sup>. Due to the rapid redox cycling

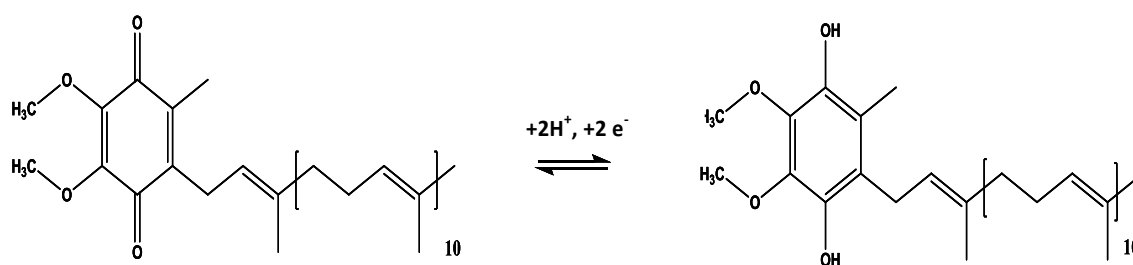


Figure 2.2: Reaction for the reduction and oxidation of ubiquinone-10.

between ubiquinol-10 and ubiquinone-10 within the mitochondrial respiratory chain during oxidative stress, a method that can selectively and simultaneously detect ubiquinone-10 and ubiquinol-10 is necessary to establish the roles of this antioxidant in the maintenance of tissue homeostasis under stressful conditions.

Several methods have been developed for the simultaneous detection of ubiquinone-10 and ubiquinol-10 using liquid chromatography coupled with UV absorbance, fluorescence or electrochemical detection (EC)<sup>22, 24-26</sup>. UV detection offers a simple and robust means to quantify analytes of interest, but requires significant sample pretreatment prior to analysis. In addition, ubiquinone and ubiquinol absorb at non-selective wavelengths (e.g. 254 nm)<sup>17, 27, 28</sup>, which in complex biological matrices, such as plasma, may result in interferences decreasing method selectivity. UV detection is typically associated with low micromolar detection limits ( $\sim 0.5 \mu\text{M}$ ); however, as Finckh *et al.* demonstrated, low nanomolar detection limits ( $\sim 4 \text{ nM}$ ) using UV absorbance can be obtained provided a sufficiently large sample volume is available<sup>29</sup>. Alternatively, fluorescence detection offers a selective and direct means to quantify ubiquinone-10 and ubiquinol-10 with low nanomolar detection limits ( $\sim 3.0 \text{ nM}$ , excitation 290 nm, emission 370 nm)<sup>24</sup>.

EC detection provides direct and selective detection of ubiquinone-10 and ubiquinol-10. This detection technique requires no sample derivatization and is selective for analytes which are inherently electrochemically active. Previous techniques have used packed carbon bed electrodes for detection, in which a generator electrode was placed upstream from the analytical cell at a potential sufficient to completely oxidize (+0.7 V vs. Ag/AgCl) or reduce (-0.7 V vs. Ag/AgCl) the analyte of interest prior to the subsequent re-oxidation or reduction within the analytical cell<sup>22, 23, 25, 26, 29-37</sup>. In addition, this detection scheme contributes to increased dead volumes and residence times, resulting in increased retention times and band broadening<sup>38</sup>. Furthermore, this detection scheme requires large sample volumes in

order to overcome the large background noise associated with the increased surface area of these packed bed electrodes to obtain the low nano-molar to pico-molar detection limits typically associated with EC detection. Reduction and oxidation potentials frequently employed by these methods are known to be sufficient for the reduction of various solvents, while simultaneously oxidizing several other biologically relevant compounds often found in plasma or tissue samples decreasing the method selectivity and sensitivity. Alternatively thin layer flow cells improve mass transport efficiencies due to decreased electrode surface area and channel thickness, improving overall the signal-to-noise ratio as compared to packed bed detectors <sup>39</sup>. Therefore, the development of an analytical method with enhanced selectivity to qualitatively assess analytes of interest is necessary to further investigate the role of ubiquinone-10 in its ability to maintain tissue homeostasis during oxidative stress.

### 2.1.3 Specific Aims of Research

The aim of the research in this chapter was to develop an analytical method using liquid chromatography with amperometric detection for the simultaneous detection of ubiquinone-10 and ubiquinol-10 in human plasma. The method discussed offers decreased total analysis time when compared to previous methods, while maintaining low nanomolar detection limits.

## 2.2 Methods

### 2.2.1 Chemicals and Reagents

Coenzyme Q<sub>10</sub> (HPLC >98%), zinc dust (<10 µm), lithium perchlorate (95%+) were purchased from Sigma (St. Louis, MO, USA). Sodium acetate and glacial acetic acid (17 M) used for the liquid chromatograph system were purchased from Fisher Scientific (Fair Lawn, NJ, USA). All chemicals were reagent grade and used as received. Solvents used for mobile phases or sample matrices (MeOH, EtOH, 1-propanol,

hexane, acetonitrile) were all HPLC grade and were obtained from Fisher Scientific (Fair Lawn, NJ, USA). Ringer's solution consisted of 147 mM NaCl, 3 mM KCl, 1 mM MgCl<sub>2</sub>, 1.3 mM CaCl<sub>2</sub> (152.3 mM ionic strength, Fisher Scientific, Fair Lawn, NJ, USA) and filtered through a 47 mm, 0.22 μm nylon filter (Fisher Scientific, Fair Lawn, NJ, USA) prior to use.

Standard solutions were prepared by dissolving 0.4-1.5 mg of ubiquinone-10 in 1.0 ml, 1-propanol:H<sub>2</sub>O (9:1 v/v). Standard solutions of ubiquinol-10 were prepared from the corresponding ubiquinone-10 using a Jones reductor. The Jones reductor, as shown in Figure 2.3, consisted of zinc dust activated with dilute sulfuric acid (0.5 M). Zinc dust (1.2-1.5 g) was placed into a 3 ml BD syringe (BD Inc., Franklin Lakes, NJ, USA) with a Millex GP 0.22 μm filter with a PES membrane (Carrigtwohill, Co. Cork, Ireland). Dilute sulfuric acid (2.0 ml) was flushed through the syringe to activate the zinc, followed by rinsing with an equal volume of water. An additional 1.0 ml of acid was added and flushed through immediately before the addition of the ubiquinone-10 standard (700 μM-1.2 mM) to ensure the reaction went to completion. Any residual ubiquinol-10 was rinsed with 250 μl 1-propanol:H<sub>2</sub>O (9:1 v/v) and was collected in a 1.5 ml microcentrifuge tube. Standards were stored in the dark at -20°C throughout the day.

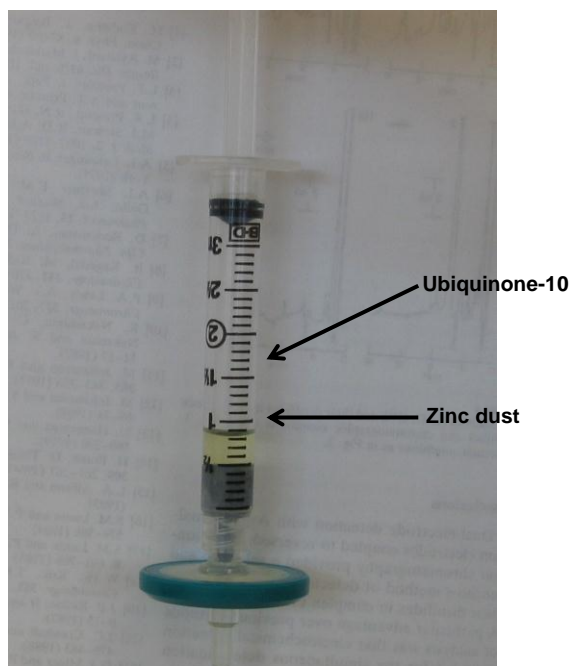
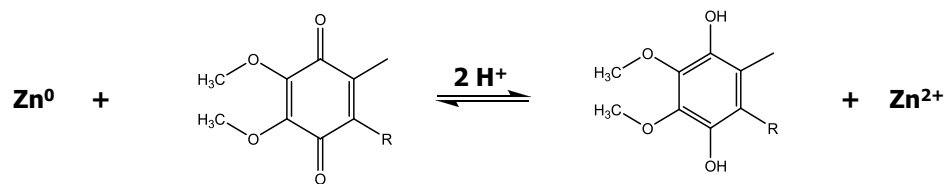


Figure 2.3: Jones reductor used for the reduction of ubiquinone-10. 1.5 g zinc dust, acidified with dilute H<sub>2</sub>SO<sub>4</sub>. Stock solution (500μl) aliquots of ubiquinone-10 filtered through Jones reductor.

Reducers were rinsed with 1.0 ml of water and then reactivated using the same procedure described above for multiple uses. A consistent decrease in peak height of ubiquinol-10 (~10%) was observed when compared to the peak height of the same concentration of ubiquinone-10. It was determined that the decrease in peak height of ubiquinol-10 was due to loss of product within the reductor and not due to the formation of ubiquinone-10 as a result of oxidation. The reuse of each reductor, for multiple reactions, was determined as well as the reproducibility of the reaction from reductor to reductor was evaluated. Deviation observed from reductor to reductor was selectively eliminated based on two criteria. First, solution color was taken into account since this has been reported previously as a means to determine formation of the quinol<sup>35</sup>. Secondly, chromatographic verification was used to ensure that there was no quinone present. Only those reducers which produced a clear solution, as well as no chromatographic evidence of the quinone were used for future method development. The relative standard deviations, based on peak heights between reducers, as well as multiple uses of a single reductor, were determined to be 6.6% and 6.2%, respectively. It was concluded that no significant variation occurred in the preparation of each reductor to notably affect the reduction of ubiquinone-10 to ubiquinol-10.

## 2.2.2 Instrumentation and Conditions

### 2.2.2.1 Method Conditions

Ubiquinone-10 has both polar and non-polar functionalities, resulting in interactions with either normal or reverse phase systems. Conventionally, normal phase systems would be a logical choice for the separation of bulky lipophilic compounds, such as ubiquinone-10, due to the strong interactions that would be expected with the stationary phase. Columns used for normal phase systems are typically silica based columns. Under normal phase conditions it has been observed that compounds such as ubiquinone, strongly adsorb on the stationary phase lowering efficiencies when compared to reverse

phase systems. For these reasons, reverse phase separations with non-aqueous mobile phases are frequently employed.

Previously developed methods have used mobile phases consisting of a wide variety of solvents (e.g. MeOH, EtOH, 1-propanol, IPA, etc.); however, these solvents often contain several trace elements that generally result in increased background noise and correspondingly poorer limits of detection. Initially, for the separation of ubiquinone-10 and ubiquinol-10 a mobile phase consisting of ACN:MeOH (75:25 v/v) with 50 mM lithium perchlorate, (utilizing a Phenomenex Gemini RP-C18, 150x2.0 mm, 5  $\mu$ m) was employed as described by Tang *et al*<sup>22</sup>. Under these conditions a total analysis time of 25 min was obtained with peak widths of over a minute. In order to improve efficiencies and decrease band broadening different ratios of ACN and MeOH were investigated. It was determined that varying the amount ACN and MeOH in the mobile phase had no significant effect on retention time or peak efficiencies. Therefore, the stationary phase was investigated to determine if changing the hydrophobicity of the column packing would decrease retention times and improve band broadening. The RP-C18 Zorbax Bonus-RP (3.5  $\mu$ m, 2.1x100 mm) provided a triply end-capped stationary phase, minimizing non-polar interactions with the incorporation of a polar amide group in the alkyl chain, modifying the interaction of ubiquinone-10 with the stationary phase, when compared to traditional RP-C18 columns, which expose long chain hydrocarbons resulting in increased interactions with the poly-unsaturated backbone of ubiquinone-10. Using this column reduced total analysis times from 25 min to 8 min, while also decreasing peak width from  $\sim$ 1.5 min to 0.62 min, respectively. The ratios of ACN and MeOH were subsequently varied to further decrease peak width and improve retention times. It was determined that a mobile phase consisting of 60:40 (% v/v) MeOH:ACN proved to give the optimal separation conditions by further reducing the retention times of ubiquinone-10 and ubiquinol-10 to 5 and 4 min, respectively.

Although lithium perchlorate is a typical inorganic salt used in non-aqueous mobile phases, for electrochemical detection, it was observed that over time precipitation of the salt from the mobile phase was accumulating at the surface of the electrodes resulting in cross-talk. Substitution of lithium perchlorate by sodium acetate (55 mM) eliminated the precipitation and resulting cross-talk while providing sufficient conductance to minimize noise.

As discussed previously, ubiquinol-10 is readily oxidized to ubiquinone-10 when exposed to oxygen at room temperature. In order to minimize loss of target analyte, glacial acetic acid (2% v/v) was added to the mobile phase described above reducing the pH to approximately six. The addition of acetic acid in the mobile phase provided supplementary protons in solution reducing any potential oxidation of ubiquinol-10 to ubiquinone-10.

All samples were analyzed by LC-EC. The system consisted of a Shimadzu LC-20AD pump and electrochemical detection was achieved with a Bioanalytical Systems LC-4C dual-electrode amperometric detector using 3.0 mm glassy carbon electrodes (Bioanalytical Systems Inc., West Lafayette, IN). A Ag/AgCl reference electrode (3 M NaCl) was used and all potentials are reported versus this electrode. Sample injections were made using a Rheodyne model 7125i injector (overfill of 25  $\mu$ l into a 5  $\mu$ l PEEK sample loop). Data was acquired using Chrom and Spec software, Chromatography Data System, version 1.5x (Ampersand International, Inc., Cleveland, OH, USA).

Separation was achieved using a Zorbax Bonus RP C18 column (2.1x100 mm, 3.5  $\mu$ m) (Agilent Technologies, Santa Clara, CA, USA). The mobile phase consisted of MeOH/ACN/glacial acetic acid (59/39/2 %v/v) with 55 mM sodium acetate at a flow rate of 0.75 ml/min. Oxygen was removed from the system by continuously purging the mobile phase with argon.

### 2.2.2.2 Sample Preparation

Pooled plasma (Invitrogen, Carlsbad, CA, USA) (100  $\mu$ l) was transferred into a 1.5 ml microcentrifuge tube. Extraction of ubiquinone-10 and ubiquinol-10 was performed as previously reported by Kalenikova<sup>15</sup>. Briefly, 100  $\mu$ l of plasma was mixed with 200  $\mu$ l ethanol and 550  $\mu$ l hexane and shaken for 10 min, followed by centrifugation at 6,700 rpm for 3 min. The analytes were extracted from the EtOH using hexane. The hexane layer was removed (500  $\mu$ l) and an additional 550  $\mu$ l of hexane was used to wash the remaining sample. The process was repeated, and the excess hexane (500  $\mu$ l) layer was added to the first aliquot with a final volume of 1.5 ml. The hexane was then evaporated to dryness under argon and reconstituted with 100  $\mu$ l 1-propanol:H<sub>2</sub>O (9:1 v/v), and immediately analyzed. Standard additions were used to determine the basal concentration of ubiquinone-10 and ubiquinol-10 in plasma samples. The concentrations determined using standard additions were then compared to basal concentrations, from unspiked plasma samples, whose concentrations were determined using standard curves. The ratio of the basal concentrations determined from the standard additions were then compared to those determined from the linear regression analysis to determine the extraction efficiency for ubiquinone-10 and ubiquinol-10 from the pooled human plasma samples.

## 2.3 Results and Discussion

### 2.3.1 Investigation of Series and Parallel Electrode Configuration

#### 2.3.1.1 Establishing Chemical Mechanism of Ubiquinone-10 in Bulk Solution

Cyclic voltammetry (CV) was used to determine the approximate peak potentials in bulk solution. Figure 2.4, shows a representative CV obtained in mobile phase. A clear reversible redox couple is observed for the chemical reduction and oxidation of ubiquinone-10.

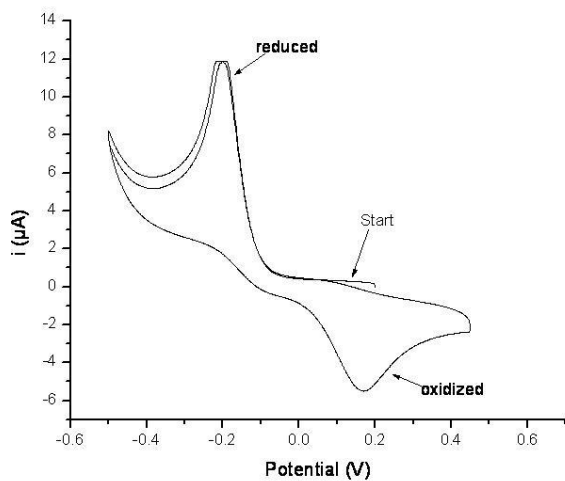
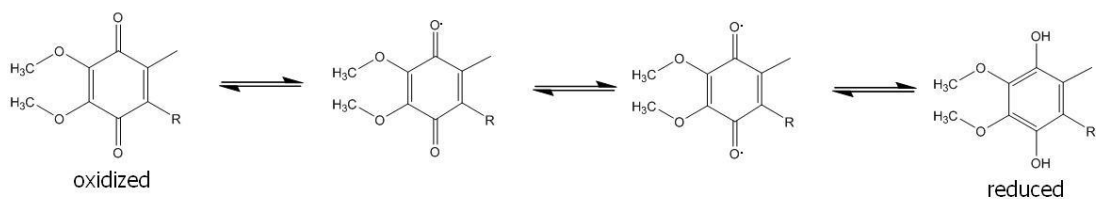


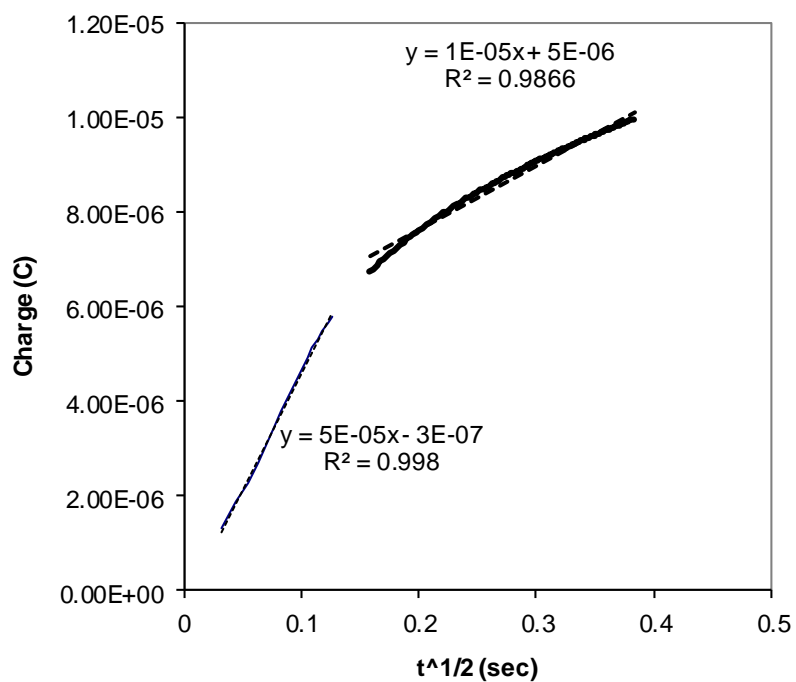
Figure 2.4: Cyclic voltammogram of ubiquinone-10. Carried out in bulk solution under mobile phase conditions (59/39/2 % (v/v), MeOH/ACN/glacial acetic acid with 55 mM sodium acetate), scan rate 100 mV/s. Ubiquinone-10 prepared in mobile at a concentration of 1.0 mM. Chemical reaction indicating short lived radicals formed while converting from the quinone and the quinol.

The reaction shown in Figure 2.4 along with the CV of ubiquinone shows a  $2e^-$ ,  $2H^+$  transfer for this reaction proceeding via a short lived intermediate radical. A chronocoulometry experiment was conducted under the same conditions as that of the CV, in order to further assess the chemical reaction. By plotting the  $t^{1/2}$  as a function of charge, the number of electrons transferred in the reaction can be determined as well as the rate at which the reactions occur. Figure 2.5 shows the plot for the reaction rates obtained for the oxidation and reduction of ubiquinone-10. From Figure 2.5, it is apparent that for both the oxidation and reduction of ubiquinone-10 the two electrons are not removed simultaneously, but instead at two different rates indicated by the change in slopes, with the removal of the first occurring at a faster rate than that of the second. The same process was observed for the reduction. From this it was concluded that there is a brief intermediate step through the radical prior to the removal or addition of the second  $e^-$  or  $H^+$ , as indicated by the reaction scheme in Figure 2.4.

#### 2.3.1.2 Establishing Optimal Working Potentials using Hydrodynamic Amperometry

Detection potentials for both electrodes were determined from hydrodynamic voltamograms (HDV), as shown in Figure 2.6. HDV's were determined by making multiple injections of a 2  $\mu$ M standard of ubiquinone-10 or ubiquinol-10 and stepping the potential in 50 mV increments between injections from high to low. Peak heights were normalized, to the largest response in order to compare chromatograms for direct and indirect detection of ubiquinone-10 and ubiquinol-10.

a



b

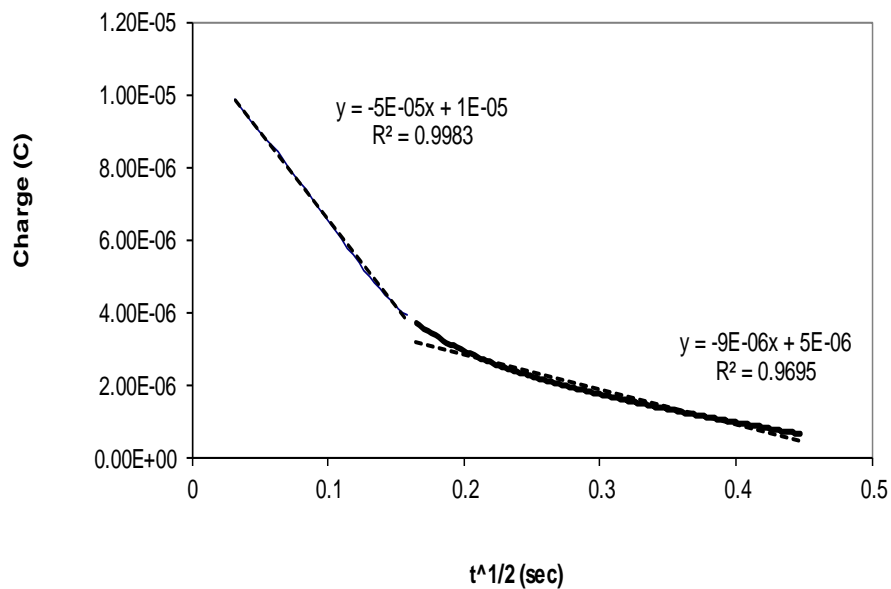


Figure 2.5: Electron transfer rates for ubiquinone-10 and ubiquinol-10. a) forward step, reduction of ubiquinone-10; b) reverse step, oxidation back to ubiquinone-10. Dashed lines indicated trend fit.

### 2.3.1.3 Series Dual Electrode Configuration

In the series configuration HDV's can be generated at the downstream electrode of the product generated at the upstream electrode. Initially, ubiquinol-10 was injected while the upstream electrode was held at +0.45 V and the downstream electrode had an applied potential of 0.0 V. For each subsequent injection of ubiquinol-10 the downstream potential was stepped down incrementally from 0.0 V to -0.50 V. Next, ubiquinone-10 was injected and the upstream electrode was held at -0.40 V, while the downstream electrode was again held at 0.0 V. Upon subsequent injections of ubiquinone-10 the downstream electrode was stepped 50 mV in the positive direction, until +0.50 V was reached. Based on the HDV, shown in Figure 2.6, detection potentials were established to be +0.45 V and -0.40 V. These potentials were chosen, because the largest analytical signal is obtained at these potentials while generating the least amount of noise.

In the series configuration selectivity is enhanced due to the ability to monitor chemically reversible processes at the downstream electrode. This is advantageous as chemically reversible redox couples, such as ubiquinone-10 and ubiquinol-10, can be easily distinguished at the downstream electrode from the chemically irreversible species, which only oxidize or reduce at the upstream electrode. This configuration was used to confirm the formation of ubiquinol-10 from ubiquinone-10 using the Jones reductor by comparing the current ratios at the peak and half wave potentials for a standard of ubiquinol-10 versus endogenous ubiquinol-10. The same experiment was performed, as mentioned above, using endogenous samples and standards to demonstrate the selectivity of this electrode configuration. Ubiquinone-10 was used as a control for this experiment. The current ratios determined for ubiquinol-10 ( $i_{+0.3/+0.45}$ ) and ubiquinone-10 ( $i_{-0.25/-0.4}$ ) standards and endogenous ubiquinol-10 and ubiquinone-10 were 0.77, 0.42 and 0.72, 0.47, respectively.

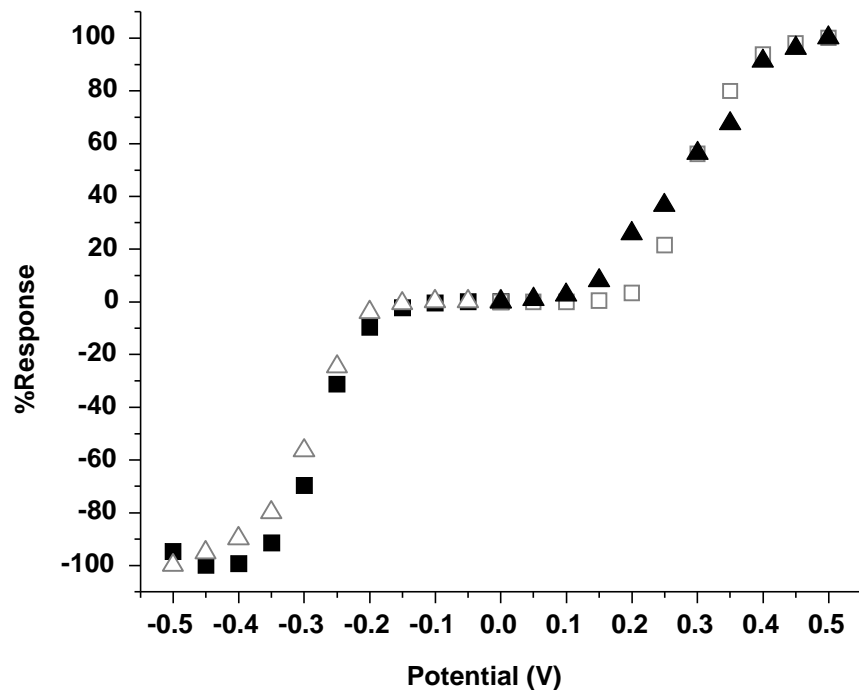


Figure 2.6: HDV of ubiquinone -10 and ubiquinol-10. Series-mode ubiquinone-10 ( □ ), series-mode ubiquinol-10 ( △ ), direct detection ubiquinone-10 ( ■ ), direct detection ubiquinol-10 ( ▲ ). Mobile phase: 59/39/2 % (v/v), MeOH/ACN/glacial acetic acid with 55 mM sodium acetate. Flow rate: 0.75 ml/min.

This shows that the Jones reductor produced only ubiquinol-10 and further demonstrates the selectivity of this electrode configuration. A representative chromatogram for the separation of ubiquinone-10 and ubiquinol-10, with the electrodes in series configuration, is shown in Figure 2.7. Good baseline resolution was obtained under these conditions, and both compounds were detected in less than 5 min, decreasing retention times previously reported<sup>22, 29, 32, 33, 40</sup>

#### 2.3.1.4 Parallel Dual Electrode Configuration

Although the series electrode configuration improves selectivity, when analyzing complex biological samples, the selectivity and LOD of the method can be improved using the electrodes in the parallel configuration. For injections with ubiquinol-10 an initial voltage of 0.0 V was applied to the electrode and incrementally increased to +0.5 V. Similarly, for ubiquinone-10 injections began at 0.0 V and the voltage was incrementally decreased to -0.5 V. Detection potentials for the oxidation and reduction electrodes were determined to be +0.45 V and -0.4 V, respectively.

In this configuration two different potentials can be monitored for simultaneous detection of reducible and oxidizable species directly. Figure 2.8 shows the response for ubiquinone-10 and ubiquinol-10 versus the response of the sample matrix with the electrodes in a parallel configuration. In this configuration the analyte of interest is seen at both the oxidation and reduction electrodes simultaneously; therefore, no subsequent re-oxidation or reduction can occur, as shown in Figure 2.8a and 2.8b. In addition, in this configuration qualitative information can be easily obtained.

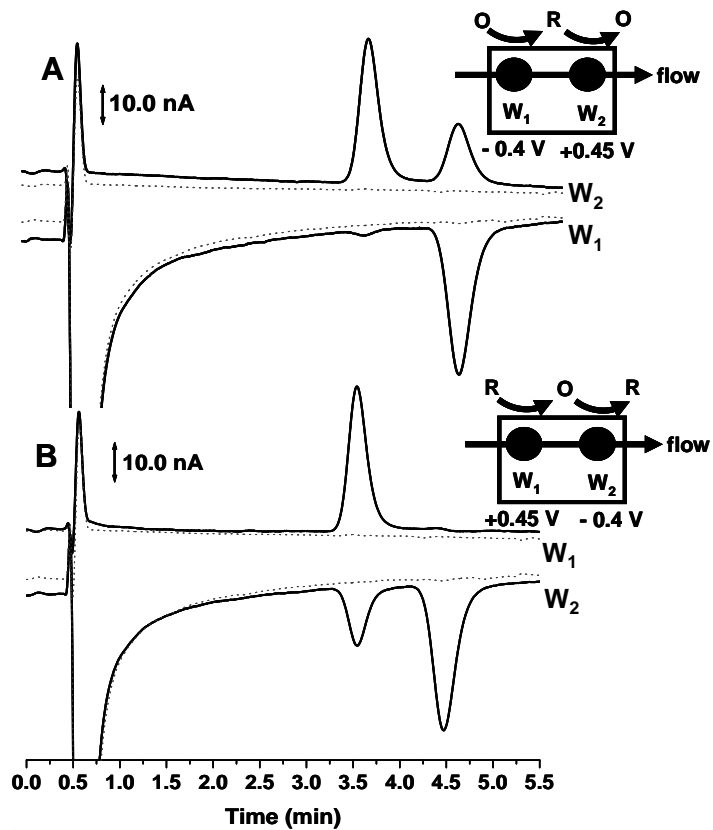


Figure 2.7: Response for ubiquinone-10 and ubiquinol-10 in series configuration. A) Injection of ubiquinone-10. B) Injection of ubiquinol-10. Mobile phase 59/39/2 % (v/v), MeOH/ACN /glacial acetic acid with 55 mM sodium acetate. Flow rate: 0.75 ml/min. Injection: 25  $\mu\text{l}$ , 5  $\mu\text{l}$  sample loop.

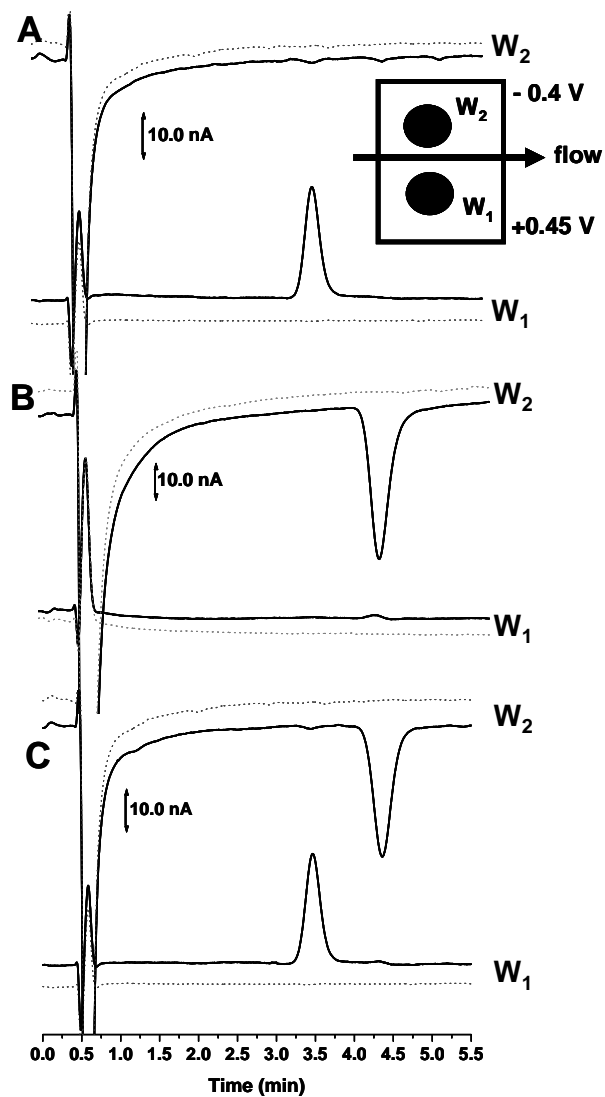


Figure 2.8: Response of ubiquinone-10 and ubiquinol -10 using parallel configuration. A) injection of ubiquinone-10. B) injection of ubiquinone-10. C) injection of both ubiquinone-10 and ubiquinol-10. Conditions were the same as reported in Figure 2.6

For the purpose of this method, this configuration qualitatively and simultaneously shows the redox state of endogenous Co-Q<sub>10</sub>, as shown in Figure 2.8c, with increased selectivity compared to previously published methods. Based on this reasoning the electrodes were used in the parallel configuration for further method validation.

### 2.2.3 Validation of Analytical Method

The calibration curves were linear over two orders of magnitude (0.05-2.0  $\mu\text{M}$ ), with correlation coefficients of 0.997-1. The limit of detection (LOD) ( $S/N = 3$ ) for this method were determined to be 5.0 nM with a RSD of 8% and 11% for ubiquinone-10 and ubiquinol-10, respectively. The limit of quantification (LOQ,  $S/N = 10$ ) was subsequently determined to be 20 nM with a RSD of 5.4% and 2.2% for ubiquinone-10 and ubiquinol-10, respectively. In addition, the intra-day and inter-day reproducibility of the method was determined by comparing peak areas and deviation in sensitivity. This was achieved by analyzing several different standard concentrations initially, followed by successive injections ( $n = 10$ ) of two standard concentrations, which were not included in the initial calibration curve. The analysis of the peak areas was then performed and it was determined that the sensitivity of the method was consistent over the course of a day, with RSD's of 7.8% and 6.0% for 0.05  $\mu\text{M}$  and 1.6% and 2.2% for 1.0  $\mu\text{M}$  for both ubiquinone-10 and ubiquinol-10, respectively. Intra-day reproducibility was determined using the same method of analysis. The deviation in method sensitivity or slope of the calibration curve was determined to be  $\pm 6\%$  and  $\pm 12\%$ , for ubiquinone-10 and ubiquinol-10, respectively. The larger deviation for ubiquinol-10 was attributed the reproducibility of the Jones reductor.

The stability of ubiquinol-10 in samples was determined over the course of a 24 hour period. Injections of the same standard concentration (1.0  $\mu\text{M}$ ) were performed every hour for 8 hours. Peak heights were compared to determine any relative changes in ubiquinol-10. From this analysis, it was determined that

there was no significant change in peak height over the course of 8 hours. The standard was then stored at -20°C overnight in the dark and the same standard was subsequently injected the following day. From this it was determined that after a 24 hour period there was significant loss in the response of ubiquinol-10 and the formation of ubiquinone-10 was observed. The loss in response of ubiquinol-10 was determined to be a result of time and not due to any freeze/thaw cycle that occurred. This suggests that loss was due to the oxidation of ubiquinol-10; therefore, standards were prepared fresh daily.

#### 2.2.3.2 Plasma Sample Analysis

Figure 2.9 shows a representative chromatogram from a plasma extraction. The method shows good selectivity for ubiquinone-10 and ubiquinol-10. In order to quantify ubiquinone-10 and ubiquinol-10 in plasma samples a calibration curve was generated. Standards of ubiquinone-10 and ubiquinol-10 were prepared as previously discussed. Standard concentrations ranged from 0.1- 2.0  $\mu\text{M}$ , with  $n=3$  injections performed for each concentration. Good linearity was obtained over the desired concentration range ( $R^2 = 0.99$ ). The concentrations of ubiquinone-10 and ubiquinol-10, determined using the generated standard curves, were calculated to be 0.42  $\mu\text{M}$  and 0.45  $\mu\text{M}$ , with RSD's of 23% and 21% ( $n = 6$ ), respectively. Plasma concentrations reported previously range from 480 nM – 2.0  $\mu\text{M}$  for ubiquinol-10 and 16 nM- 900 nM for ubiquinone-10<sup>37</sup>. These values agree well with the concentrations reported for this analysis.

Previously, there has been concern about the stability of ubiquinol-10 during the extraction from plasma<sup>22</sup>. Tang *et al* concluded in a study that both the solvent used for the extraction as well as pre-column reduction were key in the recovery of ubiquinol-10 from various types of plasma; however there was no consistent trend within the data.

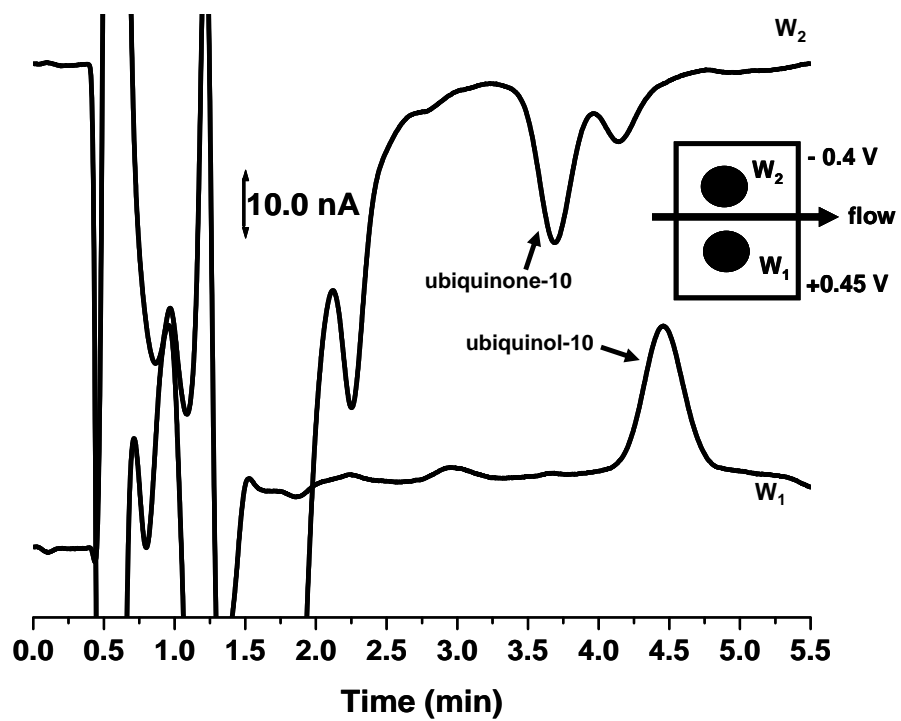


Figure 2.9: Extraction of ubiquinol-10 and ubiquinone-10 from pooled plasma. Chromatographic conditions were the same as reported in Figure 2.6.

In addition, several internal standards were tested with the optimized method, but were not included due to either elution within the void or poor capacity factors. Therefore, to validate the stability of ubiquinol-10 during extraction from plasma standard additions were performed. This was accomplished by spiking three different known concentrations of standards into separate aliquots of plasma. Table 2.1 summarizes the extraction efficiencies determined for each concentration. The deviation in values was attributed to reproducibility of the extraction. Basal concentrations were found by extrapolating the best fit line across the x-axis and were determined to be 0.51  $\mu\text{M}$  ( $\pm 14\%$ ) and 0.50  $\mu\text{M}$  ( $\pm 10\%$ ) for ubiquinone-10 and ubiquinol-10, respectively as shown in Figure 2.10. The standard additions were then compared ratiometrically to the concentrations determined from the standard curves. Based on this method of analysis, extraction efficiencies were determined to be 82% and 90% for ubiquinone-10 and ubiquinol-10, respectively. These values compare well with previously reported extraction efficiencies, specifically those reported for ubiquinol-10<sup>22</sup>. It was therefore concluded that no significant oxidation of ubiquinol-10 occurred during extraction.

<b>Spiked Concentration (nM)</b>	<b>Extraction Efficiency Ubiquinone-10</b>	<b>Extraction Efficiency Ubiquinol-10</b>
500	99.9% ± 4.3%	100% ± 11.6%
750	93.9% ± 7.1%	89.0% ± 8.0%
1000	87.8% ± 11.7%	85.9% ± 9.7%

n = 6 extractions/concentration

Table 2.1: Analysis of extraction efficiency of ubiquinone-10 and ubiquinol-10 from plasma

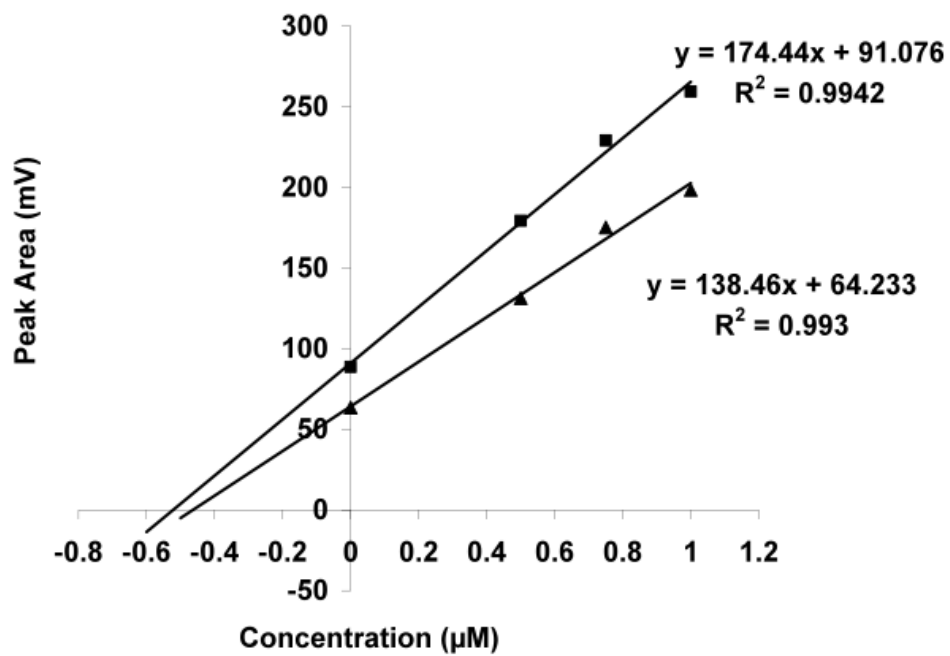


Figure 2.10: Determination of basal concentrations of ubiquinol-10 and ubiquinone-10 in pooled plasma by standard additions ( $n = 6$ ). Chromatographic conditions were the same as reported in Figure 2.6. Plasma samples were spiked to 0, 500, 750 and 1000 nM with ubiquinone-10 (■) and ubiquinol-10 (▲).

### 2.3 Conclusions

In conclusion, a robust and rapid analytical method with enhanced selectivity for the determination of ubiquinone-10 and ubiquinol-10 has been developed. This was achieved by using a dual glassy carbon electrode in a parallel electrode configuration. Total analysis times were improved based upon previously published methods, while maintaining good baseline resolution, peak efficiencies and method sensitivity for ubiquinone-10 and ubiquinol-10. These improvements allow for the determination of the redox status of ubiquinone-10 and ubiquinol-10, which will improve understanding of their role in maintaining tissue homeostasis as a result of an oxidative stress event.

## 2.4 References

1. Ames, B. N. S., Halliwell, B., Aruoma, M.K., , In *DNA and Free Radicals*. Ellis Horwood: West Sussex, England, 1993.
2. Klaunig, J. E.; Xu, Y.; Han, C.; Kamendulis, L. M.; Chen, J.; Heiser, C.; Gordon, M. S.; Mohler, E. R., III, The effect of tea consumption on oxidative stress in smokers and nonsmokers. *Proc. Soc. Exp. Biol. Med.* **1999**, *220* (Copyright (C) 2012 American Chemical Society (ACS). All Rights Reserved.), 249-254.
3. Kaneko, T.; Tahara, S.; Matsuo, M., Non-linear accumulation of 8-hydroxy-2'-deoxyguanosine, a marker of oxidized DNA damage, during aging. *Mutat. Res., DNAgging: Genet. Instab. Aging* **1996**, *316* (Copyright (C) 2012 American Chemical Society (ACS). All Rights Reserved.), 277-285.
4. Kasai, H., Analysis of a form of oxidative DNA damage, 8-hydroxy-2'-deoxyguanosine, as a marker of cellular oxidative stress during carcinogenesis. *Mutat. Res., Rev. Mutat. Res.* **1997**, *387* (Copyright (C) 2012 American Chemical Society (ACS). All Rights Reserved.), 147-163.
5. Tagesson, C., Kallberg, M., Leanderson, P., Determination of Urinary 8-Hydroxydeoxyguanosine by Coupled-Column High-Performance Liquid Chromatography with Electrochemical Detection: A Noninvasive Assay for In Vivo Oxidative DNA Damage in Humans. *Toxicology Methods* **1992**, *1* (4), 242-251.
6. Erhola, M.; Toyokuni, S.; Okada, K.; Tanaka, T.; Hiai, H.; Ochi, H.; Uchida, K.; Osawa, T.; Nieminen, M. M.; Alho, H.; Kellokumpu-Lehtinen, P., Biomarker evidence of DNA oxidation in lung cancer patients: association of urinary 8-hydroxy-2'-deoxyguanosine excretion with radiotherapy, chemotherapy, and response to treatment. *FEBS Lett.* **1997**, *409* (Copyright (C) 2012 American Chemical Society (ACS). All Rights Reserved.), 287-291.
7. Reiter, R. J., Oxidative damage in the central nervous system: protection by melatonin. *Prog. Neurobiol. (Oxford)* **1998**, *56* (Copyright (C) 2012 American Chemical Society (ACS). All Rights Reserved.), 359-384.
8. Koppal, T.; Drake, J.; Yatin, S.; Jordan, B.; Varadarajan, S.; Bettenhausen, L.; Butterfield, D. A., Peroxynitrite-induced alterations in synaptosomal membrane proteins: insight into oxidative stress in Alzheimer's disease. *J. Neurochem.* **1999**, *72* (Copyright (C) 2012 American Chemical Society (ACS). All Rights Reserved.), 310-317.
9. Spector, A., Oxidative stress-induced cataract: mechanism of action. *FASEB J.* **1995**, *9* (Copyright (C) 2012 American Chemical Society (ACS). All Rights Reserved.), 1173-82.
10. Muggli, R., *Free Radicals and Antioxidants in Nutrition*. Richelieu Press London, 1993.
11. Mechanick, J. I. In *Mitochondrial function in diabetes: pathophysiology and nutritional therapeutics*, CRC Press LLC: 2006; pp 221-263,, 1 plate.
12. Chew, G. T.; Watts, G. F., Coenzyme Q10 and diabetic endotheliopathy: oxidative stress and the 'recoupling hypothesis'. *QJM* **2004**, *97* (Copyright (C) 2012 U.S. National Library of Medicine.), 537-48.
13. Birnbaum, Y.; Hale, S. L.; Kloner, R. A., The effect of coenzyme Q10 on infarct size in a rabbit model of ischemia/reperfusion. *Cardiovasc. Res.* **1996**, *32* (Copyright (C) 2012 American Chemical Society (ACS). All Rights Reserved.), 861-868.
14. Lakomkin, V. L.; Konovalova, G. G.; Kalenikova, E. I.; Zabbarova, I. V.; Kaminnyi, A. I.; Tikhaze, A. K.; Lankin, V. Z.; Ruuge, E. K.; Kapelko, V. I., Changes in antioxidant status of myocardium during oxidative stress under the influence of coenzyme Q10. *Biochemistry (Moscow)* **2005**, *70* (Copyright (C) 2012 American Chemical Society (ACS). All Rights Reserved.), 79-84.
15. Kalenikova, E. I.; Gorodetskaya, E. A.; Kolokolchikova, E. G.; Shashurin, D. A.; Medvedev, O. S., Chronic administration of coenzyme Q10 limits postinfarct myocardial remodeling in rats. *Biochemistry (Moscow)* **2007**, *72* (Copyright (C) 2012 American Chemical Society (ACS). All Rights Reserved.), 332-338.

16. Lakomkin, V. L.; Konovalova, G. G.; Kalenikova, E. I.; Zabbarova, I. V.; Tikhaze, A. K.; Tsyplenkova, V. G.; Lankin, V. Z.; Ruuge, E. K.; Kapelko, V. I., Protection of Rat Myocardium by Coenzyme Q during Oxidative Stress Induced by Hydrogen Peroxide. *Biochemistry (Moscow, Russ. Fed.)* **2004**, *69* (Copyright (C) 2012 American Chemical Society (ACS). All Rights Reserved.), 520-526.
17. Dhanasekaran, M.; Ren, J., The emerging role of coenzyme Q-10 in aging, neurodegeneration, cardiovascular disease, cancer and diabetes mellitus. *Curr. Neurovasc. Res.* **2005**, *2* (Copyright (C) 2012 American Chemical Society (ACS). All Rights Reserved.), 447-459.
18. Whitman, G. J. R.; Niibori, K.; Yokoyama, H.; Crestanello, J. A.; Lingle, D. M.; Momeni, R., The mechanisms of coenzyme Q10 as therapy for myocardial ischemia reperfusion injury. *Mol. Aspects Med.* **1997**, *18* (Copyright (C) 2012 American Chemical Society (ACS). All Rights Reserved.), s195-s203.
19. Tarpey, M. M.; White, C. R.; Suarez, E.; Richardson, G.; Radi, R.; Freeman, B. A., Chemiluminescent detection of oxidants in vascular tissue: lucigenin but not coelenterazine enhances superoxide formation. *Circ. Res.* **1999**, *84* (Copyright (C) 2012 American Chemical Society (ACS). All Rights Reserved.), 1203-1211.
20. Beal, M. F., Mitochondrial Dysfunction and Oxidative Damage in Alzheimer's and Parkinson's Diseases and Coenzyme Q10 as a Potential Treatment. *J. Bioenerg. Biomembr.* **2004**, *36* (Copyright (C) 2012 American Chemical Society (ACS). All Rights Reserved.), 381-386.
21. Hoppe, U.; Bergemann, J.; Diembeck, W.; Ennen, J.; Gohla, S.; Harris, I.; Jacob, J.; Kielholz, J.; Mei, W.; Pollet, D.; Schachtschabel, D.; Sauermann, G.; Schreiner, V.; Stab, F.; Steckel, F., Coenzyme Q10, a cutaneous antioxidant and energizer. *BioFactors* **1999**, *9* (Copyright (C) 2012 American Chemical Society (ACS). All Rights Reserved.), 371-378.
22. Tang, P. H.; Miles, M. V.; DeGrauw, A.; Hershey, A.; Pesce, A., HPLC analysis of reduced and oxidized coenzyme Q10 in human plasma. *Clin. Chem. (Washington, DC, U. S.)* **2001**, *47* (Copyright (C) 2012 American Chemical Society (ACS). All Rights Reserved.), 256-265.
23. Tang, P. H.; de, G. T., Redox cycling of coenzyme Q9 as a new measure of plasma reducing power. *Clin. Chem. (Washington, DC, U. S.)* **2004**, *50* (Copyright (C) 2012 American Chemical Society (ACS). All Rights Reserved.), 1930-1932.
24. Andersson, S., Determination of coenzyme Q by non-aqueous reversed-phase liquid chromatography. *J. Chromatogr.* **1992**, *606* (Copyright (C) 2012 American Chemical Society (ACS). All Rights Reserved.), 272-6.
25. Finckh, B.; Kontush, A.; Commentz, J.; Hubner, C.; Burdelski, M.; Kohlschutter, A., High-performance liquid chromatography-coulometric electrochemical detection of ubiquinol 10, ubiquinone 10, carotenoids, and tocopherols in neonatal plasma. *Methods Enzymol.* **1999**, *299* (Copyright (C) 2012 American Chemical Society (ACS). All Rights Reserved.), 341-348.
26. Tang, P. H.; Miles, M. V.; Miles, L.; Quinlan, J.; Wong, B.; Wensch, A.; Bove, K., Measurement of reduced and oxidized coenzyme Q9 and coenzyme Q10 levels in mouse tissues by HPLC with coulometric detection. *Clin. Chim. Acta* **2004**, *341* (Copyright (C) 2012 American Chemical Society (ACS). All Rights Reserved.), 173-184.
27. Gay, C. A.; Stocker, R., Simultaneous determination of coenzyme Q10, cholesterol, and major cholesterylestes in human blood plasma. *Methods Enzymol.* **2004**, *378* (Copyright (C) 2012 American Chemical Society (ACS). All Rights Reserved.), 162-169.
28. Rousseau, G.; Varin, F., Determination of ubiquinone-9 and 10 levels in rat tissues and blood by high-performance liquid chromatography with ultraviolet detection. *J. Chromatogr. Sci.* **1998**, *36* (Copyright (C) 2012 American Chemical Society (ACS). All Rights Reserved.), 247-252.
29. Finckh, B.; Kontush, A.; Commentz, J.; Huebner, C.; Burdelski, M.; Kohlschuetter, A., Monitoring of ubiquinol-10, ubiquinone-10, carotenoids, and tocopherols in neonatal plasma microsamples using high-performance liquid chromatography with coulometric electrochemical detection. *Anal. Biochem.* **1995**, *232* (Copyright (C) 2012 American Chemical Society (ACS). All Rights Reserved.), 210-16.

30. Battino, M.; Leone, L.; Bompadre, S., High-performance liquid chromatography-EC assay of mitochondrial coenzyme Q9, coenzyme Q9H2, coenzyme Q10, coenzyme Q10H2, and vitamin E with a simplified on-line solid-phase extraction. *Methods Enzymol.* **2004**, *378* (Copyright (C) 2012 American Chemical Society (ACS). All Rights Reserved.), 156-162.
31. Edlund, P. O., Determination of coenzyme Q10,  $\alpha$ -tocopherol and cholesterol in biological samples by coupled-column liquid chromatography with coulometric and ultraviolet detection. *J. Chromatogr., Biomed. Appl.* **1988**, *425* (Copyright (C) 2012 American Chemical Society (ACS). All Rights Reserved.), 87-97.
32. Leray, C.; Andriamampandry, M. D.; Freund, M.; Gachet, C.; Cazenave, J.-P., Simultaneous determination of homologues of vitamin E and coenzyme Q and products of  $\alpha$ -tocopherol oxidation. *J. Lipid Res.* **1998**, *39* (Copyright (C) 2012 American Chemical Society (ACS). All Rights Reserved.), 2099-2105.
33. Menke, T.; Niklowitz, P.; Adam, S.; Weber, M.; Schluter, B.; Andler, W., Simultaneous Detection of Ubiquinol-10, Ubiquinone-10, and Tocopherols in Human Plasma Microsamples and Macrosamples as a Marker of Oxidative Damage in Neonates and Infants. *Anal. Biochem.* **2000**, *282* (Copyright (C) 2012 American Chemical Society (ACS). All Rights Reserved.), 209-217.
34. Podda, M.; Weber, C.; Traber, M. G.; Milbradt, R.; Packer, L., Sensitive high-performance liquid chromatography techniques for simultaneous determination of tocopherols, tocotrienols, ubiquinols, and ubiquinones in biological samples. *Methods Enzymol.* **1999**, *299* (Copyright (C) 2012 American Chemical Society (ACS). All Rights Reserved.), 330-341.
35. Yamamoto, Y.; Yamashita, S., Ubiquinol/ubiquinone ratio as a marker of oxidative stress. *Methods Mol. Biol. (Totowa, NJ, U. S.)* **2002**, *186* (Copyright (C) 2012 American Chemical Society (ACS). All Rights Reserved.), 241-246.
36. Yamashita, S.; Yamamoto, Y., Simultaneous detection of ubiquinol and ubiquinone in human plasma as a marker of oxidative stress. *Anal. Biochem.* **1997**, *250* (Copyright (C) 2012 American Chemical Society (ACS). All Rights Reserved.), 66-73.
37. Steele Paul, E.; Tang Peter, H.; DeGrauw Antonius, J.; Miles Michael, V., Clinical laboratory monitoring of coenzyme Q10 use in neurologic and muscular diseases. *American journal of clinical pathology* **2004**, *121 Suppl*, S113-20.
38. Kissinger, P. T., Heineman, W.R., *Laboratory Techniques in Electroanalytical Chemistry, 2nd Ed.* Marcel Dekker, Inc. : New York, 1996.
39. Roston, D. A.; Shoup, R. E.; Kissinger, P. T., Liquid chromatography/electrochemistry: thin-layer multiple electrode detection. *Anal. Chem.* **1982**, *54* (Copyright (C) 2012 American Chemical Society (ACS). All Rights Reserved.), 1417A-1418A, 1422A, 1424A, 1428A, 1430A, 1432A, 1434A.
40. Galinier, A.; Carriere, A.; Fernandez, Y.; Bessac, A. M.; Caspar-Bauguil, S.; Periquet, B.; Comtat, M.; Thouvenot, J. P.; Casteilla, L., Biological validation of coenzyme Q redox state by HPLC-EC measurement: Relationship between coenzyme Q redox state and coenzyme Q content in rat tissues. *FEBS Lett.* **2004**, *578* (Copyright (C) 2012 American Chemical Society (ACS). All Rights Reserved.), 53-57.

## Chapter 3: Development of a Parallel Dual Electrode for Capillary Electrophoresis

### 3.0 Background and Significance

A parallel-opposed dual-electrode configuration for CE as shown in Chapter 1 is desirable due to the potential for redox cycling resulting in signal enhancement, as well as improved LOD. While this configuration has been implemented in LC systems, flow rates were too fast ( $\geq 1.0$  ml/min) to allow for cycling of species between two electrodes. Capillary electrophoresis (CE) involves the electrophoretic mobility of an analyte(s) within an electric field, resulting in slower velocities across the electrode surface, potentially resulting in redox cycling. CE has commonly been coupled to UV (CE-UV) and fluorescence (CE-LIF) detectors, with limits of detection (LOD) in the low micromolar range ( $\sim 0.1 \mu\text{M}$ ) and low nanomolar range ( $\sim 5$  nM), respectively. Derivatizations for key neurotransmitters, such as dopamine have rapid degradation times making quantification of such analytes difficult, leading to inaccuracies when reporting cellular processes. Several important neurotransmitters, along with many other biological compounds are inherently electroactive, making electrochemical detection coupled to CE (CE-EC) an attractive alternative to CE-LIF. Additionally, subnanomolar LOD's comparable to CE-LIF can be achieved at a fraction of the cost<sup>1,2</sup>. Integration is relatively easy and lends itself well to miniaturization. Development of a parallel-opposed configuration for CE could improve LOD's over previously published dual electrode configurations that employed series configurations, as well as reports where only single electrodes were used (refs). Furthermore, excellent discernment in biological matrices is easily achieved using working potentials selective for the analytes of interest. In addition, large linear dynamic ranges can also be attained with EC detection<sup>3,4</sup>.

### 3.1 Introduction

#### 3.1.1 Dual-Electrode Detection

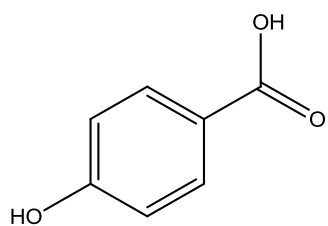
Although the previously described detection schemes adequately interface CE with EC detection, the use of dual-electrode detection for CE can improve the selectivity and sensitivity compared to single electrode detection. Initial application of a dual-electrode for CE was described for the detection of cysteine and cystine<sup>5</sup>. Lin *et al.* utilized a series configuration with the reduction electrode placed upstream from the oxidation electrode in an end-column format, LOD's were reported to be 5  $\mu\text{M}$ . Zhong and Lunte reported a series dual-Au/Hg electrode in which a tubular electrode was constructed and placed upstream from a macro disk electrode aligned with the outlet of the capillary<sup>6</sup>. The detection limit for this system was determined to be 0.5  $\mu\text{M}$ . The improvement in LOD's can be in-part explained by the larger surface areas ( $125 \mu\text{m}^2$ ) that were employed, which improved the amount of analyte detected at the downstream electrode. Holland and Lunte demonstrated another integrated approach using Pt wire electrodes<sup>7</sup>. In this system, one electrode was inserted into the separation capillary while the other was placed across the capillary outlet, the configuration offered slight improvement to detection limits ( $\sim 1 \mu\text{M}$ ) previously reported by Zare *et al.*<sup>7</sup>. Chen *et al.* reported a parallel-opposed dual-electrode configuration in order to improve sensitivity over conventional CE-EC systems through redox-cycling. Using this configuration 12 nM detection limits were obtained<sup>8,9</sup>. Microchip systems have also employed dual electrode detection schemes, both in-capillary and end-capillary<sup>10-17</sup>. While these devices allow for rapid analysis (seconds time scale), improved temporal resolution and ease of integration into automated lab-on-a chip systems, they are plagued by diminished resolution and lower efficiencies, resulting in inferior detection limits ( $> 0.2 \mu\text{M}$ ) when compared to conventional CE systems that are decoupled.

### 3.1.2 Phenolic Acids

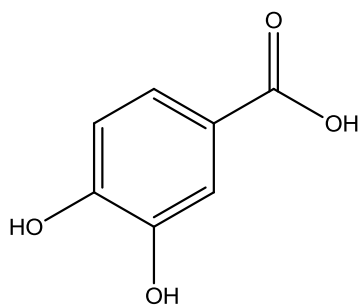
Several phenolic acids found in spirited beverages, derivatives of cinnamic acids and benzoic acids, were used to validate the dual-electrode presented in this chapter. Phenolic acids can be detected readily by UV detection, but the cinnamic acid and benzoic acid derivatives are also electroactive. Figure 3.1 shows the structures of some of the cinnamic and benzoic acid derivatives commonly found the spirited beverages, coffees, and teas<sup>3, 18-26</sup>. Each possesses hydroxyl functionalities, which are ortho, meta, or para to the carboxylic acid. 3,4-dihydroxybenzoic acid has two hydroxyl groups para and meta to the carboxylic acid. The hydroxyl groups undergo a  $2e^-$  reduction forming stable quinones, which can then be reversibly oxidized via a  $2H^+$  transfer. Conversely, 4-hydroxybenzoic acid does not form a stable quinone and instead forms a highly reactive radical, limiting the reversible oxidation-reduction obtained with 3,4-dihydroxybenzoic acid. In using these phenolic acids all potential electrochemistry's that could be encountered in any system could be assessed in order to determine the utility of the proposed dual-electrode.

### 3.1.3 Aims of Research

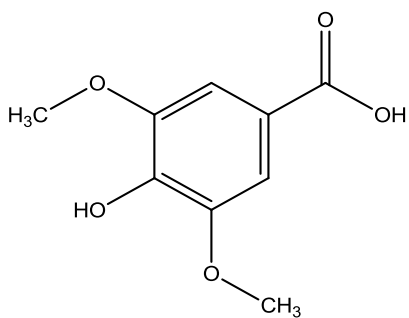
The purpose of this research was to develop an analytical detection scheme that employed a dual-parallel detection configuration that could easily be coupled to CE. Using this detection scheme issues such as diminished selectivity in complex biological samples can be improved (over conventional single electrode detection schemes), while also enhancing sensitivity.



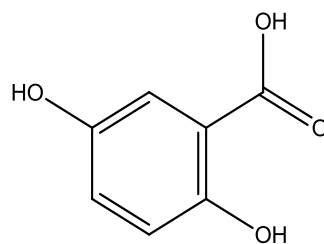
**3,4-dihydroxybenzoic acid**



**4-HBA**



**syringic acid**



**gentisic acid**

Figure 3.1: Structures of phenolic acids used to assess the parallel dual-electrode

This dual-electrode design allows for two different detection modes to be used: a redox cycling mode and a dual-potential mode. The redox cycling mode was used to enhance sensitivity and improve LOD's compared to a single working electrode. Additionally, the dual-potential mode was used to selectively identify several different phenolic acids in whiskey samples. Using this mode migration times in conjunction with current ratios were used as an orthogonal means to confirm peak identity. Furthermore, the redox cycling mode was used to confirm peak identity based on the chemical reversibility of the phenolic acids assessed.

## 3.2 Methods

### 3.2.1 Chemicals and Reagents

Isopropanol, methanol, hydrofluoric acid, hydrochloric acid, and sodium hydroxide were obtained from Fisher Scientific (Pittsburgh, PA, USA). Sodium bicarbonate, sodium tetraborate decahydrate (Borax), tetradecyltrimethylammonium bromide (TTAB), 3,4-dihydroxybenzoic acid (3,4-DHBA), 4-hydroxybenzoic acid (4-HBA), syringic acid (SA), vanillic acid (VA) and gentisic acid (GA) were purchased from Sigma-Aldrich (St. Louis, MO, USA). All chemicals were reagent grade and used as received.

### 3.2.2 Instrumentation

#### 3.2.2.1 Capillary Electrophoresis

Separations in capillary electrophoresis are based on charge-to-size ratio, the larger the discrepancy regarding the ratio the better the separation. In comparison to separations with HPLC there is no multiple paths term. Instead there is only a single term governing band broadening, diffusion. Perhaps most importantly the sample volumes and buffer volumes required for analysis are a fraction of what is required for an LC system.

Separations are carried out using fused silica capillary, filled with an aqueous buffer solution. A potential is applied across the capillary containing buffer via two electrodes, one at each end of the capillary, as shown in Figure 3.2. The walls of the capillary are lined with silanol groups which become deprotonated above pH 2. An electrical double-layer forms along the wall of the capillary with cations from the aqueous buffer forming a charged layer along the negatively charged silanol groups. A more diffuse layer of charge extends out into the bulk solution with the ions moving towards either end of the capillary (i.e. the anions move towards the anode, while the cations move towards the cathode). The solvated ions migrating towards the cathode in this case, create a bulk flow. The bulk flow or electroosmotic flow (EOF) moves at a significantly faster rate than the solvated ions resulting in net flow in one direction<sup>27</sup>.

The mobility of a particle within the field is defined as  $\mu$  and is proportional to the charge ( $q$ ) on the particle and inversely proportional to the viscosity of the buffer ( $\eta$ ) and Stokes radius ( $r$ ) as shown in equation 1.

$$\mu = \frac{q}{6\pi\eta r} \quad (1)$$

As stated earlier the separation is based on a charge-to-size ratio as ions migrate in the applied electric field. The electric field velocity ( $v$ ) of an analyte is based on the field strength ( $E$ ) and the analytes inherent electrophoretic mobility ( $\mu_e$ ), as well as the mobility the EOF ( $\mu_{EOF}$ ) equation 2 shows the mathematical relationship for these terms.

$$v = (\mu_e + \mu_{EOF})E \quad (2)$$

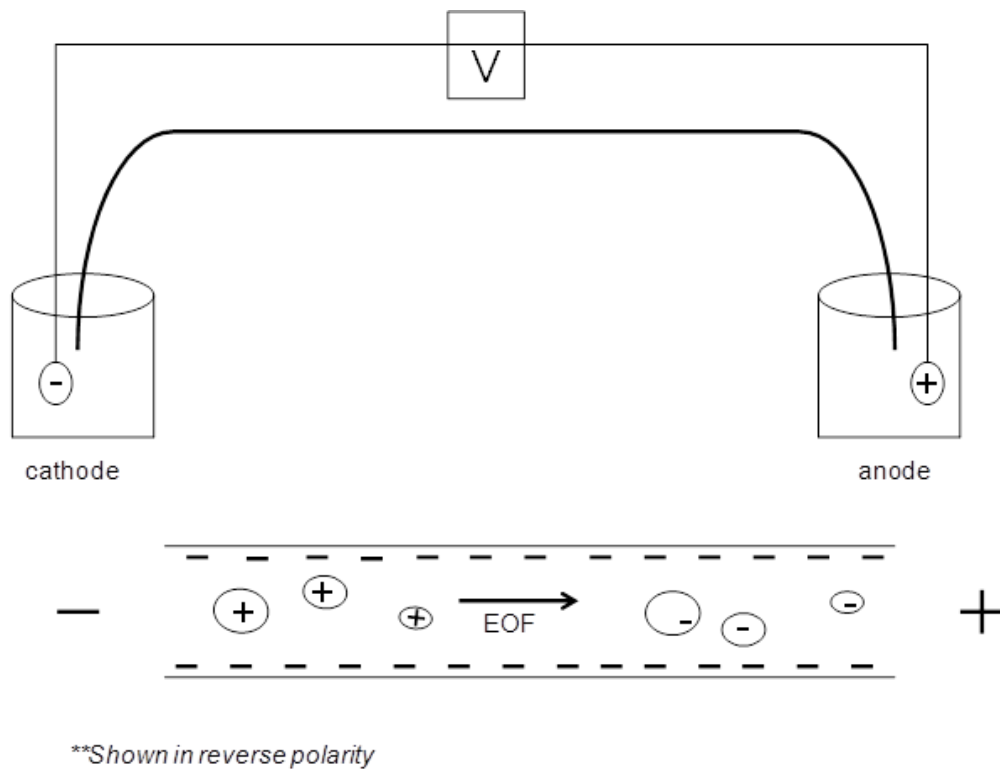


Figure 3.2: Separation of ions using capillary electrophoresis

The apparent mobility,  $\mu_{app}$ , is a function of particle charge and inversely proportional to frictional forces and electrical forces acting upon the particle. The electrical force is a function of the charge on the particle and the  $E$  (which is the applied voltage divided by the length of the capillary). The frictional force is a function of  $\eta$ ,  $r$  and  $v$ . During electrophoresis these forces are equal in magnitude, but are opposite in direction<sup>27</sup>. The second term in equation 2, is  $\mu_{EOF}$ . This term is proportional to the zeta potential ( $\zeta$ ) divided by  $\eta$ . The  $\zeta$  describes the charge on the capillary walls or the thickness of the double layer that is formed. Based on the deprotonation of the silanol groups along the capillary walls being pH dependent this should lead to the conclusion that the relative strength of the EOF is a function of pH<sup>27</sup>. At low or acidic pH  $>3$  the silanol groups will not be deprotonated, diminishing charge interactions with the buffer and any resulting separation is due completely to the  $\mu_{app}$ . Conversely at basic pH, the silanol groups are completely deprotonated resulting in strong charge-charge interactions, consequently increasing the mobility of the EOF. If analytes are stable at higher pH these conditions are preferable than lower pH because migration times are shorter with generally less diffusion or dispersion occurring.

Molecular diffusion is the primary contributor to band broadening in CE, which occurs as the analyte traverses along the length of the capillary (considering a buffer system with no added modifiers)<sup>27</sup>. Unlike LC systems there are no pumps creating parabolic flow, instead the sample is introduced to the capillary via hydrodynamic injection (pressure) or electrokinetic injection (voltage is used to drive the sample onto the capillary). Either of these injections results in a short plug of sample being injected onto the capillary. The “plug” is again pulled along by the EOF resulting in minimization of molecular dispersion. The peak efficiencies are therefore a result of the  $\mu_{app}$ ,  $E$ , the voltage applied ( $V$ ) and diffusion ( $D$ ), as shown in equation 3.

Additionally, diffusion in CE is further minimized, when compared to LC systems, by integration of on-capillary detection schemes. The polyamide coating of the fused silica can be easily flame etched, so no diffraction of light will occur at the interface of the capillary. The on-capillary detection that is possible with CE also eliminates the need for additional interfaces between the column and the detector, further minimizing dead volume<sup>27</sup>.

Lastly, another issue encountered is Joule heating. This is a result of the energy or heat produced from the applied voltage not effectively being dissipated within the capillary. If too much heat is produced within the capillary the result is convection, which is also correlated with band broadening. Joule heating can be avoided by determining the range over which the current produced from the applied voltage is linear. This effect is more pronounced in capillaries with larger inner diameters and shorter lengths, as the E is high and the resistance is low. Capillaries with longer lengths (<70 cm) and smaller inner diameters (>25  $\mu\text{m}$ ) have higher resistance more effectively dissipating the separation current over the total length of the capillary.

### 3.2.2.2 Initial Approaches to Integration of Dual-Electrode Detection with CE

#### 3.2.2.2.1 Cellulose Acetate Decoupler

Osborn and Lunte reported the use of a cellulose acetate decoupler as a way to couple CE with electrochemical detection<sup>28</sup>. Figure 3.3 illustrates the design of the cellulose acetate decoupler. In order to effectively shield the high voltage used to drive the separation in CE, laser ablation was used to create holes in the capillary.

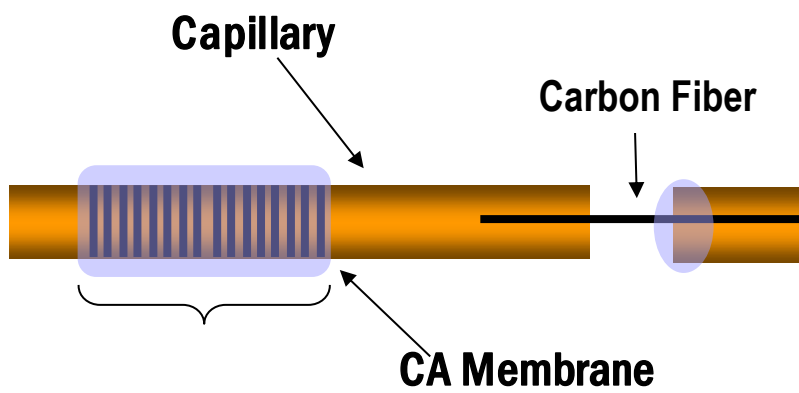


Figure 3.3: Cellulose acetate decoupler, based on Osbourn and Lunte's design, with single carbon fiber inserted into the outlet of a capillary.

In order to properly decouple the separation voltage from the detector the holes created by the ablation process had to be deep enough to pierce the inner diameter of the capillary. Osbourn optimized the depth to be  $24\ \mu\text{m}^{29}$ . In addition, the surface area or length of the decoupler was also optimized, with a surface area of 24 holes or roughly 2-3 cm resulting in a sufficient distance over which the current from the separation could be effectively dissipated <sup>29</sup>. Through use and change in location of the laser, parameters had to be re-optimized in order to gain the same conditions initially outlined by Osbourn. Table 3.1 shows the initial parameters from Osbourn and the optimization of the new parameters, using the  $\text{CO}_2$  laser.

In addition to re-optimizing the laser conditions other issues were encountered with fabrication of the decoupler. Once the ablation step has been completed, cellulose acetate was used to cover the holes in order to minimize rapid exchange of analytes of interest with bulk solution. As reported previously by Osbourn and Lunte the optimum concentration of cellulose acetate was determined to be 6% w/w<sup>28</sup>. As frequent leaking through the decoupler was encountered several different concentrations of cellulose acetate were assessed for use ranging from 3% - 10% w/w. It was also hypothesized that a potential reason for issues with leaking through the decoupler could have been due to absorption of water by the polymer, not permitting proper curing. As a result anhydrous acetone was used in place of HPLC grade acetone; this made no difference in the working operation of the decoupler. Additionally, oven temperature and drying time were also investigated; however, Osbourn's parameters of  $90^\circ\text{C}$  for 1 hour still resulted in the complete evaporation of acetone and proper curing of the cellulose without over drying. Thus, the protocol outlined by Osbourn should be used with the adjusted laser parameters of 13 % power and 3% speed with 7-8 copies.

Laser Power (dpi)	Speed	Copies	Hole Depth ( $\mu\text{m}$ )	Distance between holes ( $\mu\text{m}$ )	Surface line width ( $\mu\text{m}$ )
7-8 % <sup>a</sup>	3.1% <sup>a</sup>	6-7 <sup>a</sup>	25 <sup>a</sup>	195 <sup>a</sup>	75 <sup>a</sup>
11%	3.1%	10	13	220	60
12%	3.1%	8	10	240	80
13%	3.1%	7	20	200	80
14%	3.1%	7	14	180	NA <sup>b</sup>
15%	3.1%	6	8	240	NA <sup>b</sup>
16%	3.1%	5	12	220	NA <sup>b</sup>

Table 3.1: Laser ablation parameters for cellulose acetate decoupler

a: parameters from Osbourn and Lunte

b: majority of holes destroyed

Figure 3.4 shows an electropherogram obtained using the optimized parameters described. A single electrode was used for simplification, during complications with the fabrication of the decoupler were trying to be determined. The noise measured at the detector was 2.0 pA and the relative peaks heights for hydroquinone (HQ), dompamine (DA) and dihydroxybenzoic acid (DHBA) were 45 pA, 15, and 50 pA, respectively. The noise was greater than that reported by Osbourn and Lunte and the estimated detection limit under the same buffer conditions as reported previously were 0.5 pA. After two days the separation current was varying significantly and it was determined that the cellulose membrane had ruptured. Due to the significant issues in fabrication reproducibility other alternatives for integrating EC with CE were explored. It should be noted that prolonged exposure of cellulose acetate to NaOH will weaken and rupture the decoupler membrane, but continued flushing of 0.1 M NaOH through decouplers found not to leak should be used until separation current stabilizes. This can sometimes take up to two weeks. Stabilization is achieved with periodic flushing of an hour to two hours of 0.1 M NaOH per day with intermittent flushing of buffer for 30 min to an hour between flushes with NaOH.

#### 3.2.2.2.2 Wireless Isolated Potentiostat and End Column Detection

Isolated potentiostats have been used in conjunction with microchip electrophoresis systems as a means to achieve on-column amperometric detection.<sup>30, 31</sup> Isolated potentiostats use the working electrode as a ground for the separation current, thus placing a bias across the electrode shifting half wave potentials. Field strengths are generally much higher in microchips due to the short channel lengths and high voltages required for separation making noise at the detection electrodes in the systems much higher, even in decoupled systems. In conventional CE systems capillary column lengths are significantly longer decreasing field strengths.

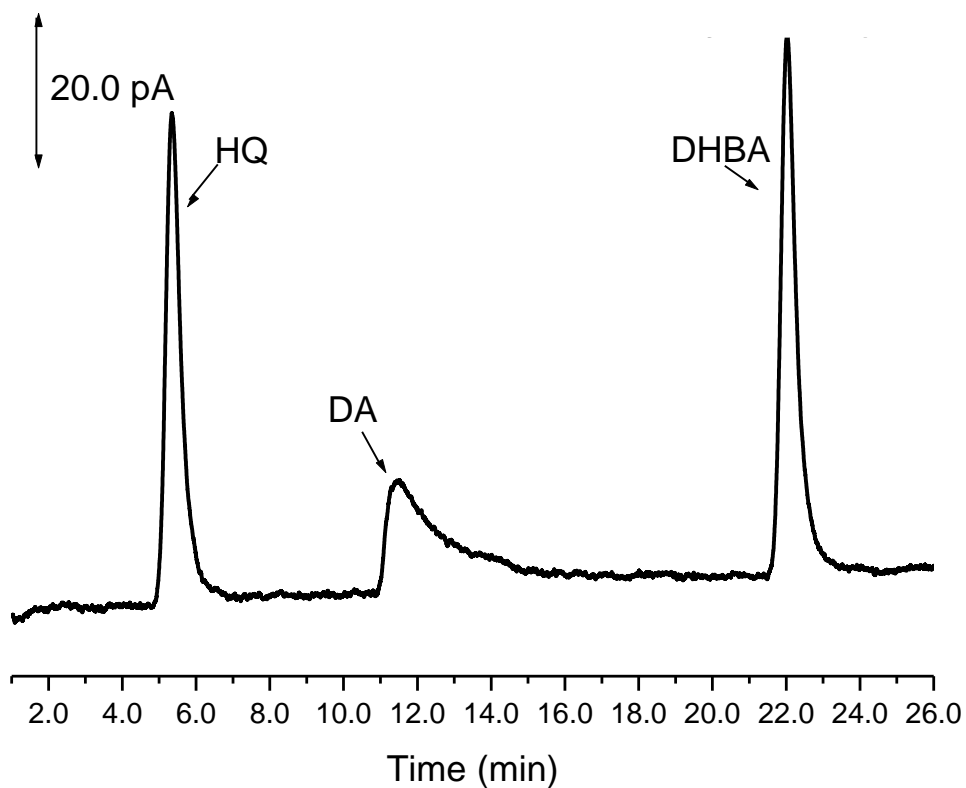


Figure 3.4: Separation of hydroquinone (HQ), dopamine (DA) and DHBA at single carbon fiber electrode using cellulose acetate decoupler. Standards prepared in 0.1 M HClO<sub>4</sub> diluted to 10 μM. Buffer: 10 mM Lithium Hydroxide, pH 6.1. Injection 3 psi, 1 sec. Separation voltage: +15 kV.

Therefore, integration of an isolated potentiostat with a conventional CE system would be possible while keeping noise low at the detector. Figure 3.5, shows an electropherogram obtained with the isolated potentiostat used by Hulvey et al.<sup>30</sup> From this electropherogram it was determined there was no significant improvement in noise at the detector compared to the noise obtained with the cellulose acetate decoupler. In addition, because the ultimate goal of the project was to integrate a dual-electrode with CE, modifications to the design of the isolated potentiostat would have been made in order to incorporate a second electrode, increasing cost.

Microchips are low cost and offer fast separations, on the order of seconds, making them desirable for portable analysis or lab-on-a-chip systems.<sup>30</sup> As discussed previously end-channel amperometric detection can also be used with microchips. As a means to simplify the fabrication issues incurred with the cellulose acetate decoupler, end-channel detection using a PDMS microchip with a Pt-electrode was assessed. The Pt-electrode was placed as close as possible to the end of the separation channel, at a distance of approximately 10-50  $\mu\text{m}$ . Using a PDMS chip with 3 cm length channel, separation was obtained for nitrate and glutathione in under 145 seconds. Although a fast analysis time was achieved detection limits were estimated to be roughly 30  $\mu\text{M}$ , making detection of low concentration electrochemically active biological compounds challenging. In addition, end-channel detection in microchip systems are often plagued with decreased resolution between analytes due to diffusion occurring within the detection reservoir.<sup>30</sup> Chips using serpentine patterns can be used to improve efficiencies and resolution; however fabrication becomes increasingly more complex. Therefore, conventional CE using HF etching, as reported by Ewing et al. was used as a simple, reproducible means to couple CE with EC detection.<sup>32, 33</sup> In addition, the etching time could be easily controlled to incorporate a depth and width that would accommodate the dual-electrode.

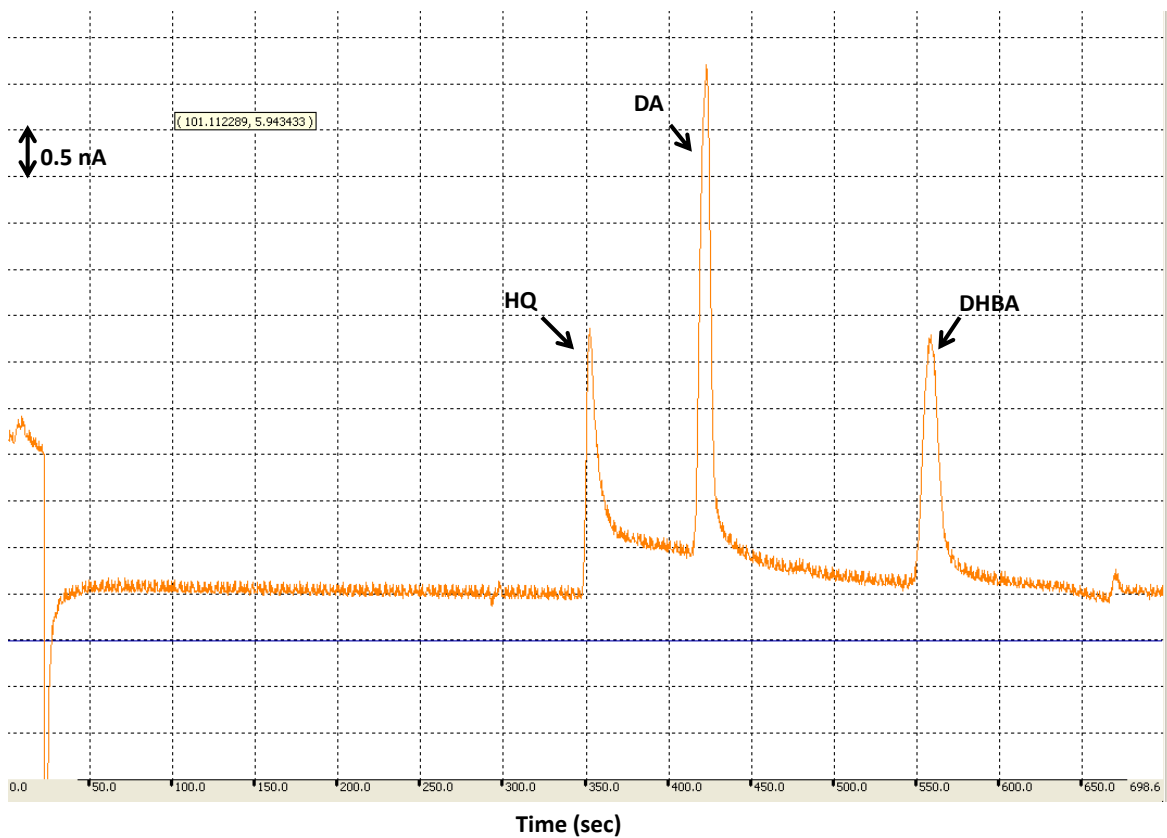


Figure 3.5: Separation of hydroquinone (HQ), dopamine (DA) and DHBA, using wireless isolated potentiostat. Capillary 50 $\mu$ m i.d., 70 cm length. Electrode bias: +0.011 V. Separation conditions same as Figure 3.4.

### 3.2.2.3 Instrumental Conditions

Electrophoresis was performed using a high voltage (0-30 kV) power supply (Spellman High Voltage, Hauppague, NY, USA). The cathodic end of the capillary was isolated in a Plexiglas box containing an interlock for the user safety. Fused silica capillaries (Polymicro Technologies, Phoenix, AZ, USA) 25  $\mu\text{m}$  i.d. and 80 cm in length were used for the separation of the phenolic acids. The capillary was placed into the EC cell which contained the BGE and served as the anodic reservoir (separations were run in reverse polarity).

In order for the dual-parallel electrode to be inserted into the separation capillary, the outlet of the capillary was modified using HF acid, a concept inspired by work described previously by Ewing et al.<sup>32</sup> Briefly, HF etching was done by submerging the outlet end of the capillary into 49% HF acid for a period of 100 min. This resulted in an opening ( $\sim 230 \mu\text{m}$ ) sufficient for insertion of the dual-parallel electrode. Furthermore, with this etch time a maximum insertion depth of  $\sim 660 \mu\text{m}$  was possible.

Prior to use electrodes were rinsed with MeOH and nanopure water. A platinum auxiliary electrode and a Ag/AgCl reference electrode (Bioanalytical Systems, West Lafayette, IN, USA) were used. The CF working electrodes were controlled by two LC-4C potentiostats (Bioanalytical Systems Inc., West Lafayette, IN, USA). All applied potentials reported were against a Ag/AgCl reference electrode. Data acquisition was performed by Chrom&Spec software (Ampersand International, Inc., Beachwood, OH, USA) at a frequency of 10 Hz per channel.

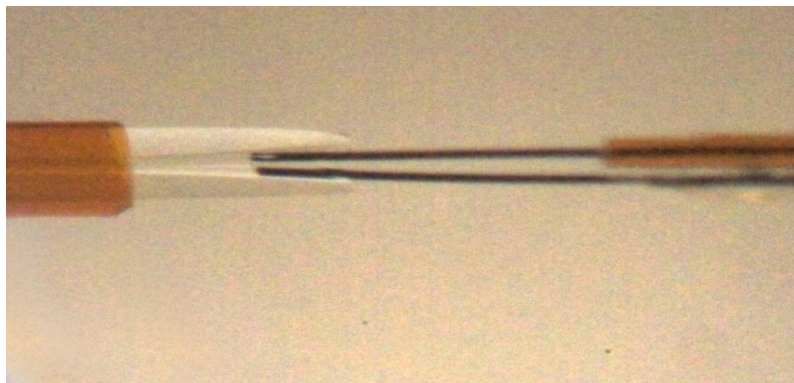
### 3.2.3 Dual-Electrode Fabrication

The dual-parallel electrode fabrication, proposed initially by Eric Crick was based on the design of the single carbon fiber (CF) electrode described previously by our lab.<sup>34, 35</sup> The modification to this design was the addition of the second 33  $\mu\text{m}$  CF to the outside of the original electrode as shown in Figure 3.6.

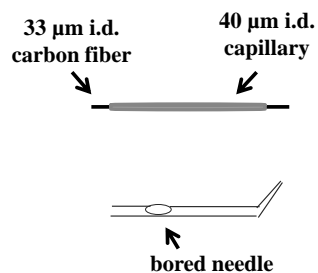
Briefly, two single 33  $\mu\text{m}$  CF (AVCO Specialty Materials, Lowell, MA, USA) electrodes were fabricated by threading the CF through fused silica capillary (105  $\mu\text{m}$  o.d., 40  $\mu\text{m}$  i.d.) leaving approximately 2 mm of CF exposed at both ends of the capillary. One of the fused silica capillary pieces was flame etched to remove the polyamide coating. This was done to ensure that the electrodes could be inserted into the opening of the capillary. One end of the exposed CF was inserted into a 23 gauge needle, which had an opening bored into the side of the needle. Each single CF was inserted into the needle until it reached the opening in the side of the needle. A drop of colloidal silver paste (Ted Pella, Redding, CA, USA) was then spread over the opening in the needle in order to make the electrical connection for the WE. The two single electrodes were then UV glued together making sure the tips of the electrodes were in alignment. The combined electrodes were then fed through a 1.5-2.0 cm length piece of fused silica capillary (658  $\mu\text{m}$  o.d, 537  $\mu\text{m}$  i.d.) for rigidity and support. Super glue was used to affix the electrodes to the support. Electrodes were trimmed using tissue scissors to a length of 1600  $\mu\text{m}$  ( $\pm$  12  $\mu\text{m}$ ) and an average width of 55  $\mu\text{m}$  ( $\pm$  9.0  $\mu\text{m}$ ).

#### 3.2.4 Experimental Conditions

All phenolic acid solutions were prepared using 1% (v/v) perchloric acid (0.1 M) in nanopure water (Millipore, Billerica, MA, USA). All samples were injected electrokinetically (-12 kV, 2 second) onto the capillary. It should be noted that without of the addition of acid to the sample matrix detection below 1.0  $\mu\text{M}$  was not possible. While the mechanism behind this separation is not well understood, the pH of the sample matrix was roughly 5 maintaining the deprotonation of the carboxylic acid, making electrokinetic injections possible.



**a**



**c**



**b**



**d**

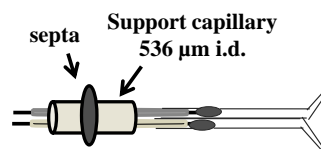


Figure 3.6: Fabrication of carbon fiber dual-electrode. a) carbon fiber inserted through 40 $\mu\text{m}$  i.d. capillary, bored 23 gauge needle. b) single carbon fiber electrode with colloidal silver paste over bored needle hole. c) two single carbon fiber electrodes joined together with UV glue. d) assembled dual electrode inserted through support capillary.

The BGE for this research was 75 mM sodium tetraborate, 0.5 mM TTAB, pH 8.4. The buffer was pH adjusted using concentrated HCl. Analytes were baseline resolved in less than 25 min using a separation voltage of -12 kV. The dual-electrodes were inserted a depth of 374  $\mu\text{m}$  ( $\pm 19 \mu\text{m}$ ). The oxidation and reduction potentials used to detect the phenolic acids were +800 mV and -200 mV versus Ag/AgCl, respectively.

Whiskey samples were diluted 1:1 with 1% (v/v) perchloric acid (0.1 M) and spiked with 250 nM 4-HBA standard. Prior to dilution the whiskey was filtered through 0.22  $\mu\text{m}$  sized Millex GP syringe filter. Samples were then injected directly onto the capillary for analysis. The separation voltage was -10 kV for the analysis of whiskey samples, in order to minimize co-migration of various phenolic acids contained in the sample. The sample was injected as previously described. In order to account for the variability in migration times, all elution times were normalized to the migration time of 4-HBA.

### 3.3 Results and Discussion

#### 3.3.1 Optimization of Working Potentials

A mixture of four phenolic acids, possessing different electrochemical properties (3,4-DHBA, 4-HBA, SA and GA) were used to evaluate the dual-electrode design. Both SA and GA are relatively easily oxidized while 3,4-DHBA and 4-HBA oxidize at higher potentials. While both GA and 3,4-DHBA exhibit chemically reversible electrochemistry, the oxidation of SA and 4-HBA are chemically irreversible. Electrophoretically assisted hydrodynamic voltammograms (HDV) were generated to optimize working electrode potentials for the oxidation and reduction of the analytes of interest and are shown in Figure 3.7. An oxidation potential of +800 mV versus Ag/AgCl was determined to be on the current plateau for all four compounds. A reduction potential of -200 mV versus Ag/AgCl was determined to be needed to reduce the oxidized form of GA and 3,4-DHBA.

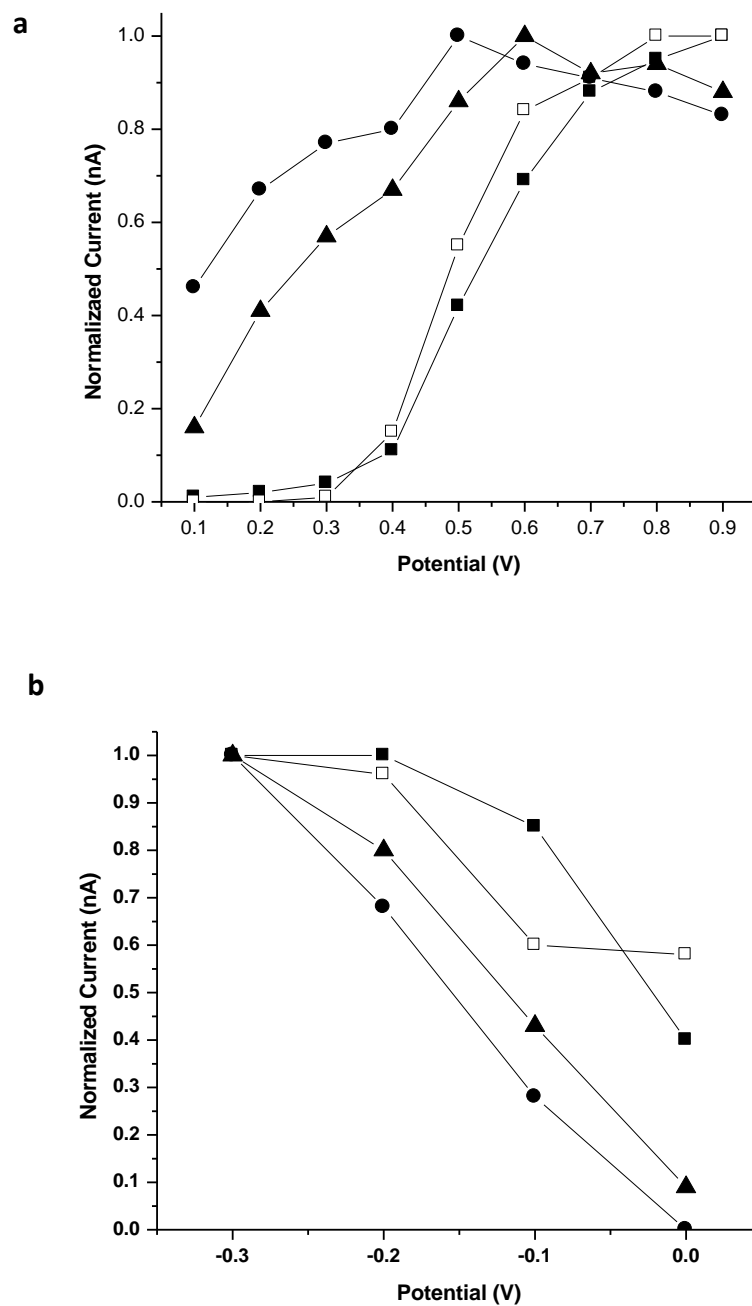


Figure 3.7: HDV's generated with reduced phenolic acids. Separation conditions: 75 mM tetraborate, 0.5 mM TTAB, pH 8.4, -12 kV. Injection: 2 sec, -10 kV. Standards diluted in 1.0 mM HClO<sub>4</sub>. a) WE<sub>1</sub> = +0.8 V, WE<sub>2</sub>, voltage varied from +0.9 V- +0.1 V. b) WE<sub>1</sub> = +0.8 V, WE<sub>2</sub>, voltage varied from -0.3 V- 0.0V. 3,4-DHBA (■), 4-HBA (□), SA (▲), GA (●). n = 1

It should be noted that the surfaces of carbon fibers vary from electrode to electrode; therefore, it was important to establish proper working potentials for each set of electrodes. Due to the variability between each set of electrodes error bars were omitted in Figure 3.7. Working potentials were established for each set of electrodes by assessing the peak heights for the current ratios at +500 mV/+800 mV and +200 mV/+800 mV. Responses that were within 0.1-0.2 of the initial HDV generate were determined to be acceptable. The same assessment was also used to establish the reduction potential for each set of electrodes.

### 3.3.2 Redox Cycling Mode

To test the ability of the parallel dual-electrode system for redox-cycling, one electrode ( $WE_1$ ) was held at +800 mV and the second electrode ( $WE_2$ ) was held at a potential of -200 mV versus Ag/AgCl. Figure 3.8 shows that with both electrodes on, responses were observed at both electrodes for the injected reduced phenolic acids. Liquid chromatography with dual electrode detection (LC-EC), using a series configuration elicits similar characteristics<sup>36</sup>. In the series configuration an analyte oxidized at  $WE_1$  can diffuse to  $WE_2$  where it is reduced. The mixture of phenolic acids was also injected without  $WE_1$  on and no response was observed at  $WE_2$  (data not shown). With only  $WE_1$  on, the response detected was smaller than in the dual-electrode mode. This demonstrated that complete redox cycling was occurring in the parallel dual-electrode, as shown in Figure 3.9. Based on the response observed in Figure 3.8, it was determined that the parallel dual-electrode configuration allows for multiple redox-cycling events to occur for a given analyte. This can be explained by determining the linear velocity of each analyte along the electrodes, as well as the residence times of each analyte spent between the electrodes. The linear velocity was determined by taking the length of the capillary (0.08 m) divided by the migration time, in seconds of an analyte.

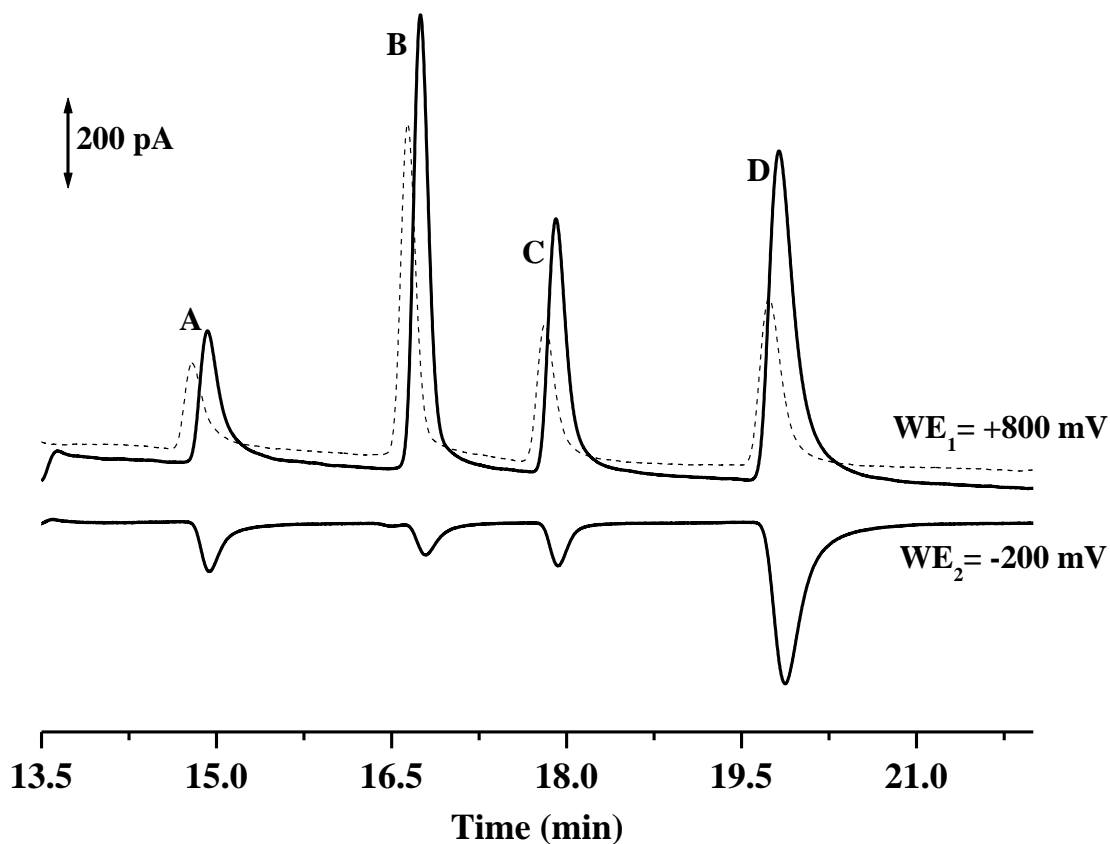


Figure 3.8: Parallel dual-electrode in redox-cycling mode. Response observed for reduced phenolic acids. Separation conditions: 75 mM tetraborate, 0.5 mM TTAB, pH 8.4, -12 kV. Injection: 2 sec, -10 kV. Standards diluted in 1.0 mM HClO<sub>4</sub>. A) 3,4-DHBA, B) 4-HBA, C) SA and D) GA. ( - - ) WE<sub>1</sub> on, ( — ) both WE<sub>1</sub> and WE<sub>2</sub> on.

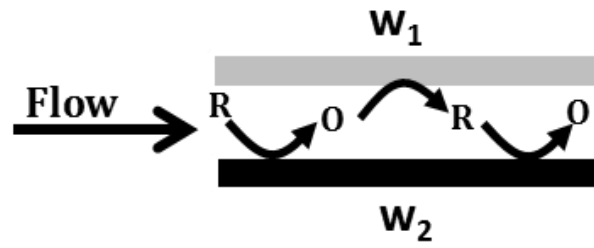


Figure 3.9: Mechanism for redox cycling with parallel dual-electrode.

Intuitively, velocity will decrease with increasing migration times, which should result in increased residence times for later migrating analytes. Residence times were then determined by taking the time an analyte spent on the electrode divided by the time it would take the analyte to cross from WE<sub>1</sub> to WE<sub>2</sub> one time. Based on these calculations and the observed increase in response when both electrodes are on, as shown in Figure 3.8, a signal enhancement can be calculated for each analyte by calculating the percent change in observed peak area using equation 4.

$$\text{—————} \quad (4)$$

Table 3.2 summarizes the data obtained using the parallel dual-electrode in redox cycling mode. Initially, the collection efficiencies were determined for each analyte in order to determine what percentage of analyte was being reduced at the second electrode. This was done by dividing the peak height at WE<sub>2</sub> by the peak height at WE<sub>1</sub>. The calculated values varied from 8% to 62% collection efficiency for 4-HBA and GA, respectively. The variability in collection efficiencies were directly correlated to chemical reversibility. 4-HBA is a chemically irreversible compound, which involves a one electron, one proton transfer, resulting in the formation of a highly reactive free radical; the mechanism for SA follows the same mechanism. Conversely, 3,4-DHBA and GA are chemically reversible species going through a two electron, two proton transfer resulting in the formation of quinone moieties that can be reduced back to their respective quinols. In addition to the collection efficiencies determined, signal enhancement for each analyte was also determined. The signal enhancement was calculated by dividing the slope of the curve from the linear regression analysis of WE<sub>1</sub> in redox-cycling mode, by the slope of WE<sub>1</sub> when only a single electrode was used. The same trends observed for collection efficiencies were also observed for the signal enhancements.

	Calculated Linear Velocity ( $\mu\text{m}/\text{sec}$ )	Calculated redox cycling	Sensitivity Single Electrode +800 mV (fA/nM)	Collection Efficiency	Signal Enhancement	Sensitivity Redox Cycling Mode, $w_1$ , +800 mV (fA/nM)	Sensitivity Redox Cycling Mode, $w_2$ , -200 mV (fA/nM)
<b>3,4-DHBA</b>	90	8	$550 \pm 10$	$31 \pm 9\%$	1.35	$730 \pm 30$	$260 \pm 50$
<b>4-HBA</b>	80	7	$1230 \pm 50$	$6.2 \pm 0\%$	1.05	$1300 \pm 80$	$115 \pm 5$
<b>SA</b>	74	7	$920 \pm 40$	$15 \pm 4\%$	1.12	$1030 \pm 50$	$180 \pm 20$
<b>GA</b>	68	6	$530 \pm 40$	$62 \pm 20\%$	1.72	$890 \pm 50$	$560 \pm 20$

Table 3.2: Data summarizing the collection efficiencies, signal enhancement and calculated cycling for the dual-electrode in redox cycling mode. Standard deviations reported based on peak heights ( $n = 5$ ).

That is, approximately a 2-fold increase in signal was determined for GA, while there was virtually no signal enhancement observed for 4-HBA. Furthermore, a linear trend was observed for the parallel dual-electrode, at both electrodes, of over two orders of magnitude (100 nM- 4.0 nM), with correlation coefficients of 0.92-0.99.

The reproducibility of the dual-electrode fabrication was investigated by comparing the sensitivities of three different dual-electrode sets. This was done by using linear regression analysis for one electrode set, with the sensitivities from subsequent sets of electrodes being compared at a concentration of 60 nM. The values shown in Table 3.3 represent the relative standard deviations for the determined peak heights between three different sets of electrodes. No significant deviation was observed for 3,4-DHBA, 4-HBA, SA or GA using this method of analysis at WE<sub>1</sub>. The deviation at WE<sub>2</sub> for 4-HBA was slightly higher compared to the other analytes. This was attributed to the diminished response at WE<sub>2</sub> for 4-HBA compared to the other analytes. There is minimal variability within the fabrication process that would significantly alter the response. It should be noted that while there was minimal variability in response from electrode to electrode, the amount of redox cycling observed is directly related to the working potential applied. Brief HDV's should be run for each new set of electrodes to ensure that there is minimal variability in signal enhancements and collection efficiencies. Additionally, the reproducibility between injections was also determined for n = 8 injections, by comparing peak heights. The data shown in Table 3.3, represents the relative standard deviations in the peak heights for both electrodes at a concentration of 1.0 μM. It was determined that there was less than 10% variation in peak heights between injections.

	<b>Injection Reproducibility, WE<sub>1</sub></b>	<b>Injection Reproducibility, WE<sub>2</sub></b>	<b>Electrode Fabrication Reproducibility, WE<sub>1</sub></b>	<b>Electrode Fabrication Reproducibility, WE<sub>2</sub></b>
<b>3,4-DHBA</b>	9.8%	9.8%	10%	10%
<b>4-HBA</b>	7.8%	14%	8.8%	12%
<b>SA</b>	8.8%	12%	4.5%	4.3%
<b>GA</b>	9.4%	6.2%	0.20%	0.30%

Table 3.3: Data summarizing injection reproducibility and reproducibility of electrode fabrication.

Relative standard deviations reported, based on peak height.

### 3.3.3 Dual-Potential Mode

The dual-potential mode is a selective configuration that is useful when analyzing complex biological matrices. Current ratios can be obtained in this configuration and used in conjunction with migration times to identify sample components. In Figure 3.10,  $WE_1$  was held at a potential of +800 mV, while  $WE_2$  was held at a potential of +500 mV versus Ag/AgCl. At a potential of +500 mV approximately ~35% of the current for 3,4-DHBA and 4-HBA was observed relative to +800 mV, while approximately ~85% of the current was observed for SA and GA. The ratio of the current response at these two potentials ( $i_{+500\text{ mV}}/i_{+800\text{ mV}}$ ) is characteristic of each compound and can be used in confirming the identity of peaks in actual samples. The current ratio in essence represents a two-point voltammogram. As a compound's electrochemical characteristics are orthogonal to its electrophoretic migration characteristics, using both properties to identify peaks in complex samples provides significantly higher confidence than using migration alone.

#### 3.3.3.1 Whiskey Analysis

Analysis of a whiskey sample was used to demonstrate the utility of the parallel-dual electrode for the analysis of complex samples. For this analysis several additional phenolic acid standards were characterized by CE with dual-electrode detection. Analytes were selected based on a previous report by Roston et al. which profiled several different spirits by LCEC<sup>37</sup>.

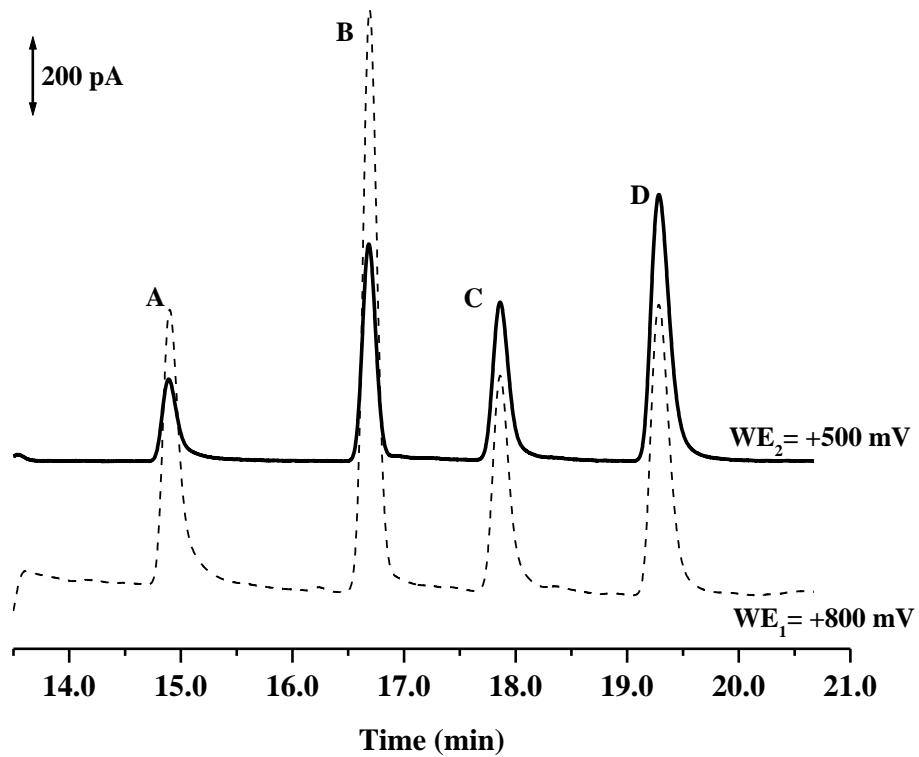


Figure 3.10: Response from injected reduced phenolic acids using dual-potential mode. Separation conditions the same as reported in Figure 3.9. A) 3,4-DHBA, B) 4-HBA, C) SA and D) GA.

In order to minimize co-migration of these additional phenolic acids the separation voltage was decreased to -10 kV. The migration and electrochemical properties of all of the standards tested are shown in Table 3.4.

A sample of whiskey was analyzed with the electrodes in both the dual-potential mode at two different current ratios (+800 mV and +500 mV versus Ag/AgCl, +800 mV and +200 mV versus AgAgCl) in order to improve peak identification based on a compounds ability to more or less easily oxidized. Additionally, redox cycling mode (+800 mV and -250 mV versus Ag/AgCl) was also employed to further enhance selectivity based on chemical reversibility of peaks within the whiskey sample. Nine peaks were identified from these electrohpherograms, as shown in Figures 3.11-3.13. Preliminary peak identities were made based on comparing the migration times of the peaks in the whiskey sample to those of the phenolic acid standards. It should be noted migration time in CE is a poor indication of peak identity. For this system, intraday variability and interday variability with respect to migration were found to be 0.5 min and 1.25 min, respectively. In order to minimize variability in migration time, as mentioned previously, 4-HBA was used as an internal standard for migration time. As shown in Figures 3.10-3.12, 4-HBA migrates between Peaks 2 and 3 and with no response observed from the whiskey sample between these two peaks it was spiked in with no issue of interference. Based on migration time alone, Peak 1 was tentatively identified as 3,4-DHBA or 3,4-DHPA, Peak 2 as 3,4-DHPA or gallic acid, Peak 3 as VA, Peak 5 as either p-coumaric acid or SA, Peak 6 as either p-coumaric acid or ferulic acid, and Peak 7 as GA. The migration time for Peak 8 correlated with that of GA as well, while Peak 9 did not match the migration times of any of the available standards, making identification of peak 9 impossible.

	<b>Time (min)</b>	<b>i ratio (+500 mV/+800 mV)</b>	<b>i ratio (+200 mV/+800 mV)</b>	<b>i ratio (-250 mV/+800 mV)</b>
<b>3,4-DHBA</b>	18.0 ± 0.2	0.21 ± 0.03	ND <sup>a</sup>	0.31 ± 0.09
<b>Peak 1</b>	18.2 ± 0.3	0.34 ± 0.04	0.052 ± 0.003	0.2 ± 0.1
<b>3,4-DHPA</b>	18.5 ± 0.1	0.95 ± 0.05	0.04 ± 0.01	0.54 ± 0.03
<b>Peak 2</b>	18.6 ± 0.2	0.97 ± 0.03	0.09 ± 0.01	NR <sup>c</sup>
<b>Gallic acid</b>	18.65 ± 0.03	1.15 ± 0.09	0.12 ± 0.03	NR <sup>c</sup>
<b>4-HBA</b>	20.2 ± 0.0	0.33 ± 0.04	ND <sup>a</sup>	0.062 ± 0.004
<b>vanillic acid</b>	20.9 ± 0.1	1.14 ± 0.07	0.023 ± 0.001	0.26 ± 0.04
<b>Peak 3</b>	21.0 ± 0.4	1.16 ± 0.04	0.25 ± 0.01	0.31 ± 0.01
<b>Peak 4</b>	21.3 ± 0.1	1.4 ± 0.1	BLOD <sup>b</sup>	BLOD <sup>b</sup>
<b>Peak 5</b>	21.6 ± 0.1	1.10 ± 0.04	0.3 ± 0.1	0.19 ± 0.01
<b>SA</b>	21.7 ± 0.2	1.06 ± 0.04	0.230 ± 0.006	0.15 ± 0.04
<b>p-coumaric acid</b>	21.7 ± 0.0	0.69 ± 0.06	0.005 ± 0.001	NR <sup>c</sup>
<b>Peak 6</b>	22.1 ± 0.3	0.85 ± 0.07	0.04 ± 0.02	BLOD <sup>b</sup>
<b>ferulic acid</b>	22.3 ± 0.1	1.30 ± 0.08	0.32 ± 0.05	0.25 ± 0.01
<b>Peak 7</b>	22.8 ± 0.3	0.74 ± 0.01	0.09 ± 0.02	0.14 ± 0.01
<b>GA</b>	22.9 ± 0.3	1.71 ± 0.08	0.93 ± 0.05	0.6 ± 0.2
<b>Peak 8</b>	23.3 ± 0.3	0.93 ± 0.07	0.14 ± 0.02	0.03 ± 0.01
<b>Peak 9</b>	24.9 ± 0.5	ND <sup>a</sup>	ND <sup>a</sup>	ND <sup>a</sup>

Table 3.4: Analysis of migration times and current ratios using dual-potential mode and redox cycling mode for standards and unknown peaks in the whiskey sample. Separation conditions were the same as reported in Figure 3.11

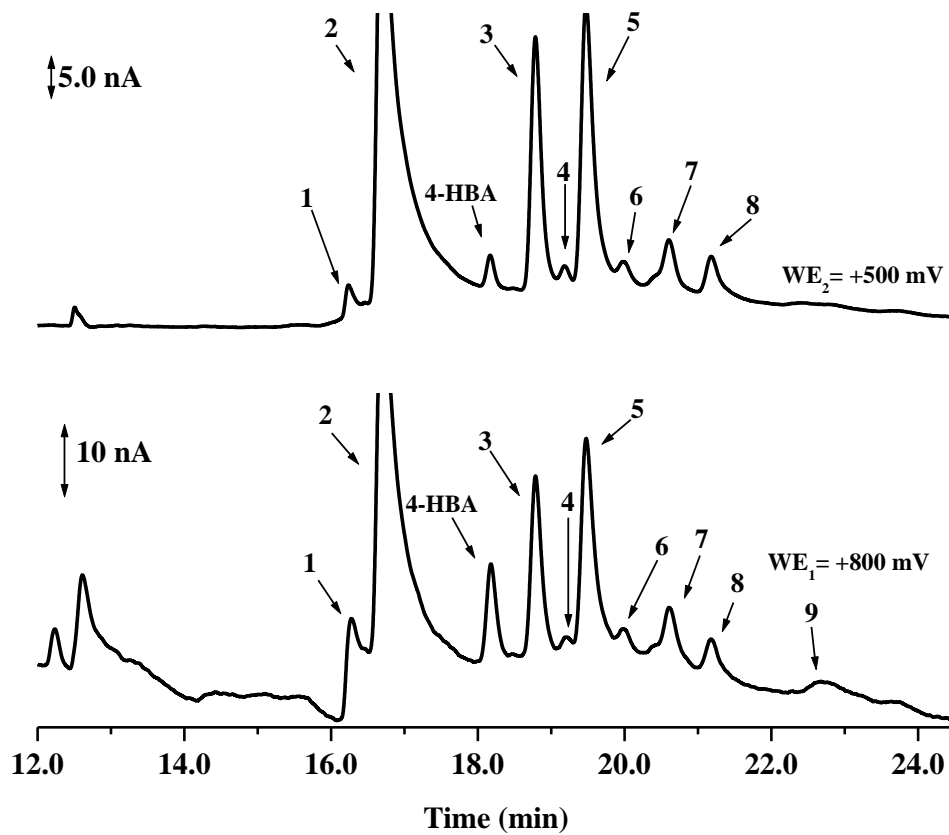


Figure 3.11: Response from whiskey sample using electrodes in dual-potential mode. Separation conditions: 75 mM tetraborate, 0.5 mM TTAB, pH 8.4, -10 kV. Injection: 2 sec, -12 kV. Samples diluted with 1.0 mM  $\text{HClO}_4$ .

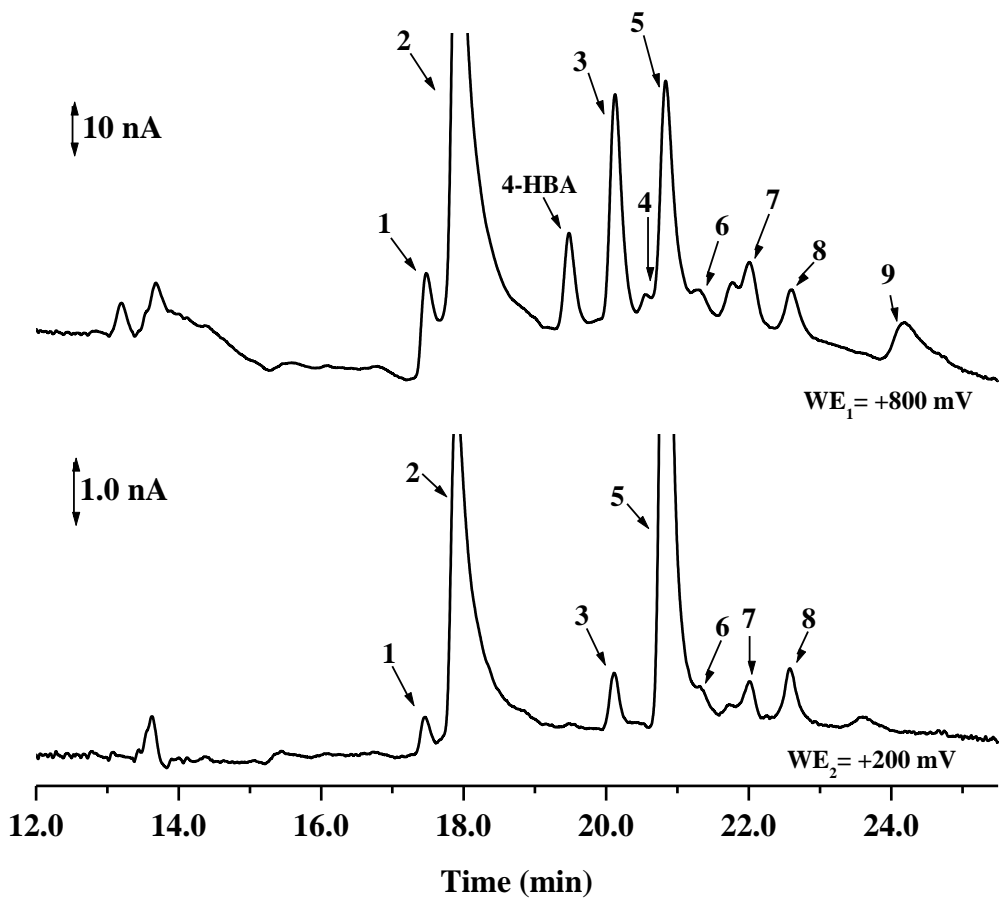


Figure 3.12: Response from whiskey sample using electrodes in dual-potential mode. Conditions were the same as reported in Figure 3.11.

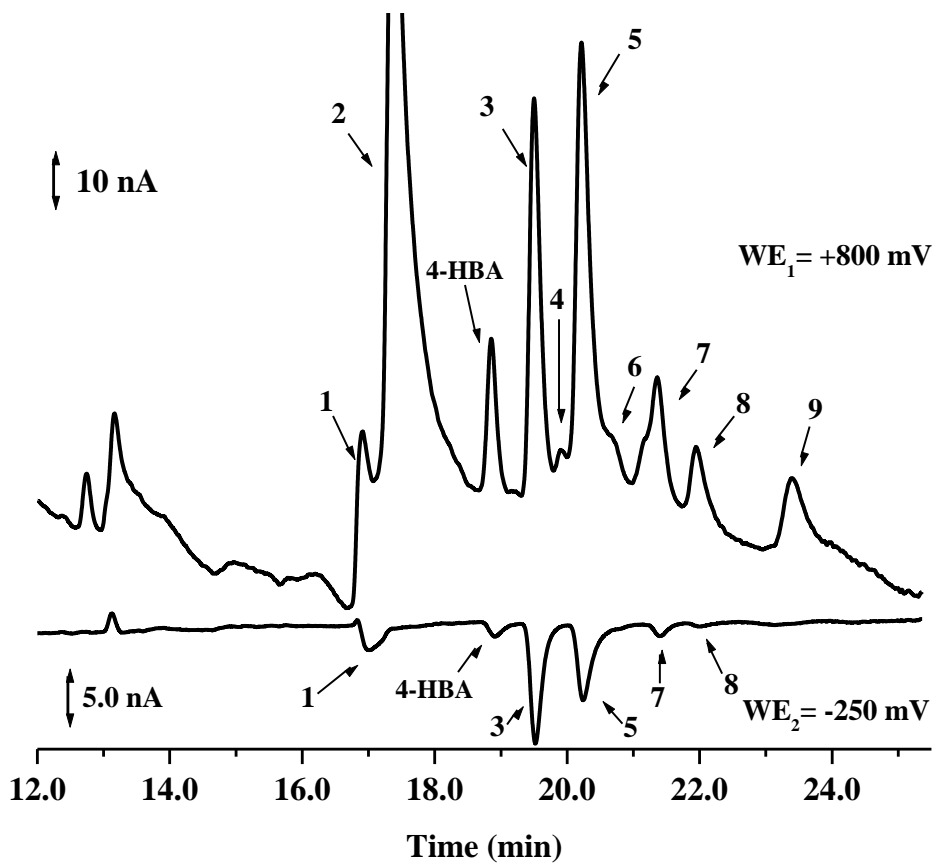


Figure 3.13: Response from whiskey sample using electrodes in redox cycling mode. Separation conditions were the same as reported in Figure 3.11.

The whiskey sample was then spiked with standards to more accurately make migration-based peak identity assignments. Based on linear regression analysis peak concentrations in the whiskey sample were roughly established. Analytes were then spiked in at concentrations that would effectively double the peak height of the corresponding peak of interest. This was done in order to ensure that spiked concentrations would not swamp out neighboring peaks of interest. These spiking experiments confirmed the identities of Peaks 1, 2, 3 and 5 based on migration as, 3,4-DHBA, gallic acid, VA and SA. Furthermore, it was determined through spiking that p-coumaric acid correlated Peak 6, ferulic acid matched with Peak 7 and GA co-migrated with Peak 8.

Using electrochemistry as an orthogonal means to confirm migration-based peak identity, Peak 1 was assigned as 3,4-DHBA. Analysis based on both oxidation potential ( $i_{+500\text{ mV}}/i_{+800\text{ mV}}$ , dual-potential mode) and chemical reversibility ( $i_{-200\text{ mV}}/i_{+800\text{ mV}}$ , redox cycling mode) confirmed this identification as shown in Table 3.4. Although, the electrochemistry at the second oxidative dual-potential ( $i_{+200\text{ mV}}/i_{+800\text{ mV}}$ ) correlated with the electrochemistry of 3,4-DHPA two other current ratios used in Table 5 in conjunction with spiking indicated that Peak 1 was 3,4-DHBA and not 3,4-DHPA. Peak 2 was determined to be chemically irreversible as shown in Table 3.4, indicating that the migration-based assignment of gallic acid was correct. Using both the dual-potential mode as well as the redox cycling mode Peaks 3 and 5 were confirmed as VA and SA, respectively. Peak 6 was present at low concentration (~10 nM) as determined by linear regression analysis, making the integration of Peak 6 difficult to reproduce from injection to injection. However, even with this difficulty the electrochemistry determined in Table 5 without spiking experiments correlated well with that of the p-coumaric acid standard. With the spiking analysis performed at both 20 nM and 40 nM for p-coumaric acid current ratios of 0.71 and 0.71 were obtained in dual-potential mode, respectively. This then confirmed Peak 6 as p-coumaric acid. As

previously stated spiking experiments were also performed with ferulic acid and co-migration was observed with Peak 7, the electrochemistry could not be accurately quantified, suggesting the presence of multiple species. Although through spiking and migration-based peak identity GA was determined to co-migrate with Peak 8, the electrochemistry determined for Peak 8 did not correlate with that of the standard for GA. In this case Peak 8 was to be baseline resolved from Peaks 7 and 9 and did not have any apparent fronting, tailing or shoulders indicating that unlike Peak 7 this peak represented only one unknown. Spiking experiments at 150 nM and 250 nM showed increasing asymmetry with increasing concentration on the leading side of the peak. This example, as well as that of Peak 7, has clearly demonstrated the utility of the newly developed parallel dual-electrode. Relying on only migration-based peak identity within complex matrices would lead to incorrect identification of peaks. Instead the analytes inherent electrochemical properties, in this instance, were used in an orthogonal analysis to better establish peak identities.

### 3.4 Conclusions

A parallel dual-electrode was developed for CE. The detector has been shown to work in both a redox cycling mode as well as dual-potential mode. In redox-cycling mode a 2-fold enhancement in sensitivity was achieved via complete redox cycling of analytes between electrodes. Offers improvement in detection limits compared to previously published dual-electrode systems as well as applications where only single electrodes were employed. In addition, the dual-potential mode can be used as an additional means of confirming migration based peak identities.

### 3.5 References

1. Weng, Q.; Xu, G.; Yuan, K.; Tang, P., Determination of monoamines in urine by capillary electrophoresis with field-amplified sample stacking and amperometric detection. *J. Chromatogr., B: Anal. Technol. Biomed. Life Sci.* **2006**, *835* (Copyright (C) 2012 American Chemical Society (ACS). All Rights Reserved.), 55-61.
2. Xu, J.-J.; Wang, A.-J.; Chen, H.-Y., Electrochemical detection modes for microchip capillary electrophoresis. *TrAC, Trends Anal. Chem.* **2007**, *26* (Copyright (C) 2012 American Chemical Society (ACS). All Rights Reserved.), 125-132.
3. Bhat, S. H.; Azmi, A. S.; Hadi, S. M., Prooxidant DNA breakage induced by caffeic acid in human peripheral lymphocytes: Involvement of endogenous copper and a putative mechanism for anticancer properties. *Toxicol. Appl. Pharmacol.* **2007**, *218* (Copyright (C) 2012 American Chemical Society (ACS). All Rights Reserved.), 249-255.
4. Kong, Y.; Chen, H.; Wang, Y.; Soper, S. A., Fabrication of a gold microelectrode for amperometric detection on a polycarbonate electrophoresis chip by photodirected electroless plating. *Electrophoresis* **2006**, *27* (14), 2940-2950.
5. Lin, B. L.; Colon, L. A.; Zare, R. N., Dual electrochemical detection of cysteine and cystine in capillary zone electrophoresis. *J. Chromatogr., A* **1994**, *680* (1), 263-70.
6. Zhong, M.; Lunte, S. M., Tubular-Wire Dual Electrode for Detection of Thiols and Disulfides by Capillary Electrophoresis/Electrochemistry. *Anal. Chem.* **1999**, *71* (1), 251-255.
7. Holland, L. A.; Lunte, S. M., Postcolumn Reaction Detection with Dual-Electrode Capillary Electrophoresis-Electrochemistry and Electrogenerated Bromine. *Anal. Chem.* **1999**, *71* (2), 407-412.
8. Chen, D.-c.; Chang, S.-S.; Chen, C.-h., Parallel-Opposed Dual-Electrode Detector with Recycling Amperometric Enhancement for Capillary Electrophoresis. *Anal. Chem.* **1999**, *71* (15), 3200-3205.
9. Chen, D. c.; Zhan, D. Z.; Cheng, C. W.; Liu, A. C.; Chen, C. h., Determination of urine catecholamines by capillary electrophoresis with dual-electrode amperometric detection. *J. Chromatogr., B Biomed. Sci. Appl.* **2001**, *750* (1), 33-39.
10. Mecker, L. C.; Martin, R. S., Use of micromolded carbon dual electrodes with a palladium decoupler for amperometric detection in microchip electrophoresis. *Electrophoresis* **2006**, *27* (24), 5032-5042.
11. Lai, C.-C. J.; Chen, C.-h.; Ko, F.-H., In-channel dual-electrode amperometric detection in electrophoretic chips with a palladium film decoupler. *J. Chromatogr., A* **2004**, *1023* (1), 143-150.
12. Castano-Alvarez, M.; Fernandez-Abedul, M. T.; Costa-Garcia, A., Amperometric detector designs for capillary electrophoresis microchips. *J. Chromatogr., A* **2006**, *1109* (2), 291-299.
13. Du, F.; Fung, Y. S., Development of CE-dual opposite carbon-fiber micro-disk electrode detection for peak purity assessment of polyphenols in red wine. *Electrophoresis* **2010**, *31* (13), 2192-2199.
14. Martin, R. S.; Gawron, A. J.; Fogarty, B. A.; Regan, F. B.; Dempsey, E.; Lunte, S. M., Carbon paste-based electrochemical detectors for microchip capillary electrophoresis/electrochemistry. *Analyst (Cambridge, U. K.)* **2001**, *126* (3), 277-280.
15. Martin, R. S.; Gawron, A. J.; Lunte, S. M.; Henry, C. S., Dual-Electrode Electrochemical Detection for Poly(dimethylsiloxane)-Fabricated Capillary Electrophoresis Microchips. *Anal. Chem.* **2000**, *72* (14), 3196-3202.

16. Fischer, D. J.; Vandaveer, W. R. I. V.; Grigsby, R. J.; Lunte, S. M., Pyrolyzed photoresist carbon electrodes for microchip electrophoresis with dual-electrode amperometric detection. *Electroanalysis* **2005**, *17* (13), 1153-1159.
17. Pai, R. S.; Walsh, K. M.; Crain, M. M.; Roussel, T. J., Jr.; Jackson, D. J.; Baldwin, R. P.; Keynton, R. S.; Naber, J. F., Fully Integrated Three-Dimensional Electrodes for Electrochemical Detection in Microchips: Fabrication, Characterization, and Applications. *Anal. Chem. (Washington, DC, U. S.)* **2009**, *81* (12), 4762-4769.
18. Gerhauser, C., Beer constituents as potential cancer chemopreventive agents. *Eur J Cancer* **2005**, *41* (Copyright (C) 2012 U.S. National Library of Medicine.), 1941-54.
19. Clifford, M. N., Chlorogenic acids and other cinnamates - nature, occurrence and dietary burden. *J. Sci. Food Agric.* **1999**, *79* (Copyright (C) 2012 American Chemical Society (ACS). All Rights Reserved.), 362-372.
20. Leifert, W. R.; Abeywardena, M. Y., Grape seed and red wine polyphenol extracts inhibit cellular cholesterol uptake, cell proliferation, and 5-lipoxygenase activity. *Nutr. Res. (N. Y., NY, U. S.)* **2008**, *28* (Copyright (C) 2012 American Chemical Society (ACS). All Rights Reserved.), 729-737.
21. Freedman, J. E.; Parker, C., III; Li, L.; Perlman, J. A.; Frei, B.; Ivanov, V.; Deak, L. R.; Iafrafi, M. D.; Folts, J. D., Select flavonoids and whole juice from purple grapes inhibit platelet function and enhance nitric oxide release. *Circulation* **2001**, *103* (Copyright (C) 2012 American Chemical Society (ACS). All Rights Reserved.), 2792-2798.
22. Taubert, D.; Berkels, R.; Klaus, W.; Roesen, R., Nitric oxide formation and corresponding relaxation of porcine coronary arteries induced by plant phenols: Essential structural features. *J. Cardiovasc. Pharmacol.* **2002**, *40* (Copyright (C) 2012 American Chemical Society (ACS). All Rights Reserved.), 701-713.
23. Stoclet, J.-C.; Chataigneau, T.; Ndiaye, M.; Oak, M.-H.; El, B. J.; Chataigneau, M.; Schini-Kerth, V. B., Vascular protection by dietary polyphenols. *Eur. J. Pharmacol.* **2004**, *500* (Copyright (C) 2012 American Chemical Society (ACS). All Rights Reserved.), 299-313.
24. Rodrigo, R.; Miranda, A.; Vergara, L., Modulation of endogenous antioxidant system by wine polyphenols in human disease. *Clin. Chim. Acta* **2011**, *412* (Copyright (C) 2012 American Chemical Society (ACS). All Rights Reserved.), 410-424.
25. Lee, Y. S., Role of NADPH oxidase-mediated generation of reactive oxygen species in the mechanism of apoptosis induced by phenolic acids in HepG2 human hepatoma cells. *Arch. Pharmacol. Res.* **2005**, *28* (Copyright (C) 2012 American Chemical Society (ACS). All Rights Reserved.), 1183-1189.
26. Yeh, C.-T.; Yen, G.-C., Induction of hepatic antioxidant enzymes by phenolic acids in rats is accompanied by increased levels of multidrug resistance-associated protein 3 mRNA expression. *J. Nutr.* **2006**, *136* (Copyright (C) 2012 American Chemical Society (ACS). All Rights Reserved.), 11-15.
27. Landers, J. P., *Handbook of Capillary Electrophoresis, 2nd Ed.* CRC Press: Boca Raton, FL, 1997.
28. Osbourn, D. M.; Lunte, C. E., Cellulose Acetate Decoupler for On-Column Electrochemical Detection in Capillary Electrophoresis. *Anal. Chem.* **2001**, *73* (24), 5961-5964.
29. Osbourn, D. Instrumentation and methods for capillary electrophoresis. University of Kansas, 2004.
30. Gunasekara, D. B.; Hulvey, M. K.; Lunte, S. M., In-channel amperometric detection for microchip electrophoresis using a wireless isolated potentiostat. *Electrophoresis* **2011**, *32* (Copyright (C) 2012 American Chemical Society (ACS). All Rights Reserved.), 832-837.
31. Lunte, S. M.; Martin, R. S.; Lunte, C. E., Capillary electrophoresis/electrochemistry: Instrument design and bioanalytical applications. *Electroanal. Methods Biol. Mater.* **2002**, 461-490.

32. Powell, P. R.; Woods, L. A.; Ewing, A. G., Characterization of etched electrochemical detection for electrophoresis in micron inner diameter capillaries. *J. Sep. Sci.* **2005**, *28* (18), 2540-2545.
33. Wallingford, R. A.; Ewing, A. G., Capillary zone electrophoresis with electrochemical detection. *Anal. Chem.* **1987**, *59* (14), 1762-6.
34. Park, S.; Lunte, S. M.; Lunte, C. E., A perfluorosulfonated ionomer joint for capillary electrophoresis with on-column electrochemical detection. *Anal. Chem.* **1995**, *67* (5), 911-18.
35. Crick, E. W. *In vivo* microdialysis coupled with electrophysiology for the measurement and analysis of epileptic seizures. University of Kansas, 2007.
36. Roston, D. A.; Shoup, R. E.; Kissinger, P. T., Liquid chromatography/electrochemistry: thin-layer multiple electrode detection. *Anal. Chem.* **1982**, *54* (13), 1417A-1418A, 1422A, 1424A, 1428A, 1430A, 1432A, 1434A.
37. Roston, D. A.; Kissinger, P. T., Identification of phenolic constituents in commercial beverages by liquid chromatography with electrochemical detection. *Anal. Chem.* **1981**, *53* (11), 1695-9.

## Chapter 4: Development of a Dual-Au/Hg Electrode Capillary Electrophoresis Method for the Determination of Thiols and Disulfides

### 4.0 Background and Significance

Thiol to disulfide ratios have long been important markers of tissue redox homeostasis or disruption of homeostasis as a result of oxidative stress. As oxidative stress events are key in the progression of several neurological diseases it is important to be able to monitor endogenous markers that are directly associated with damage or maintained tissue homeostasis in order to better understand the biological implications of these diseases. Several methods have been developed for the analysis of thiols and disulfides by fluorescence, UV and electrochemical detection<sup>1-33</sup>. Predominately, these methods have focused on glutathione (GSH) and its disulfide (GSSG) in conjunction with one additional thiol, either homocysteine or cysteine.

### 4.1 Introduction

The focus of this work was on low molecular weight thiols and their corresponding disulfides. Specifically, low molecular weight thiols, homocysteine, cysteine, and glutathione, shown in Figure 4.1 are of significant interest due to their antioxidant properties. The thiol or “sulfhydryl” group (S-H) is highly reactive at neutral to slightly basic pH. The reactivity of these thiols, is directly related to the proximity of the ionizable groups. The carboxyl groups are stabilizing, while amino groups reduce the pKa of thiol further<sup>34</sup>. Consequently, cysteine has the lowest pKa. Due to the reactivity of the thiolate anion, cytotoxic effects have been observed at low concentrations (<μM). At these cellular concentrations thiolate anion will readily oxidize other cellular components. At higher concentration (>μM) thiolate anions will react with themselves rapidly to form disulfides.

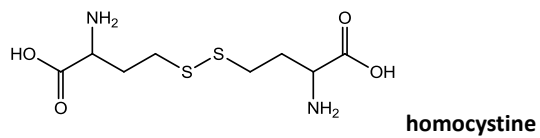
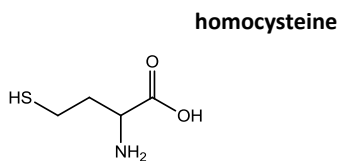
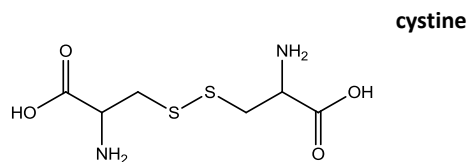
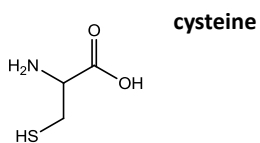
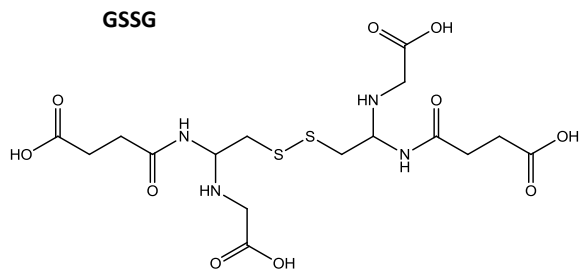
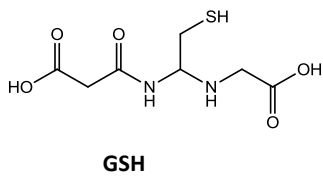


Figure 4.1: Structures of low molecular weight thiols and disulfides. pka values for functional groups on low molecular weight thiols and disulfides: COOH = 1.0-2.2, SH = 8.0-8.8, NH<sub>2</sub> = 9.4-10.8.

Under oxidative stress conditions this redox chemistry works to scavenge free radicals, maintain reduced forms of proteins, prevent lipid peroxidation and subsequent breakdown of cell membranes, as well as provide crucial regeneration of methionine<sup>35,36</sup>.

#### 4.1.1 Endogenous Antioxidants

Figure 4.2 shows the metabolic pathway associated with general sulfur metabolism. From the generalized scheme, homocysteine is produced through transmethylation, which upon reaction with serine produces cysteine. Cysteine then reacts with  $\gamma$ -glutamylcysteine and glycine to produce glutathione.

As shown in Figure 4.2 homocysteine plays a central role in regenerating methionine via transmethylation while competing equally with the transsulfuration pathway to form cysteine. The conversion of homocysteine to cysteine is irreversible making it a key part in sulfur metabolism<sup>35</sup>. Genetic deficiencies in either of these pathways (*i.e.* transsulfuration or transmethylation) lead to accumulation of homocysteine. The result of this accumulation has been reported to contribute to the development of neurological disorders amongst other physical impairments<sup>35-37</sup>. Furthermore, oxidation of homocysteine with free radicals has been shown to aid in endothelial dysfunction increasing propensity of lipid peroxidation<sup>35</sup>.

Cysteine is perhaps the most critical component in sulfur metabolism. It serves as an essential building block for most endogenous non-sulfur containing compounds and is key in the synthesis of glutathione. In addition, it is incorporated in the backbone of most proteins, acting as the sole source of thiols<sup>35,36</sup>.

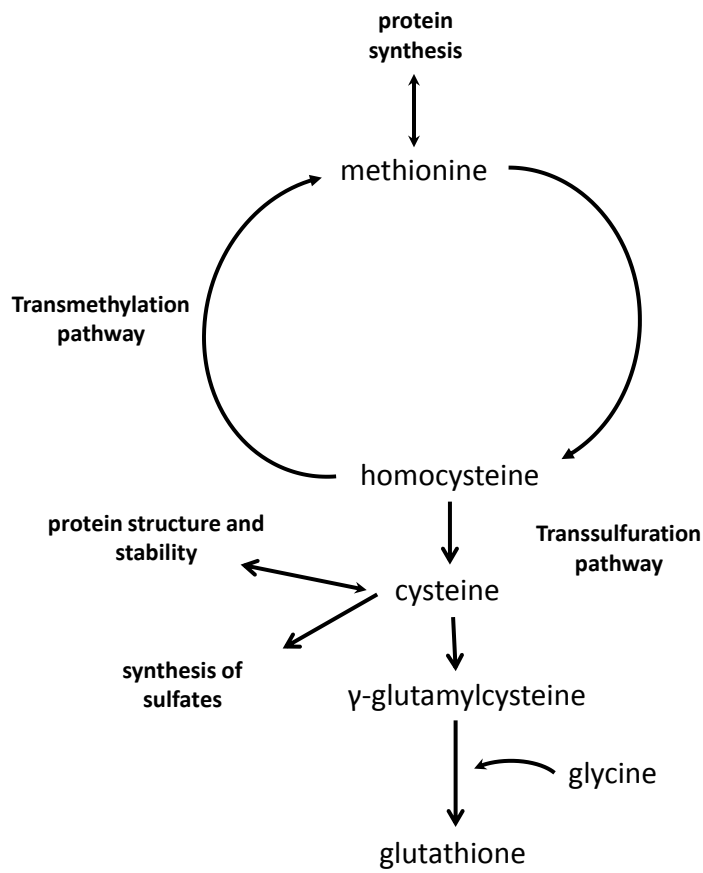
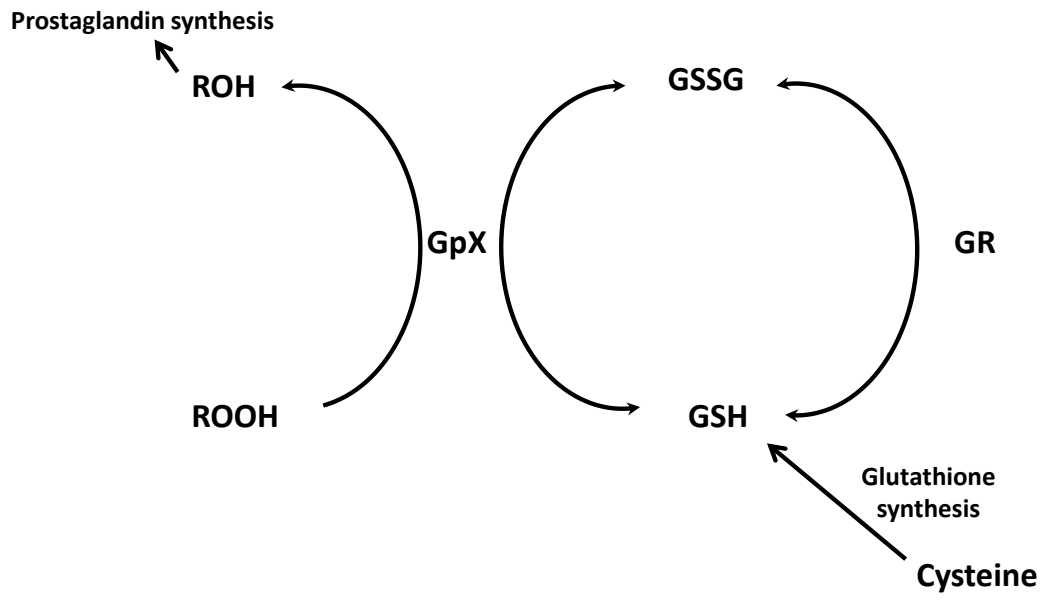


Figure 4.2: Metabolic pathway of methionine, adapted from Bayle<sup>36</sup>.

Cysteine is present in equilibrium with its disulfide, cystine. Cystine is transported into the cell via reduction to cysteine. Like glutathione, cysteine can also scavenge free radicals and is important in the synthesis of taurine, which is known to regulate production of intracellular  $\text{Ca}^{2+}$ . Liang *et al.* reported in their investigation of mitochondrial redox status as a result of seizures a decrease in cysteine, which they concluded was a contributing factor in the observed decrease in production of GSH and an increase in mitochondrial ratio of GSH/GSSG<sup>38</sup>. Reid and Jahoer reported intracellular cysteine increased in people deficient in cysteine with a diet supplemented with N-actylcysteine. With an increase in intracellular cysteine and a correlated increase intracellular GSH, resulting in enhanced cytoprotective effects<sup>39</sup>.

GSH is synthesized from  $\gamma$ -glutamylcysteine and glycine. GSH and its disulfide (GSSG) are the most widely studied endogenous markers of oxidative stress. GSH is present in high concentration within the tissue (mM) and is present in tens of micromolar in the plasma. Similar in its cytoprotective effects to cysteine, GSH is also involved in amino acid transport via the  $\gamma$ -glutamyl cycle, functions as a co-enzyme in several reactions (*e.g.* leukotriene synthesis, cyclooxygenase synthesis)<sup>35</sup>.

The primary function of GSH is its involvement in mitigation of oxidative stress through the scavenging of free radicals and detoxification of  $\text{H}_2\text{O}_2$ . Reduction of  $\text{H}_2\text{O}_2$  is critical, and if not effectively reduced to  $\text{H}_2\text{O}$  it can go on to cause lipid peroxidation and oxidative damage to DNA. While catalase can reduce  $\text{H}_2\text{O}_2$  to  $\text{H}_2\text{O}$ , it is thought that both cytosolic and extracellular  $\text{H}_2\text{O}_2$  are reduced preferentially by glutathione reductase. The reaction is a two-step process in which  $\text{H}_2\text{O}_2$  is reduced with 2 molecules of GSH and glutathione peroxidase, producing GSSG and  $\text{H}_2\text{O}$ . GSSG then reacts with NADPH, which reduces the disulfide back to GSH, the reaction is shown in Figure 4.3<sup>35</sup>.



(1)

(2)

Figure 4.3: Reduction of peroxides via oxidation of glutathione. GpX (glutathione peroxidase), GR (glutathione reductase), ROOH is peroxide, most commonly hydrogen peroxide.

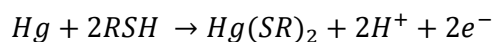
#### 4.1.2 Analysis of Thiols and Disulfides

Based on the biological significance of these low molecular weight thiols and disulfides in maintaining tissue redox homeostasis, development of an analytical method to simultaneously and selectively detect these analytes is of importance. Several approaches for the separation and detection of these analytes have been reported previously, although very few have achieved separation and detection of all six analytes proposed for this work. Furthermore, methods reported in the literature have primarily dealt with matrices from urine, plasma or tissue. In these types of matrices there is generally significant sample pretreatment prior to analysis with reconstitution of the extracted analytes in an ideal matrix. Dialysis samples eliminate difficulties in separations encountered with the previously mentioned matrices. The semi-permeable membrane used in these experiments eliminates large molecular weight species resulting in cleaner samples allowing for direct injection.

##### 4.1.2.1 Liquid Chromatography (LC)

Initially the separation of thiols and disulfides was carried out using LC, prior to CE being developed. Several detectors have been coupled with LC systems including: UV<sup>2, 15</sup>, fluorescence<sup>21, 22</sup>, electrochemical (EC)<sup>1, 13, 17, 20, 25, 28</sup> and more recently, mass spectrometry (MS)<sup>7, 40</sup>. Methods that have been reported for fluorescence require derivatization for detection of the both thiols and disulfides<sup>21, 22</sup>. Although, the derivatization process is time consuming, the sensitivity and detection limits (LOD) are comparable to EC (nM), if not improved in some cases (pM). UV detection has also been coupled to LC for the detection of thiols and disulfides<sup>2, 15</sup>. UV detection of these analytes without derivatization is only possible at non-selective wavelengths (200 nm). In order to increase selectivity thiols and disulfides are tagged with chromophores; however, path length is still a limiting factor in the sensitivity of this detection scheme, yielding LOD to tens of micromolar.

EC detection coupled with LC has overwhelmingly been used throughout the literature for the detection of thiols and disulfides. The thiol moiety is electrochemically reactive and can be oxidized directly using a carbon electrode at a voltage of  $\sim + 1.0$  V vs. Ag/AgCl<sup>17</sup>. Detection at this working potential is not selective as several biologically relevant compounds will oxidize under these conditions; consequently noise is increased diminishing LOD. This can be overcome with the use of a Hg amalgam electrode. Saetre and Rubenstein were the first to report using a pooled Hg electrode coupled with LC for the separation and detection of thiol compounds<sup>25</sup>. Using a Hg electrode certain species, such as thiols can be oxidized<sup>1, 20, 28</sup> indirectly via the oxidation of Hg. The reaction for the indirect oxidation of thiol with Hg is shown below:



Using this type of electrode the oxidation of thiol containing species is reduced to + 0.1 V vs. Ag/AgCl. Not only is the selectivity of the reaction improved through the complexation with Hg, but the potential at which the reaction occurs is also more selective compared to that at a carbon surface. The integration of the pooled Hg electrode as reported by Rubenstein and Saetre, was similar in design to thin-layer cell reported by Kissinger *et al.*<sup>41</sup>. Although, Saetre and Rubenstein demonstrated that thiol compounds could be selectively detected using a Hg electrode; however, the design of the cell incurred issues with uncompensated resistance and poor peak efficiencies (2 min wide peaks)<sup>25</sup>. Allison and Shoup were the first to report on the integration of a thin-layer dual Au/Hg amalgam electrode for the detection of thiols and disulfides in one chromatographic run<sup>1</sup>. This was achieved by using a dual Au electrode amalgamated with Hg in a series configuration, as shown in Figure 4.4. The upstream electrode in this case acts as a generator electrode, and is used to reduce disulfides.

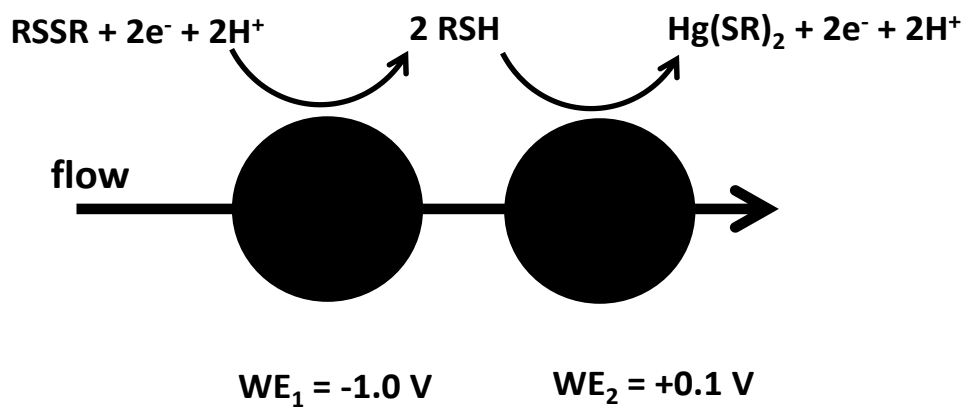


Figure 4.4: Thin layer dual Au/Hg electrode, electrodes shown in series configuration. Reduction of disulfides at the upstream or generator electrode. Detection of reduced thiols and disulfides occurring at the downstream oxidation electrode.

The subsequent oxidation of thiols and reduced disulfides is then monitored at the downstream electrode. Several other reports in the literature have used this same detection scheme for the analysis of thiols and disulfides<sup>13, 20, 28</sup>. Because of the similarity in structures between low molecular weight thiols and disulfides, especially cysteine and homocysteine which differ only by an additional carbon, separation can sometimes be arduous. Most methods that have successfully separated low molecular weight thiols, disulfides and even mixed disulfides have used acidic mobile phase conditions (pH < 3) with an ion-pairing agent, typically sodium octyl sulfate (SOS)<sup>13, 28</sup>. Under these conditions the carboxylic acid is protonated, along with the sulfhydryl and amine moieties resulting in overall net positive charge. SOS, which is a negatively charged ion-pairing agent, can then easily interact with these analytes based on charge-charge interactions resulting in resolution between analytes such as homocysteine and cysteine.

In addition to LCEC systems, improved selectivity and sensitivity can be maintained by coupling LC with mass spectrometry (MS)<sup>7, 40</sup>. LC-MS has become the tool of choice for the detection of several species over the last decade, especially for the detection of proteins. The chromatography in these methods typically does not result in base line resolution between analytes of interest. Instead, the authors rely on the selectivity of detector to reliably distinguish peaks of interest. In addition, these methods require a derivatization step, using either Ellman's reagent or iodoacetic acid to improve sensitivity<sup>7, 40</sup>.

While LC systems have the advantage of an added phase in the separation (*i.e.* partitioning between the mobile phase and stationary phase), resolution between structurally similar analytes easier, the exception being ion-pairing systems. However, injection volumes are quite large (5-20 $\mu$ l) making their application to small volume biological samples, such as dialysate difficult. It should be noted that with the onset and more routine use of capillary LC columns, as well as UHPLC systems that these issues can be overcome.

#### 4.1.2.2 Capillary Electrophoresis (CE)

CE yields highly efficient separations and is well suited to low volume sampling, as the total capillary volume is on the order of hundreds of nanoliters to tens of microliters. Injection volumes are typically within the nL-pL range, making integration with microdialysis sampling ideal. Primarily separations for thiols and disulfides with CE have been done using normal polarity, where order of migration would be cations, neutrals, then anions and have been integrated with several detection schemes: UV<sup>9, 14, 26, 42</sup>, fluorescence<sup>5, 12, 16, 18, 43</sup>, and EC<sup>3, 8, 10, 19, 23, 24, 29, 30, 32, 33, 44-47</sup>. The small diameters of the separation capillaries, typically  $\leq 75 \mu\text{m}$ , place restraints on spectroscopic methods as they limit path length significantly. In addition, as with LC methods discussed previously, derivatization is required to enhance selectivity for UV methods.<sup>14, 42</sup> Some reports have used UV detection for thiols and disulfides without derivatization and instead incorporated sample stacking methods to enhance sensitivity<sup>9, 26</sup>.

Several approaches using on-capillary and off-capillary detection have been reported for the detection of thiols and disulfides<sup>10, 23, 24, 29, 30, 33, 45, 47</sup>. Chen *et al.* and Wang *et al.* both employed off-capillary detection using single carbon electrodes for the analysis of reduced thiols<sup>30, 45</sup>. However, as mentioned previously oxidation potentials at these electrode are  $\geq + 1.0 \text{ V vs. Ag/AgCl}$ , which result in high background noise in addition to diminished selectivity. Aside from single Au/Hg electrodes being reported for detection of reduced thiols in CEEC<sup>23, 24</sup>, other approaches including pulsed electrochemical detection (PED), integrated pulsed amperometric detection (IPAD) and carbon electrodes with chemically modified surfaces have also been investigated<sup>29, 31, 33, 47</sup>. Two electrode surface modifications have been routinely used, cobalt-phthalocyanine and ruthenium-cyanide. While oxidation potentials are reduced from + 1.0 V to +0.6 V and +0.85 V, respectively, these electrode are prone to short life spans due in part to lack of protons in the buffer systems required to catalyze oxidation at the electrode or to surface fouling. Surface fouling is also experienced when using noble metal electrodes for the detection

of sulfur containing compounds<sup>29</sup>. This is thought to be the result of the two lone pairs of electrons on the sulfur resulting in the oxidation of the metal surface. Consequently, oxides form on the surface passivating the electrode. If reduction at the surface cannot occur then further electrode fouling will result. Johnson and Owens both investigated surface cleaning techniques (PED and IPAD) in order to increase electrode lifetime and maintain better sensitivity<sup>29, 47</sup>.

The issue with single electrode detection is that only the thiol or the disulfide can be detected. The exception to this being application of PED, IPAD and mixed ruthenium-cyanide electrodes. Integration of dual-electrode detection using the series configuration, as Allison and Shoup reported for LCEC systems, would be ideal for CE. Application of a dual-Au/Hg electrode would still result in an indirect detection scheme, but there is no requirement for catalysts in order for the reaction to take place and detection does require additional cleaning from injection to injection. There are several reports on various dual Au/Hg electrode fabrications for the analysis of thiols and disulfides<sup>19, 48</sup>. All employ a series configuration, in which the upstream electrode acts as a “generator” electrode and the downstream electrode, held at a low oxidation potential (+0.1 V) is used for detection. Zare *et al.* used a Pd field decoupler in conjunction with dual-electrode detection. In this scheme the upstream electrode was placed 2 cm downstream from the decoupler<sup>19</sup>. The electrode was placed inside the capillary by etching the capillary to expose the inner diameter; the electrode was fixed with epoxy, as shown in Figure 4.5.

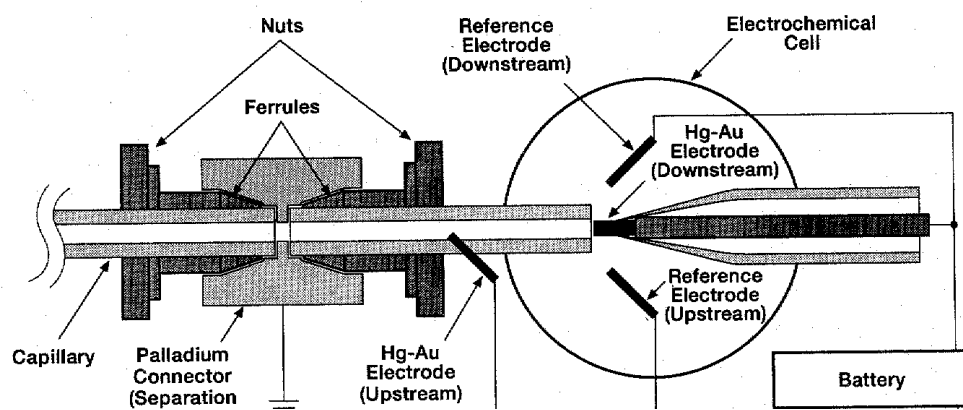


Figure 4.5: Dual Au/Hg electrode in series configuration, with permission<sup>19</sup>. Electrodes integrated with capillary electrophoresis using an electrical decoupler.

A macro electrode was then positioned just outside the capillary outlet and was used for the detection of cysteine and cysteine. LOD's were reported to be 5  $\mu\text{M}$  and 100  $\mu\text{M}$ , respectively. With this design loss in efficiency was due to the distance of the electrodes in relation to the separation capillary<sup>19</sup>. Zhong and Lunte, reported the use of tubular-wire dual electrode configuration<sup>48</sup>. LOD of for this system were reported to be 0.5  $\mu\text{M}$ . The limitation to this design was the large mismatch in size between the tube and the wire, as seen in Figure 4.6. As a result a large dead volume occurs at the detector, leading to peak broadening and subsequent decrease in analyte signal. Attempts to use larger diameter wires were made, but insertion without electrical contact posed challenges<sup>8, 48</sup>. Holland and Lunte, also employed the use of a dual-electrode for the detection of thiols and disulfides, but used indirect detection via oxidation of bromide ( $\text{Br}^-$ ) to bromine ( $\text{Br}_2$ ) at Pt electrodes<sup>8</sup>. The downstream electrode is used as the detection electrode where electrogenerated bromine is measured. The response is proportional to the concentration of reacted analyte present<sup>8</sup>. Holland found that a wire-wire configuration, shown in Figure 4.7, resulted in the best LOD. In this configuration, upstream Pt electrode was inserted into the capillary disrupting the flow of buffer and allowing for better reaction of  $\text{Br}^-$  with the thiols present. The detection electrode was composed of a second Pt wire placed across the outlet of the capillary without making contact with the upstream electrode<sup>8</sup>. This configuration resulted in LOD's of 80 nM due in part to limited diffusion of the analyte away from the electrode surface.

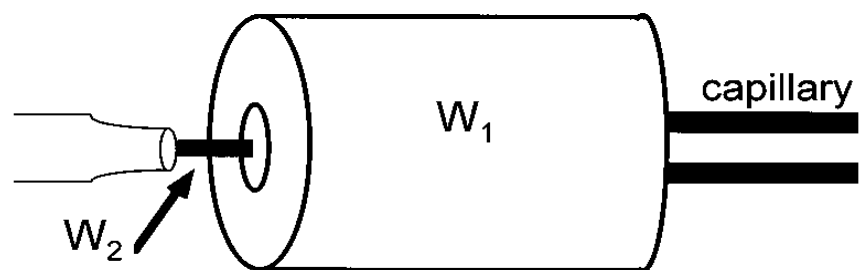


Figure 4.6: Tubular-wire dual Au/Hg electrode configuration from Holland et al. with permission<sup>8</sup>.

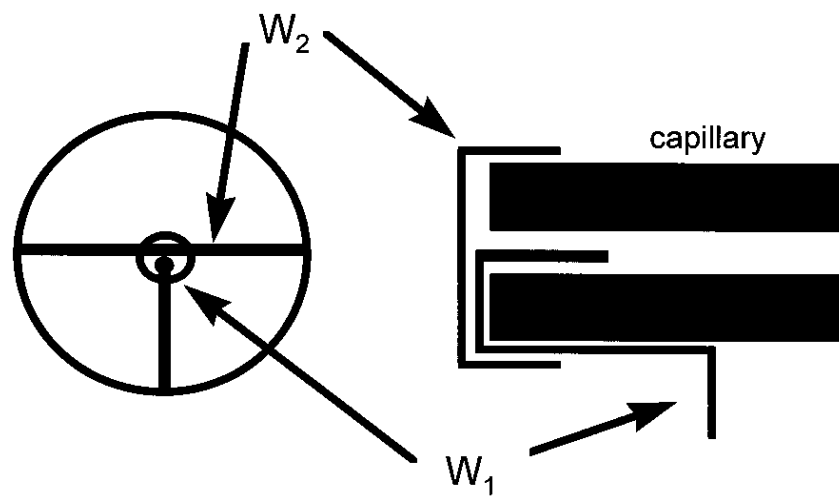


Figure 4.7: Wire-wire dual Pt electrode configuration from Holland et al. with permission <sup>8</sup>.

Although, dual-electrode detection allows for thiols and disulfides to be detected in one injection with no derivatization, fabrication of these detectors in conjunction with integration to CE makes them less appealing. None-the-less the selectivity and sensitivity that can be achieved with this mode of detection makes the development of more robust and sensitive detection schemes of great interest.

#### 4.1.3 Specific Aims

The aim of this research was to take the previously developed parallel-dual electrode from Chapter 3 and fabricate a dual-Au/Hg amalgam electrode for the detection of thiols and disulfides. The signal enhancement and thus the improvement in sensitivity observed for the carbon-fiber dual electrode through redox-cycling would be advantageous for the detection of low molecular weight thiols and disulfides, such as cysteine and homocysteine, which are not present in high concentrations within the brain. In addition, most methods, with the exception of the CE-UV method reported by Rabenstein *et al.*, only assess one or two of the thiols and disulfides, most notably glutathione and GSSG. Therefore, in addition to implementing the dual-parallel electrode design, the second focus was to develop a method for the detection of homocysteine, cysteine, glutathione and their corresponding symmetrical disulfides.

## 4.2 Experimental

### 4.2.1 Chemicals and Reagents

Sodium tetraborate decahydrate (Borax), tetradecyltrimethylammonium bromide (TTAB), methyl- $\beta$ -cyclodextrin, glutathione (GSH), glutathione oxidized (GSSG), cysteine (Cys), cystine (Cys<sub>ox</sub>), homocysteine (Hcy), homocystine (Hcy<sub>ox</sub>) and N-ethylmaleimide (NEM) were all obtained from Sigma-

Aldrich (St. Louis, MO, USA). Anhydrous sodium phosphate dibasic was purchased from Fisher Scientific (Pittsburgh, PA, USA).

#### 4.2.2 Dual Au/Hg Electrode Fabrication

The dual-parallel Au/Hg electrode fabrication was based on the design of the dual CF electrode described in Chapter 3. For this application 25  $\mu\text{m}$  diameter Au wire (Goodfellow, Oakdale, PA, USA) were used in place of the carbon fiber electrodes, as previously described. Briefly, two single 25  $\mu\text{m}$  Au electrodes were fabricated by threading the Au wire through fused silica capillary (105  $\mu\text{m}$  o.d., 40  $\mu\text{m}$  i.d.) leaving approximately 2 mm of Au exposed at both ends of the capillary. One of the fused silica capillary pieces was flame etched to remove the polyamide coating. This was done to ensure that the electrodes could be inserted into the opening of the capillary. One end of the exposed Au wire was inserted into a 23 gauge needle, which had an opening bored into the side of the needle. Each single Au wire was inserted into the needle until it reached the opening in the side of the needle. A drop of colloidal silver paste (Ted Pella, Redding, CA, USA) was then spread over the opening in the needle in order to make the electrical connection for the WE's. At this point the single electrodes were cleaned by filling a 10 mL beaker with 100 % EtOH for 1 min, submerging the exposed Au surface. This was followed by a 30 sec cleaning with H<sub>2</sub>O. A 5 mL beaker was used to contain 50 g of Hg (Sigma Aldrich, St. Louis, MO, USA, electronic grade). The exposed Au wires were submerged into the Hg and exposed for 12 sec before being removed. Times for Hg amalgamation were based off of those reported by O'Shea and Lunte<sup>23</sup>. Times were varied to optimize Hg coating; 4, 8, 10 and 12 sec amalgamations were tested. Times of 4 and 8 sec were found to be too short to adequately amalgamate the surface of the electrode. 10 and 12 seconds resulted in sufficient coating without dissolving the Au wire. No appreciable difference in noise was observed between the two times; therefore, 12 sec was used for the amalgamation of all Au electrodes. The single electrodes were allowed to equilibrate for a minimum of

10 hours (or overnight) prior to use. The two single electrodes were then UV glued together making sure the tips of the electrodes were in alignment. The combined electrodes were then fed through a 1.5-2.0 cm length piece of fused silica capillary (658  $\mu\text{m}$  o.d, 537  $\mu\text{m}$  i.d.) for rigidity and support. Super glue was used to affix the electrodes to the support. Electrodes were trimmed using tissue scissors to a length of 1600  $\mu\text{m}$  ( $\pm 12 \mu\text{m}$ ) and an average width of 55  $\mu\text{m}$  ( $\pm 9.0 \mu\text{m}$ ).

#### 4.2.3 Instrumentation and Separation Conditions

##### 4.2.3.1 Micellar Electrokinetic Chromatography

In Micellar Electrokinetic Chromatography (MEKC) species interact with micelles that are added to the buffer solution, with the separation occurring based on charge-charge interaction. This occurs through the formation of micelles. Micelles are formed via micelle molecules that aggregate above the critical micelle concentration (CMC). Above the CMC surfactant molecules interact with one another with the hydrophobic tails lining the inside of the micelles while the head groups that are hydrophilic and charged comprise the outside surface. Based on this arrangement partitioning either occurs based on hydrophobic interactions or ionic attraction.

The mobility of the micelles is slower than the EOF with migration toward either the cathode or anode based on the respective charge of the micelle. Because the micelles are migrating in the field as well, an additional window for migration is formed. Neutral molecules migrating with the EOF will partition between these two phases, resulting in the ability to resolve neutral molecules.

#### 4.2.3.2 Separation conditions and electrode pretreatment

Electrophoresis was performed using a high voltage (0-30 kV) power supply (Spellman High Voltage, Hauppague, NY, USA). The cathodic end of the capillary was isolated in a Plexiglas box containing an interlock for the user safety. Fused silica capillaries (Polymicro Technologies, Phoenix, AZ, USA) 25  $\mu\text{m}$  i.d. and 80 cm in length were used for the separation of the thiols. The outlet of the capillary was placed into the EC cell containing BGE.

In order for the dual-parallel electrode to be inserted into the separation capillary, the outlet of the capillary was modified using HF acid, a concept inspired by work described previously by Ewing *et al.*<sup>49</sup>. Briefly, HF etching was done by submerging the outlet end of the capillary into 49% HF acid for a period of 100 min. This resulted in an opening ( $\sim 230 \mu\text{m}$ ) sufficient for insertion of the dual-parallel electrode. Furthermore, with this etch time a maximum insertion depth of  $\sim 660 \mu\text{m}$  was possible.

Prior to placing electrodes into the CE system, cyclic voltammograms were run as a means to precondition the electrode surfaces. Electrodes were then placed in BGE, six successive scans were run from +0.3 V to -1.0 V. The electrodes were then immediately placed into the detection cell. After insertion into the capillary, electrodes were slowly increased to estimated working potentials ( $WE_1 = +0.1$  V and  $WE_2 = -1.0$  V). BGE was allowed to flow through the capillary at 40 psi for 1 hour with the electrode on, followed by 1 hour with separation voltage at -21 kV. This time was sufficient for the background current to stabilize at both electrodes. A platinum auxiliary electrode and a Ag/AgCl reference electrode (Bioanalytical Systems, West Lafayette, IN, USA) were used. The Au/Hg working electrodes were controlled by two LC-4C potentiostats (Bioanalytical Systems Inc., West Lafayette, IN, USA). All applied potentials reported were against a Ag/AgCl reference electrode. Data acquisition was performed with Chrom&Spec software (Ampersand International, Inc., Beachwood, OH, USA) at a frequency of 10 Hz per channel.

#### 4.2.4 Standard and Sample Preparation

Stock solutions of each analyte were prepared weekly in 0.1 M HClO<sub>4</sub>, except for cystine in this case 0.1 M HCl was used, due to solubility. All stock solutions were prepared to a final volume of 1.0 mL. Stock solutions were diluted in aCSF (145 mM NaCl, 2.7 mM KCl, 1.0 mM MgCl<sub>2</sub>, 1.2 mM CaCl<sub>2</sub>, 0.45 mM NaH<sub>2</sub>PO<sub>4</sub>, 2.33 mM Na<sub>2</sub>HPO<sub>4</sub>, pH 7.4) containing 0.1 mM EDTA and 1.0 mM HClO<sub>4</sub> in order to keep the concentration of acid constant at a concentration of 2.0 mM.

Liver dialysate samples were obtained using the same surgical procedure, probe dimensions and probe implantation as reported by Price and Lunte<sup>50</sup>. After implantation, the probe was flushed for 30 min with aCSF prior to sample collection. Samples were collected every 30 minutes at a flow rate of 1 μL/min. The collection vials each contained 3 μL of 2.0 mM HClO<sub>4</sub> and 0.1 mM EDTA. Samples were immediately placed in the freezer at -20°C until they could be analyzed. Under these conditions samples were stable for at least 24 hours. In order to observe damage induced from oxidative stress. Doxorubicin was dosed at a concentration of 2 mg/mL for 1 hour at a flow rate of 1 μL/min. After 1 hour the syringe was switched back to aCSF and samples continued to be collected for an additional 90 minutes. This time had been shown previously to be adequate for the clearance of doxorubicin and reestablishment of basal concentrations of GSH and GSSG<sup>50</sup>. For experiments using NEM 0.5 μL of 0.16 M NEM was added to 10 μL aliquot of a given sample and allowed to react for 5 min. Samples were then directly injected onto the system. The same conditions used for the in vivo studies with NEM were also applied to standard solutions.

#### 4.3.0 Results and Discussion

##### 4.3.1 Method Development

As mentioned previously, several CE methods have been published to separate thiols and disulfides in various biological matrices, namely plasma and urine. Currently, only one method using CE-UV has separated all three reduced thiols and their corresponding disulfides in one injection<sup>42</sup>. In this method normal polarity (+15 kV) was employed with a 0.1 M phosphate pH 2.3 buffer. Stocks were prepared in 1.0 M HCl and diluted in run buffer prior to analysis. As pH 2.3 is below the pKa of the carboxylic acid functional group all of the analytes had an overall net positive charge. Under these conditions all six analytes were baseline resolved from each other in less than 20 min using a 50  $\mu\text{m}$  i.d. capillary x 50 cm (300 V/cm). Although the separation length of the capillary and capillary i.d. could not be used with end column detection, the buffer conditions were used as an initial starting point for the method development. A 75 cm length, 25  $\mu\text{m}$  i.d. capillary was used with the buffer conditions reported by Rabenstein *et al.* Under these conditions no response was observed before 80 min. Acidic buffers have no EOF with subsequent slow migration of analytes through the field, which was only exacerbated by the longer capillary lengths used for end column detection proposed here in. Therefore, these conditions were not further pursued.

###### 4.3.1.1 Normal Polarity

In normal polarity the cathode is placed at the outlet and the anode is placed at the inlet of the capillary. The order of ions migrating in the field is cations, neutrals, and then anions. The initial approach for the separation of these analytes was to use a high pH buffer (pH  $\geq$  9) creating a strong EOF with rapid analysis times. At basic pH there would be a net negative charge on each of the analytes theoretically

creating the largest discrepancies in migration times. Due to the similarities in structure between the analytes especially Cys, Cys<sub>ox</sub>, Hcy and Hcy<sub>ox</sub> conditions that would provide the greatest difference electrophoretic migration, while still maintaining rapid analysis, was desirable. Therefore, 40 mM borate pH 9.0 buffer was chosen. Under these conditions Cys and GSH could not be effectively separated. In addition, there was concern about on-capillary oxidation of thiols due to the basic conditions; however, no significant evidence of this was observed. Methods by O'Shea and Lunte for the analysis of Cys, GSH and GSH had used 10 mM MES, pH 5.5 buffer, with a 95 cm x 75 µm i.d. capillary, separation carried out at +30 kV<sup>23</sup>. MES is a zwitterionic buffer with low conductivity, meaning that higher concentrations can be used without significantly increasing background noise. Under these conditions resolution could not be obtained between Hcy and Cys. Two more acidic buffers were used to try and separate the thiols and disulfides, 20 mM acetate pH 4 and 20 mM phosphate pH 2.5. A broad peak was observed at 80 min in the acetate buffer and no response was observed in the phosphate buffer after 40 min. Furthermore, addition of solvents, varying the pH, ionic strength and separation voltages were also assessed in order to better resolve the analytes of interest.

#### 4.3.1.2 MEKC Approach using Normal Polarity

In order to gain better resolution between the analytes surfactant was added to several of the buffers mentioned in the previous section. Initially, 10 mM SDS was added to the 40 mM borate, pH 9 buffer. The addition of surfactants, above their critical micelle concentrations (CMC) provides an additional separation phase by which analytes partition in and out of the micelles based on charge interactions. Under these conditions, resolution could be obtained between Cys and GSH with migration times less than 25 min. Upon addition of Cys<sub>ox</sub> and Hcy<sub>ox</sub> to the sample mixture resolution could not be obtained between these analytes and Cys. As summarized in Table 4.1, several different surfactants (*i.e.* cationic and neutral surfactants, cyclodextrins) were evaluated in order to achieve separation.

Buffer	Migration Time (min)	Issues	Things Tried	Outcome
Boric Acid	10 min, Hcy	Poor response for GSH Potential on-capillary oxidation	Increasing and decreasing ionic strength pH (8-9.5) Concentration of SDS (10-80 mM )	Concerned about on-capillary oxidation  could not resolve disulfides (Hcy <sub>ox</sub> /Cys <sub>ox</sub> from Cys,
MES	9.5 min, Hcy 13 min, GSH	Co-migration of Hcy and Cys	Surfactants (TTAB, SOS, $\beta$ -CD) Ionic Strength Solvents (MeOH, ACN) pH 4-6.5 Separation Voltages	Not able to separate Hcy and Cys
20 mM Acetate, pH 4.0	Broad "peak" 80 min GSH	Long migration times	-	-
20 mM Phosphate, pH 2.5	No response after 45 min	-	-	-
95:5 (v/v) Tris/Phosphate, 5 mM sulfate- $\beta$ -cyclodextrin, pH 7: 1,4-dioxane	19 min, Hcy 20 min, Hcy <sub>ox</sub> /Cys 20.5 min, Cys <sub>ox</sub> 30 min, GSH 35.5, GSSG	Poor response for GSSG Co-migration between Cys and Hcy <sub>ox</sub>	Increasing ionic strength Increasing pH (8-9) Increasing or decreasing $\beta$ -CD or 1,4:dioxane	Could not separate Cys and Hcy <sub>ox</sub>

Table 4.1: Summary of normal polarity buffer conditions.

The various types of surfactants were added to change the charge-charge interactions. Cyclodextrins have been traditionally used to separate aromatic compounds. Integration of charged species, such as sulfates on to cyclodextrins created additional negative charge effect slowing electrophoretic mobility<sup>51</sup>. Although no significant interaction was expected between the thiols and disulfides with cyclodextrins any minimal interaction based on charge or change in viscosity was seen as a potential advantage in the separation of these compounds. As Hcy and Cys differ only by one carbon, their electrophoretic mobility's will be essentially identical under more acidic or even basic conditions where they will carry the same net charge. They only differ marginally in the pKa of the sulfhydryl group, due to their slightly different reactivity and distance from the electrophilic amine. Therefore, the focus was turned to a more neutral to slightly basic pH range (pH 7-8). A report by Zhong et al. used a tris/phosphate buffer in conjunction with sulfated- $\beta$ -cyclodextrin, methyl cellulose and 1,4 dioxane at pH 7 for the separation of protein isomers<sup>52</sup>. For this buffer 40 mM tris pH 7 was attained, pH adjusting with 0.1 M Sodium phosphate (monobasic) pH 2.0. Sulfated- $\beta$ -cyclodextrin was added at a concentration of 2.0 mM. Under these conditions Hcy and Cys were not baseline resolved. The concentration was then increased to 5 mM sulfated- $\beta$ -cyclodextrin and better resolution was obtained. No additional improvement in resolution was obtained with higher concentrations of cyclodextrin. The viscosity of the buffer can also be used to enhance separations often by disrupting the charge-charge interactions with the walls of the capillary or surfactants. The addition of 5 % (v/v) 1,4-dioxane to the buffer achieved baseline resolution between Hcy and Cys. Addition of oxidized Hcy and Cys, Hcy<sub>ox</sub> and Cys<sub>ox</sub>, respectively resulted in co-migration with Cys, Figure 4.8. Addition of more 1,4-dioxane at 10% and 20% (v/v) had no additional effect on the separation. The pH and ionic strength were increased in separate steps, but resolution could not be improved under these buffer conditions. It is likely that the addition of sulfated- $\beta$ -cyclodextrin minimized any charge-charge interactions of the standards with the wall of the capillary, but only to a limited point. The limited charge-charge interactions that may have occurred between the

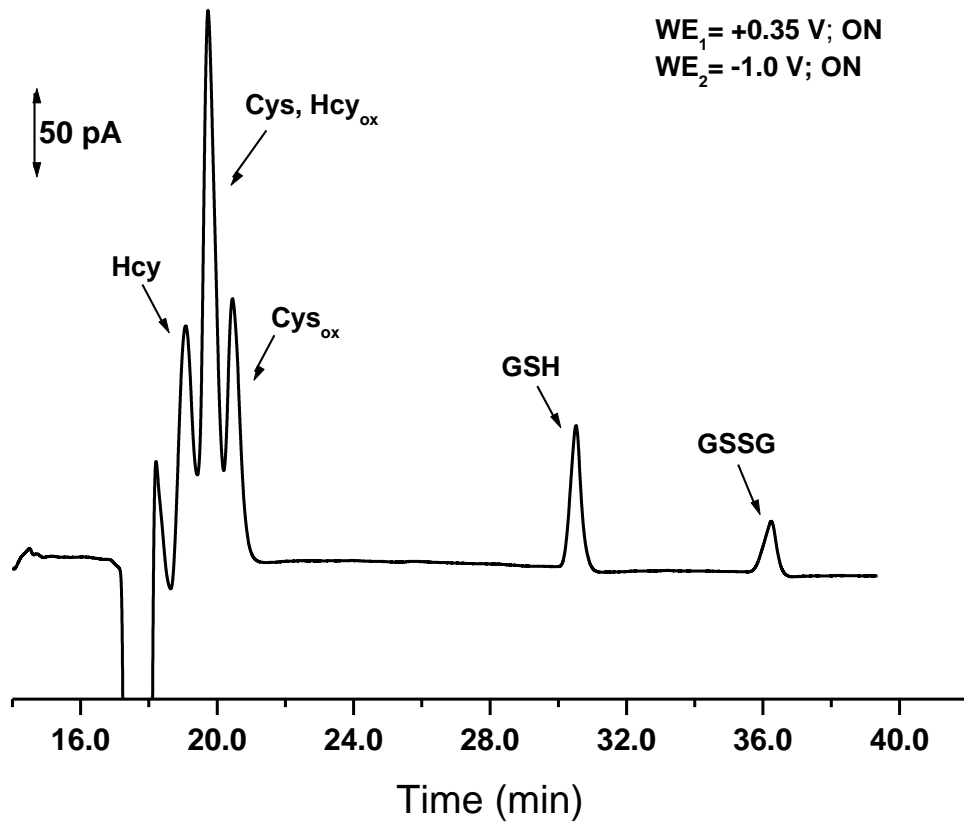


Figure 4.8 Injection of all six standards with both electrodes on. Separation conditions: 40 mM Tris, 5 mM sulfated- $\beta$ -cyclodextrin, pH 7.0 (adjust with 0.1 M monobasic sodium phosphate anhydrous (pH 2.0)) with 5% (v/v) 1,4-dioxane; +17 kV. Injection: 23 psi, 6 sec. Standards: 100 $\mu$ M diluted in 50  $\mu$ M EDTA.

negatively charged sulfhydryl and amine moieties was likely diminished at higher pH, due to deprotonation of the amine. Consequently no improvement in separation was observed even with the addition of more 1,4-dioxane or sulfated- $\beta$ -cyclodextrin.

#### 4.3.1.3 Reversed Polarity

In negative polarity the order of migration is reversed from that of normal polarity by switching the polarity on the electrodes at both the inlet and outlet. The addition of TTAB to the buffer is used to change the charge on the walls of the capillary thereby reversing the EOF. Under normal polarity conditions better responses and separations were achieved in either neutral buffers or more basic buffers. In both neutral and basic buffers, the analytes will be negatively charged or neutral migrating against or with the EOF. Therefore by running the separation in reversed polarity the disulfides and thiols will migrate at the front of the sample zone instead of the back, taking further advantage of their varying charge states, potentially improving resolution not attained with normal polarity.

From the normal polarity mode a 10 mM borate/ 10 mM phosphate/ 5 mM SDS, pH 8.2 buffer shown in Figure 4.9, resulted in baseline resolution between all of the analytes except for Cys, Hcy<sub>ox</sub> and Cys<sub>ox</sub> without the complex buffer conditions used to attain the same separation at pH 7 with the tris/phosphate buffer. Therefore, this buffer was initially used for the separation in negative polarity, with the exception that no SDS was used, but instead TTAB (0.5 mM) was added to reverse the EOF. This resulted in the co-migration of GSSG and GSH, Cys<sub>ox</sub> and Cys, Hcy and Hcy<sub>ox</sub>. As the ionic strength of this buffer is far less than that of Ringer's (~100 mM), it was assumed that severe de-stacking would occur; therefore, these conditions were not further pursued. Instead pH mediated base stacking, which was developed in our lab was tried<sup>9,53</sup>.

pH mediated stacking was developed in order to improve peak efficiencies in dialysate samples without diluting the sample matrix or extraction from the sample matrix.

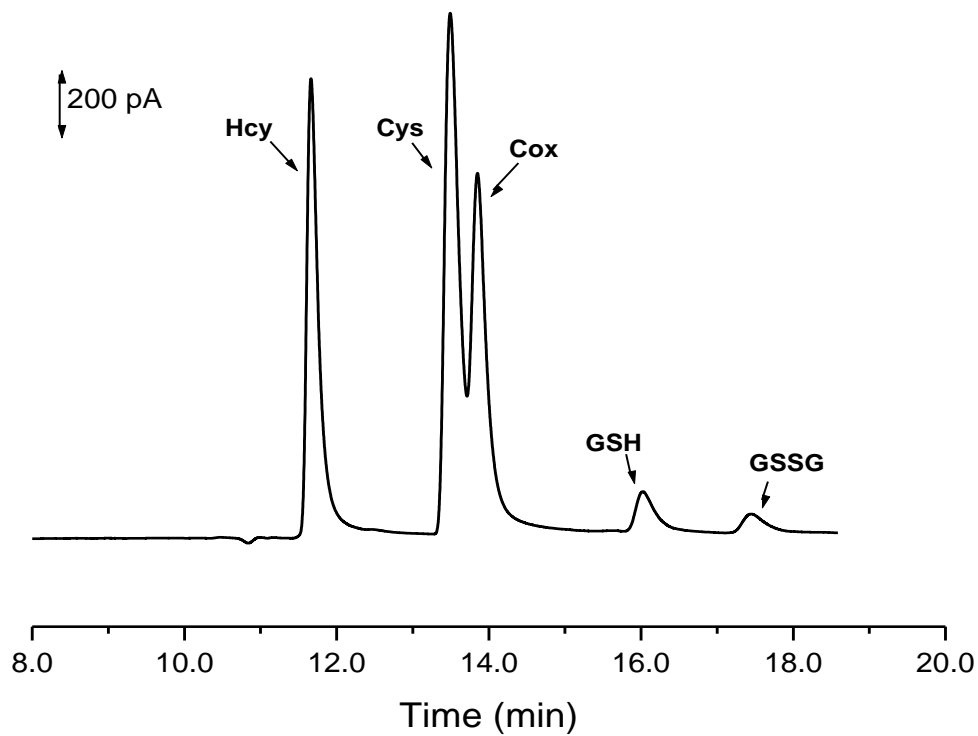


Figure 4.9: Injection of thiols, Cox and GSSG. Separation conditions: 10 mM borate/10 mM dibasic phosphate, 5 mM SDS, pH 8.2; + 17 kV. Injection: 15 psi, 3 sec.  $WE_1 = +0.1$  V,  $WE_2 = -1.0$  V. Standard concentrations 25  $\mu$ M thiols, 50  $\mu$ M GSSG diluted with 1.0 mM  $HClO_4$ /50  $\mu$ M EDTA.

High ionic strength samples, such as dialysate, result in de-stacking due to the high conductivity sample zone in the presence of low field strength<sup>53</sup>. In pH mediated base stacking, a weak base generally an ammonium salt is effectively titrated on capillary using 0.1 M NaOH<sup>9, 53</sup>. Titration of the sample zone with base creates an area of low conductivity through which anions can then move quickly through and stack at the front of the zone. Hoque and Lunte applied this methodology for the separation of GSH and GSSG in dialysate samples using CE-UV. In this method a 50  $\mu\text{m}$  i.d. capillary (60 cm total, 45 cm effective length) with a buffer consisting of 100 mM ammonium hydroxide, 0.5 mM TTAB at pH 8.4 was used as the background electrolyte (BGE). Stacking was achieved by EKI, 30 sec of sample followed by 60 sec of 0.1 M NaOH both at  $-10\text{ kV}$ <sup>9</sup>. Under these conditions a 26-fold increase in response was observed when compared to an injection of dialysate with no base stacking. Using these buffer conditions for CEEC with the dual Au/Hg electrode and a capillary length of 80 cm (25  $\mu\text{m}$  i.d.), only one peak was observed when all six analytes were injected. Various injection lengths were tried with these conditions, but no further resolution was obtained. Arnett and Lunte had also published a report using pH mediated stacking for the analysis of 8-oxoguanine and 8-hydroxy-2'-deoxyguanosine. For this method a 40 mM borate/50 mM Tris, pH 8.6 was used for the separation, with a 60 sec EKI of sample, followed by a 15 sec EKI of 0.1 M NaOH. Similar conditions were tried to separate out the thiols and disulfides. Varying injection times for both the sample and base were tried with no improvement in resolution. Additionally, a large peak migrating just after the analytes was consistently observed. It was determined that this peak was the result of untitrated base, which was found to strip the Hg from the surface of the Au electrodes. As a result, pH base mediated stacking was not further explored.

In reversed polarity the best response observed had been with the low ionic strength borate/phosphate buffer first mentioned. Resolution between analytes was not observed under the low ionic strength conditions; as a result ionic strength was increased until no further improvement in resolution was observed. Separations conditions consisting of 50 mM borate/ 50 mM phosphate, 0.5 mM TTAB, pH 8.2

resulted in some resolution, not baseline, of GSH and GSSG; however, no resolution was obtained for the later migrating peaks, shown in Figure 4.10. In order to decrease the effect of the EOF and thereby slow the separation down the pH of the BGE was decreased from 8.2 to 7.4. This adjustment in pH resulted in a decrease in resolution between Cys and Cys<sub>ox</sub>, but an increased resolution between the later migrating standards, as shown in Figure 4.11. In order to improve resolution between standard peaks, several different surfactants were added to the BGE at both pH 8.2 and pH 7.4. Negatively charged surfactants such as, SDS and sulfated- $\beta$ -cyclodextrin were determined to interact to a large extent with TTAB. This resulted in significant drag on the EOF resulting in long migration times (+ 40 min) with significant peak broadening. At lower concentrations or concentrations below the CMC ( $\leq 5$  mM), as is the case for SDS, no significant improvement in resolution was observed. A zwitterionic surfactant, CHAPS was also investigated. Because CHAPS possess both positive and negative charges it was thought that there would be a stronger charge-charge interaction between Cys, Cys<sub>ox</sub>, Hcy and Hcy<sub>ox</sub> primarily because of the negatively charged carboxylic acid and the positively charged amine present on all of these analytes. In addition, it was also thought that if the charge-charge based interaction between the analytes and CHAPS was not significant, the CHAPS might decrease any potential interaction of the analytes with the TTAB perhaps also improving the resolution. Above the CMC (5.0 mM) the same effects observed with the negatively charged surfactants also effected this separation. However, at a concentration well below the CMC (2.0 mM) baseline resolution was obtained between Cys<sub>ox</sub> and Cys, but diminished between GSH and GSSG. As a result, the addition of neutral cyclodextrins was then tried. The choice of adding neutral cyclodextrins was not desirable due to strong interaction with the EOF and subsequently longer migration times that were likely. An initial concentration of 10 mM methyl- $\beta$ -cyclodextrin was added to the BGE. Significantly longer migration times were observed (50 min for GSSG), as a result a much smaller concentration was then added, 50  $\mu$ M.

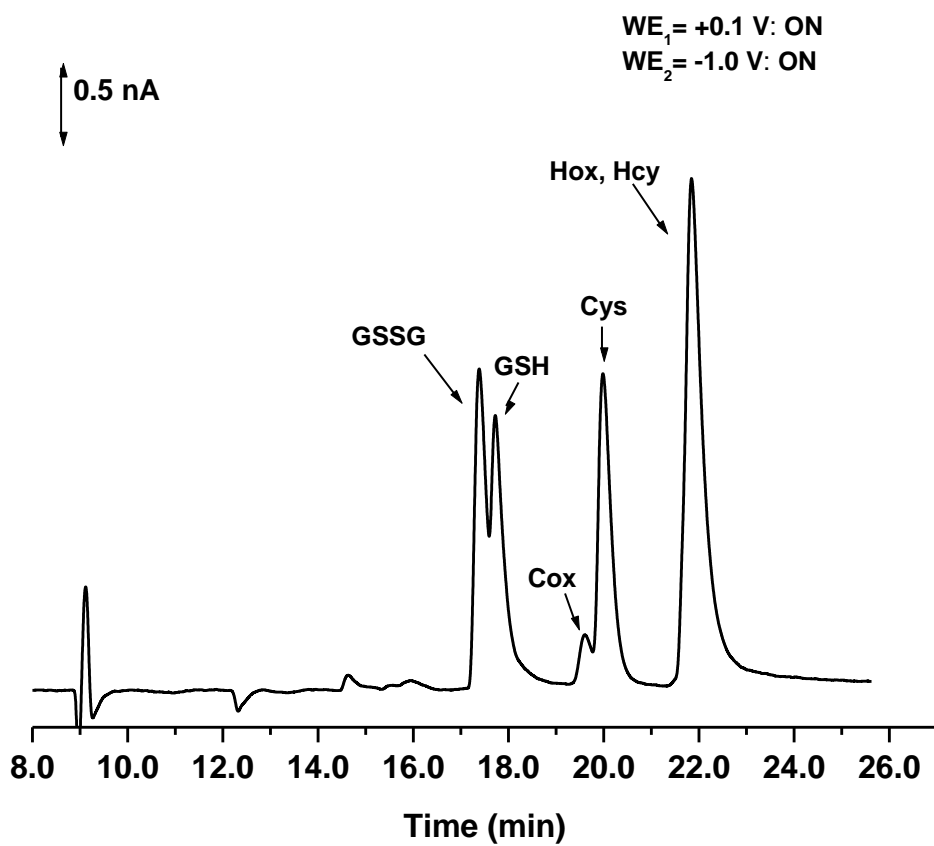


Figure 4.10 Injection of all six standards. Separation conditions: 50 mM borate/50 mM phosphate, 0.5 mM TTAB, pH 8.2; -15 kV. Standards were diluted to 50  $\mu$ M and 100  $\mu$ M, thiols and disulfides, respectively with 1.0 mM HClO<sub>4</sub>/50  $\mu$ M EDTA.

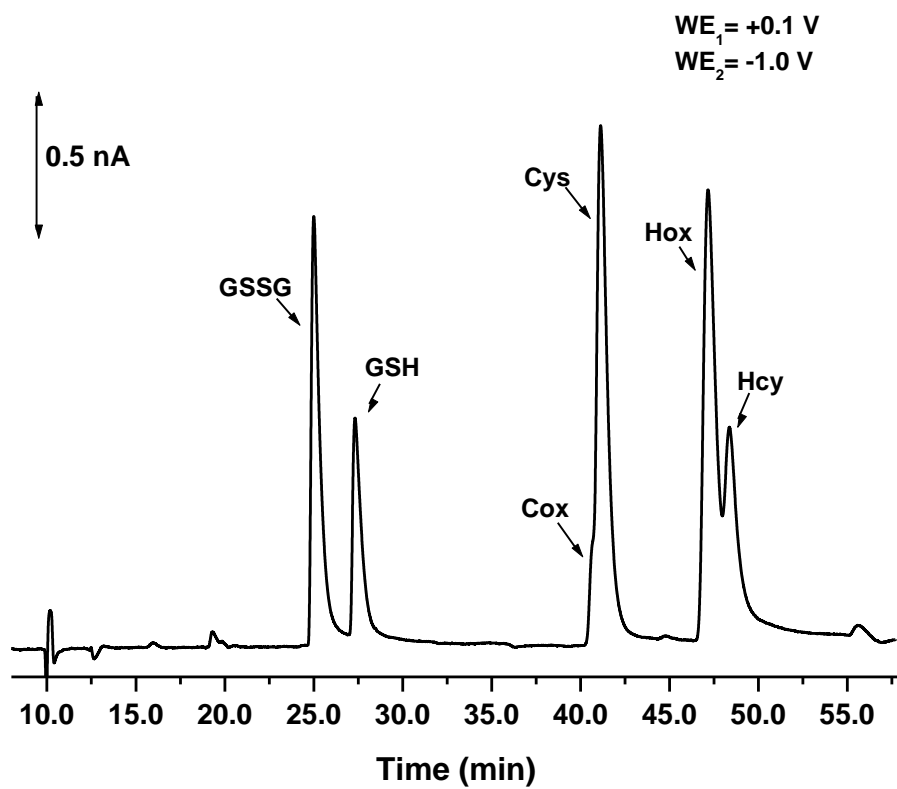


Figure 4.11: Injection of all six standards. Conditions were the same as reported in Figure 4.10 except the pH of the buffer was decreased to pH 7.4.

Figure 4.12, shows the addition of 75  $\mu$ M methyl- $\beta$ -cyclodextrin to the BGE. Capillary length was also investigated as a means to improve the resolution between the analytes. By increasing the capillary length selectivity can be improved by providing the analytes more time in the electric field. The capillary length was increased to 97 cm, but no improvement was observed in resolution between Cys and Cys<sub>ox</sub>. Although, these conditions did not significantly improve the separation over those shown in Figure 4.12 the increased capillary length resulted in decreased separation currents and subsequently decreased noise at the detector. These conditions were therefore used to evaluate the dual Au/Hg electrode. Table 4.2 summarizes the results from this section.

#### 4.3.2 Dual-Au/Hg Electrode

Hydrodynamic voltammograms (HDV) were initially generated to establish optimum working potentials for the reduction and oxidation of the thiols and disulfides. The oxidation potential was established first by injecting the reduced thiols. For this set of experiments WE2 was turned off and WE1 was incrementally stepped from -100 mV to +100 mV. Potentials above +100 mV showed a significant decrease in response, which was attributed to the oxidation of Hg. Based on the HDV shown in Figure 4.13 A the optimum working potential for the oxidation of thiols was determined to be +0.05 V. After the working potential for the oxidation of the thiols was determined the reduction potential for the disulfides was established. In this case only disulfides were injected. WE1 was held at +50 mV while adjusting the voltage applied to WE2 from -900 mV to -1.3 V. The noise at WE2 was too high to monitor the response at this electrode; consequently the reoxidation occurring at WE1 was used to determine the optimum reduction potential for WE2. The normalized response is shown in Figure 4.13 B. It should be noted that significant variation in optimum applied voltage differs from electrode to electrode. Variations between  $\pm$  50 mV were frequently observed between sets of electrodes.

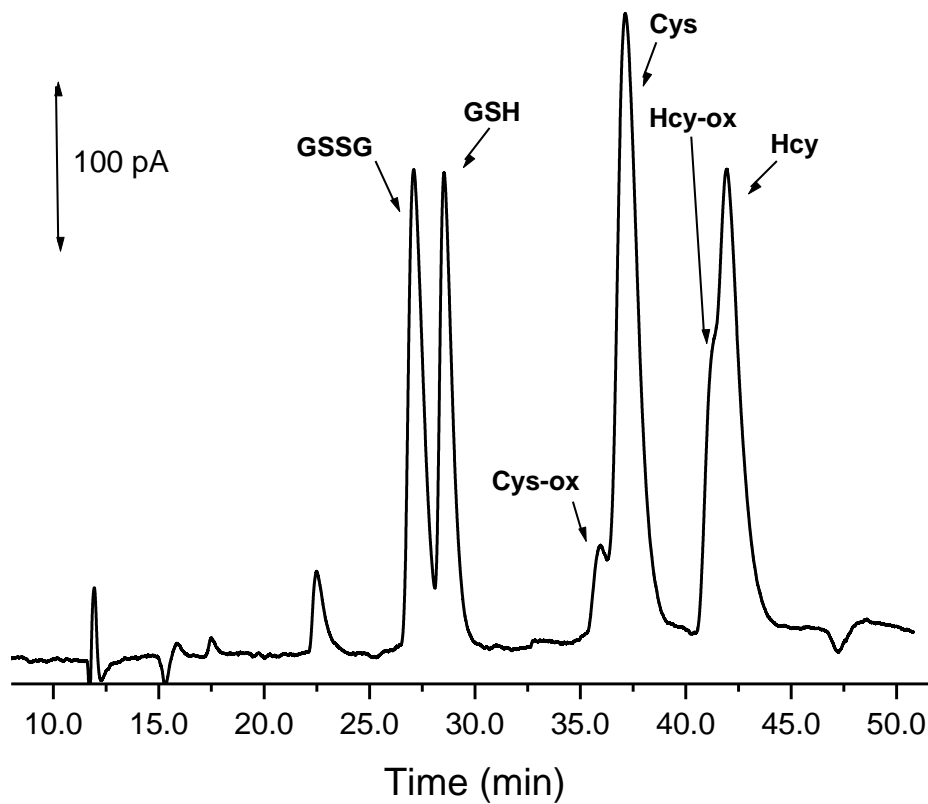


Figure 4.12: Injection of all six standards. Separation conditions: 60 mM Borate/60 mM Phosphate, 0.5 mM TTAB, 75  $\mu$ M methyl- $\beta$ -cyclodextrin, pH 7.4; -12 kV. Injection 15 psi, 3sec. Standards diluted to 25  $\mu$ M and 50  $\mu$ M for thiols and disulfides, respectively.

<b>Buffer</b>	<b>Migration Time (min)</b>	<b>Issues</b>	<b>Things Tried</b>	<b>Outcome</b>
10 mM Borate/10 mM Phosphate, pH 8.2	12-18 min	Co-migration	-	Not able to separate standards
100 mM Ammonium Hydroxide, pH 8.4	16 min	Co-migration	Varying sample injection time/base times	Not able to separate standards
40 mM Borate/50 mM Tris, pH 8.1	12-20 min	Co-migration	Varying sample injection times/base times, increasing concentration of Tris	Not able to separate standards, large amounts of base strip electrodes
50 mM Borate/ 50 mM Phosphate, pH 7.4	20-36 min	Co-migration	Varying concentrations of both borate and phosphate, increasing pH, addition of surfactants (negative, zwitterionic, neutral)	Not able to separate standards

Table 4.2 Summary of buffer conditions used to separate thiols and disulfides in negative polarity.

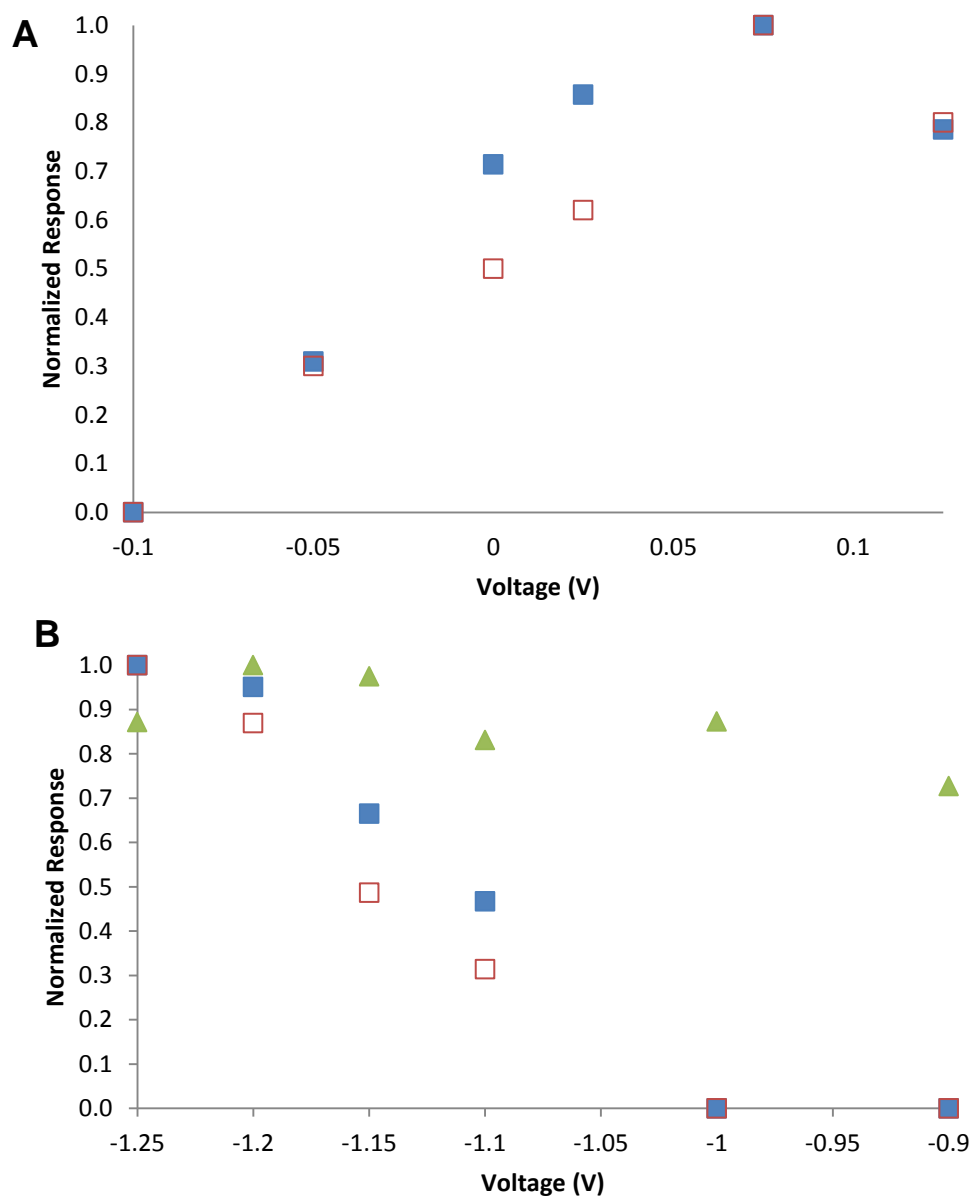


Figure 4.13: Hydrodynamic voltammograms. A) Voltammetry of GSH using the dual electrode with WE<sub>1</sub> on only (■) and both WE<sub>1</sub> and WE<sub>2</sub> turned on (□). B) Response of Cys<sub>ox</sub> (□), Hcy<sub>ox</sub> (▲), and GSSG (■) at WE<sub>1</sub> with voltage varied at WE<sub>2</sub>.

Therefore, several points over the expected potential range should be run to establish the correct voltages prior to using each set of electrodes. Because the electrodes can be operated in a parallel opposed mode an HDV with both electrodes on was constructed to confirm no change in voltammetry. This was done by injecting only the thiols holding  $WE_2$  at  $-1.225$  V and varying the voltage at  $WE_1$  from  $-50$  mV to  $+0.1$  V. From this it was determined that the voltammetry at the oxidation electrode was unchanged whether operating the system as a single electrode or in a parallel opposed configuration.

#### 4.3.2.1 Mechanism of Response for Dual Au/Hg Electrode

As discussed previously all of the dual-electrode detection schemes used to date for the determination of thiols and disulfides have used electrodes in a series configuration, as Alison and Shoup initially published<sup>1</sup>. In the series configuration as shown in Figure 4.14, the upstream electrode is held at a reduction voltage ( $-1.0$  V), which effectively reduces all of the disulfides, while the downstream electrode is used for the detection of the thiols and reduced disulfides. This occurs through complexation of the thiol moiety with Hg by which Hg is reduced by the Au electrode surface. Because of the configuration of the proposed dual Au/Hg amalgam electrode it was unclear if this set of electrodes would behave in a more “traditional” series configuration or if redox cycling would be observed for these electrodes as well. It was initially thought that redox cycling would likely not occur with these electrode based on the difference in the electrochemical mechanism compared with that discussed in Chapter 3. With the parallel-opposed dual carbon fiber electrode developed in Chapter 3; reduced phenolic acids were injected and oxidized at the first working electrode, then reduced at the second working electrode and subsequently reoxidized at the first working electrode.

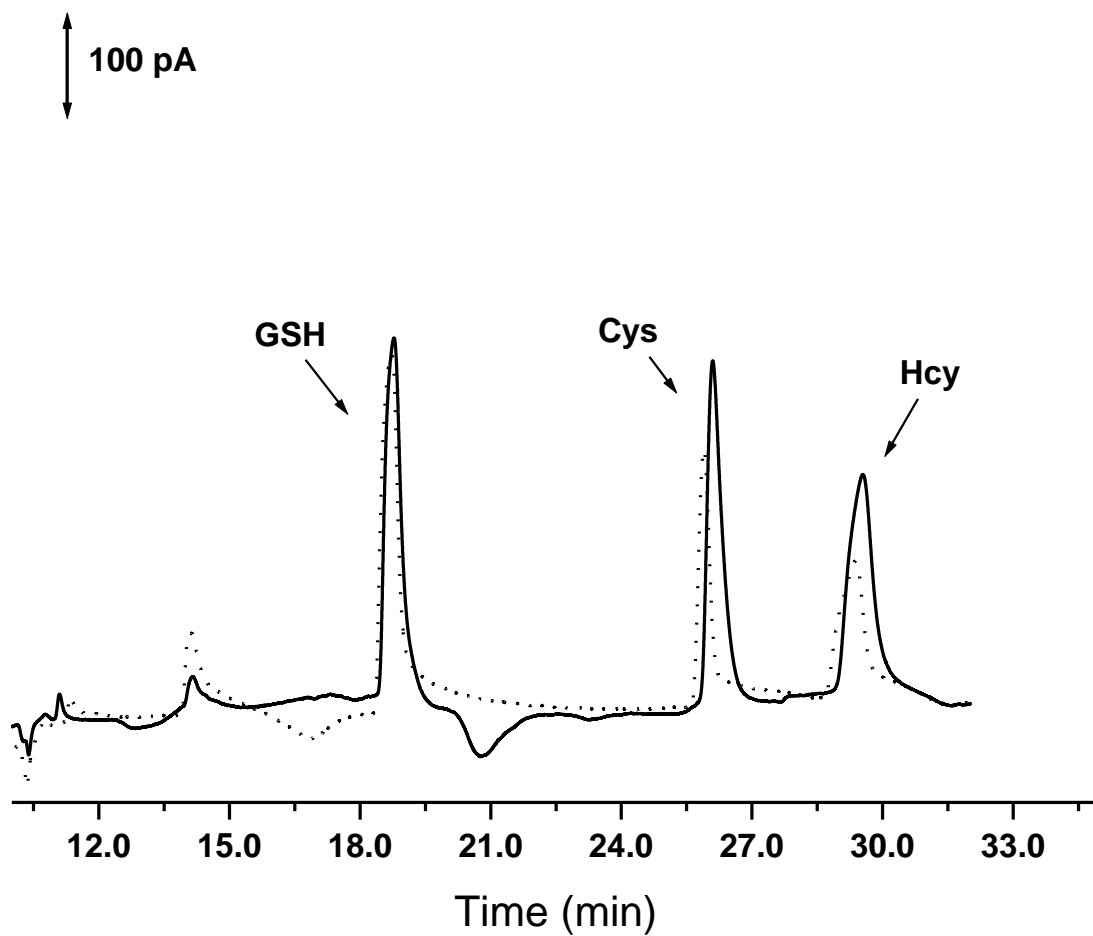


Figure 4.14: Observed signal enhancement of reduced thiols at WE<sub>1</sub>(+0.05 V). Response with both electrodes turned on (—) and with only WE<sub>1</sub> on (---). Conditions: 20 mM Borate/20 mM phosphate, 50 μM methyl-β-cyclodextrin, 0.5 mM TTAB, pH 7.4. Injection: 15 psi, 5 sec. Separation: -21 kV. Standards diluted in aCSF with 1.0 mM HClO<sub>4</sub><sup>-</sup>/0.1 mM EDTA.

Using the 20 mM borate/20 mM phosphate, 0.5 mM TTAB, 50  $\mu$ M methyl- $\beta$ -cyclodextrin, pH 7.4 buffer the electrochemical mechanism was investigated. Due to the applied voltage at WE<sub>2</sub> (-1.225 V) significant baseline noise was observed; therefore, the electrochemical mechanism for the dual Au/Hg electrode was only determined for the thiols using the response at WE<sub>1</sub> (+0.05 V). First the reduced thiols were injected with only WE<sub>1</sub> on. A response was observed for all three analytes of interest. The same standard solution was injected again with both WE<sub>1</sub> and WE<sub>2</sub> on. From Figure 4.14 a minimal increase in response for all three thiols was observed when both electrodes were on compared to the response observed when only using a single electrode. For GSH no signal enhancement was observed and less than 1% signal enhancement was observed for Cys and Hcy. Therefore, no redox cycling was determined to occur with the dual Au/Hg electrode. The mechanism of action is different between these electrodes and the carbon fiber electrodes developed in Chapter 3. In order for redox cycling to be observed with these electrodes Hg(SR)<sub>2</sub> would need to be reduced at WE<sub>2</sub>, as Hg does not participate in the reduction of the thiol it would not be likely that signal enhancement would have been observed.

Under the separation conditions obtained using the 20 mM borate/20 mM phosphate, 0.5 mM TTAB, 50  $\mu$ M methyl- $\beta$ -cyclodextrin, pH 7.4, baseline resolution was not obtained between Cys and Cys<sub>ox</sub>, as well as Hcy and Hcy<sub>ox</sub>, as mentioned previously. This would normally be problematic; however, the dual electrode detector can be manipulated so that the response from each analyte can be determined by using the electrodes in single electrode mode or as a dual electrode. As shown in Figure 4.15 A, when both the reduction and oxidation electrodes are on responses were observed for both disulfides and reduced thiols. The response for the disulfides observed at the oxidation electrode is dependent upon the reduction of the disulfides at WE<sub>2</sub>. If the reduction electrode is turned off and only the oxidation electrode is on then the response from only the thiols was observed, as shown in Figure 4.15 B. Because the second potentiostat uses the first potentiostat as a reference for the applied potential, WE<sub>2</sub> cannot be used independently to assess the response of only the disulfides. In order to determine the response

from only the disulfides NEM was added to the sample matrix. Upon the addition of NEM to the sample matrix the reduced thiols become non-electroactive<sup>20</sup>. As shown in Figure 4.15 C, with both electrodes turned on, in the presence of NEM, no response was observed for the reduced thiols. Furthermore, with both electrodes turned off in the presence of NEM no response was observed (Figure 4.15 D) for either the reduced thiols or the disulfides, which could then be used as a control to confirm both thiol and disulfide peak assignments in dialysate samples. This showed that although co-migration occurred between the later migrating analytes the detector along with the chemical reactivity of these analytes could be used to successfully distinguish the analytes from one another.

A linear range of the dual Au/Hg electrode was observed between 30 $\mu$ M-5 $\mu$ M. These values were reported to be in the range of thiol and disulfide concentrations in liver dialysate<sup>50</sup>. The LOD for GSH was determined to be 1.0  $\mu$ M with no response observed for the other analytes of interest below 5.0  $\mu$ M. These LOD's showed no significant improvement over previously reported methods using dual electrode detection<sup>8, 19, 48</sup>. However, the other previously reported dual electrode systems were all decoupled systems; therefore, LODs using this dual electrode in a decoupled system could significantly improve upon those previously published detection schemes.

#### 4.3.2.1 Monitoring Redox Status *In Vivo*

The ability to monitor thiol tissue redox status *in vivo* is of significant interest due to the roles of these compounds in maintaining cell viability as a result of oxidative injury. Using the conditions for the developed method, baseline resolution was only obtained for GSH and GSSG. However, as shown previously in Figures 4.15 A- 4.15 D utilization if the detector as a single or dual electrode could be used to obtain the response from only the thiols and the chemical reactivity of the reduced thiols with NEM could be used to obtain the response from only the disulfides.

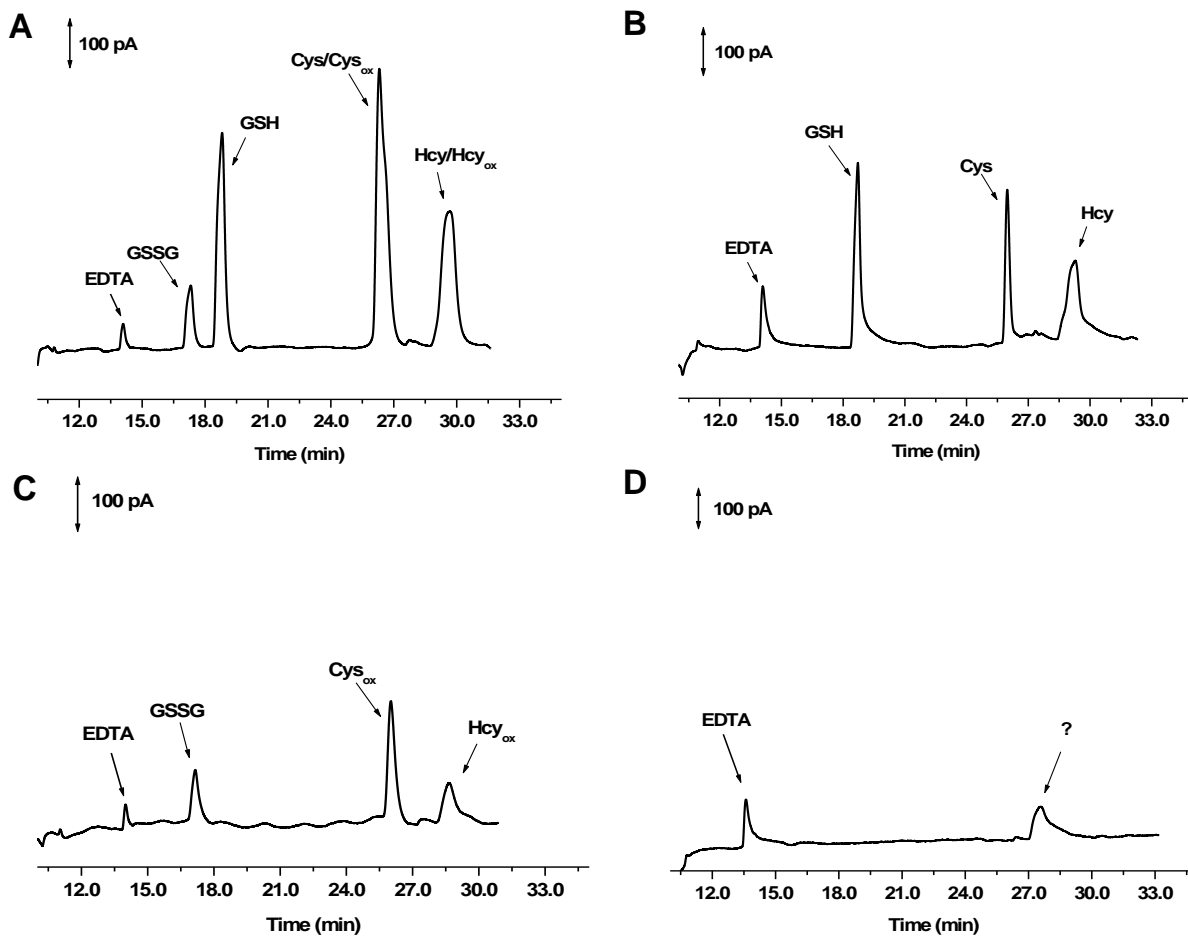


Figure 4.15: Response of reduced thiols and disulfides with both electrodes on (A), with WE<sub>1</sub> only (B), both electrodes on with 0.5  $\mu$ L of 0.16 M NEM added to sample matrix (C), and WE<sub>1</sub> on only with 0.5  $\mu$ L of 0.16 M NEM added to the sample matrix (D). Separation conditions were the same as reported in Figure 4.14.

Using these parameters redox status could be accurately evaluated *in vivo*. Migration times were used to assign peak identities. By comparing the migration times of the standards to the peaks observed in the dialysate samples peaks 1, 2, 3 and 4 were determined to be GSSG, GSH, Cys/Cys<sub>ox</sub> and Hcy<sub>ox</sub>/Hcy, respectively. In order to confirm that thiol and disulfide peaks were assigned correctly, three separate injections of a basal dialysate were made, as shown in Figure 4.16 A-C. In Figure 4.16 A both WE<sub>1</sub> and WE<sub>2</sub> were turned on and responses from both reduced thiols and disulfides were observed. In order to determine if the thiol peaks were assigned correctly, NEM was added to the sample matrix, which resulted in no response observed for the peak identified as GSH and the response for the peak assigned as Cys/Cys<sub>ox</sub> was changed to reflect the difference in response between the thiol and disulfide, as shown in Figure 4.16 B. To then ensure that the disulfide peaks were also assigned correctly the same sample spiked with NEM was then injected again with only WE<sub>1</sub> turned on, Figure 4.16 C. In this case no responses were observed for either the disulfides or the reduced thiols further indicating that peak identification was correctly assigned and that no other species were determined to interfere.

A short experiment to determine if the Au/Hg dual electrode was capable of determining redox status *in vivo* was carried out in the liver. Oxidative injury was caused by dosing doxorubicin directly to the liver through the implanted probe, as referenced to in the methods section. Figure 4.17 shows the changes observed in concentration as a function of time. No response was observed for Hcy or Hcy<sub>ox</sub> throughout the duration of the experiment. This was thought to potentially be due to the presence of these two analytes being below the LOD for this system or more likely that the role of these two analytes is known to be predominately intracellular<sup>36, 37, 39, 48, 54</sup>. Responses were observed for GSSG, GSH, Cys and Cys<sub>ox</sub> throughout the experiment. Under basal conditions a large response was observed for GSH, while the response was significantly less for GSSG indicative of no oxidative injury occurring. The observed responses were similar for that of Cys and Cys<sub>ox</sub>.

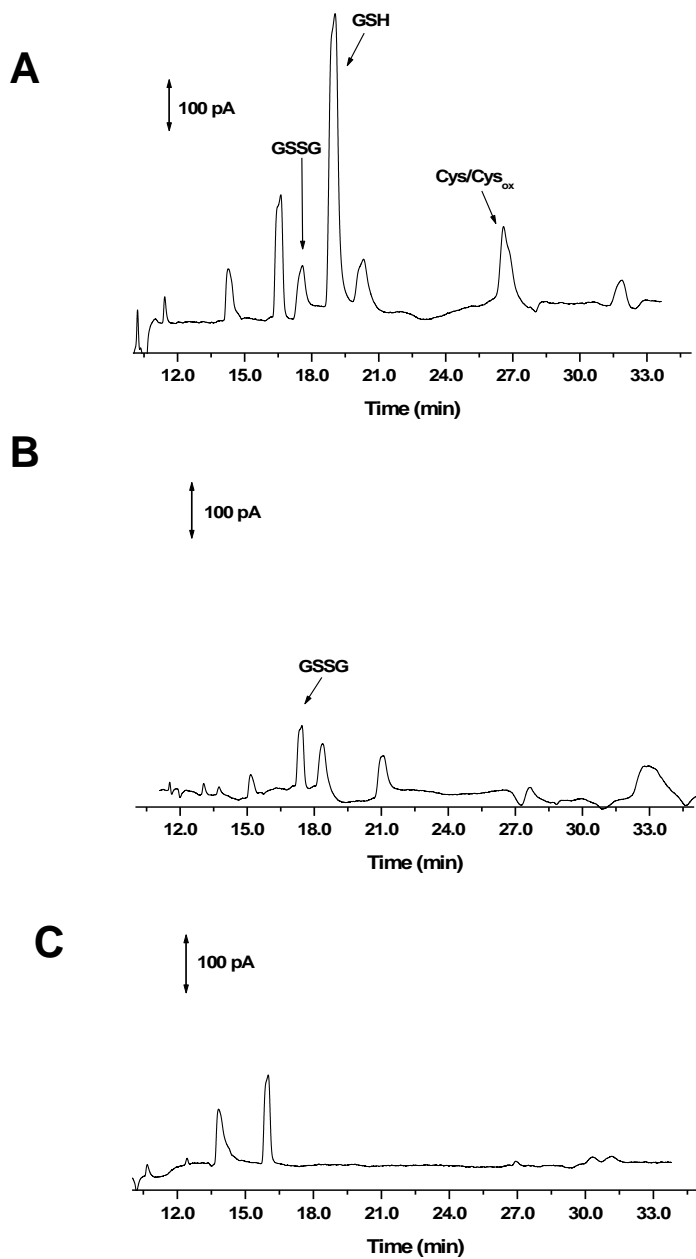


Figure 4.16: Response of reduced thiols and disulfides in basal liver dialysate. A) both WE<sub>1</sub> and WE<sub>2</sub> turned on, B) both WE<sub>1</sub> and WE<sub>2</sub> turned on, but 0.5  $\mu$ L of 0.16 M NEM added to 10  $\mu$ L aliquot of basal liver dialysate and C) WE<sub>2</sub> turned off with addition of same concentration of NEM to the sample matrix. Separation conditions were the same as reported in Figure 4.14.

However, when doxorubicin was dosed through the probe the response from GSH decreased from 40  $\mu\text{M}$  to 1.4  $\mu\text{M}$ , while GSSG remained relatively unchanged. However, the responses between  $\text{Cys}_{\text{ox}}$  and Cys changed dramatically. As the chemistry of Cys dictates the production of GSH the observed decrease in GSH concentration and relatively unchanged concentration in GSSG is logical<sup>36</sup>. After stopping the dose with doxorubicin, concentrations of GSH and Cys begin to increase, although the ratio of reduced to oxidized GSH/GSSG and Cys/ $\text{Cys}_{\text{ox}}$  were not the same prior to oxidative injury.

#### 4.4 Conclusions

The dual Au/Hg electrode developed in this chapter was capable of determining redox status *in vivo*. Although, several approaches for method development were tried to achieve baseline resolution between Cys/ $\text{Cys}_{\text{ox}}$  and Hcy/ $\text{Hcy}_{\text{ox}}$ , none proved to be successful. However, the electrochemistries of the reduced thiols and disulfides, as well as the chemical reactivity were used to obtain the responses of either the disulfides or the reduced thiols. This made it possible to determine the changes in redox status as a result of oxidative injury *in vivo*. Furthermore, the mechanism of action was determined for the electrodes in the parallel opposed configuration. As reported in Chapter 3, signal enhancement was observed when the dual CF electrode was operated as dual electrode compared to a single electrode. As the mechanism of action is different with the dual Au/Hg electrode versus the CF, it was unknown if the electrodes would behave in the same fashion as the dual CF. No appreciable signal enhancement was observed for the dual Au/Hg electrode indicating that the difference in the chemical responses at the electrodes ultimately dictates signal enhancement.

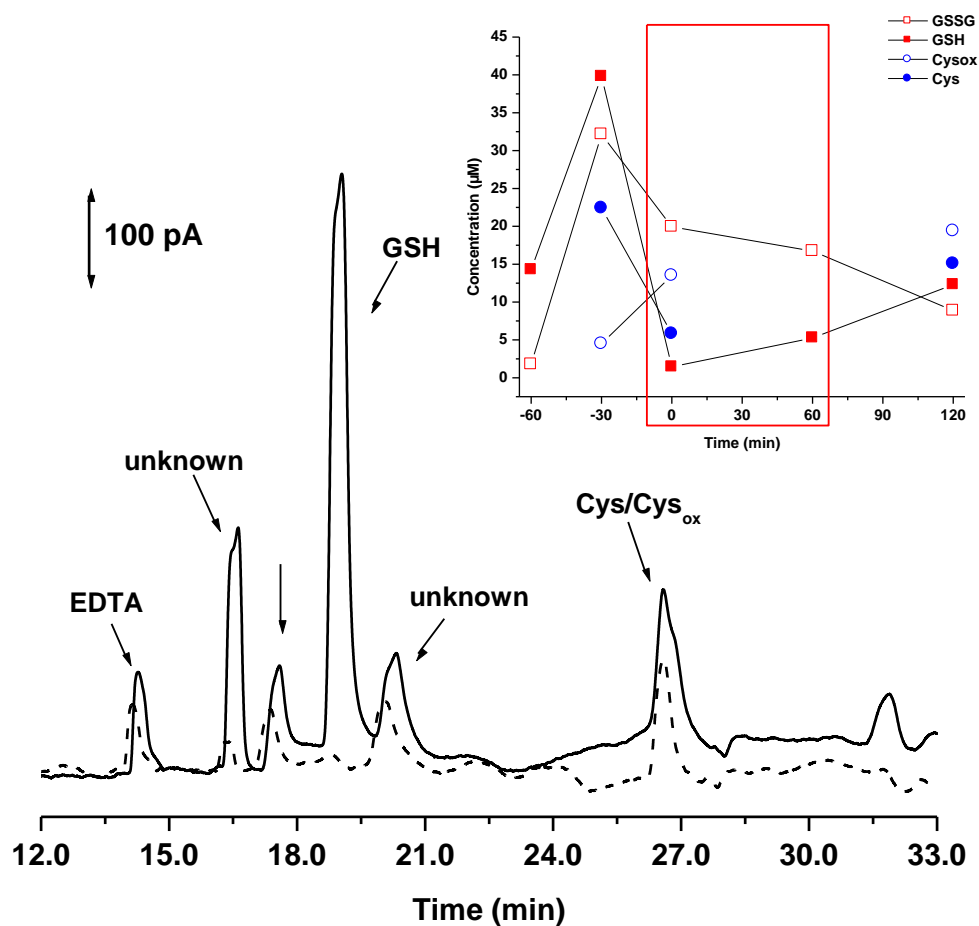


Figure 4.17: Changes in thiol tissue redox status as a function of chemically induced oxidative stress. Response before chemically induced oxidative stress ( ——— ). Inset concentration as a function of time, box indicates time period for perfusion of doxorubicin through the probe at 1  $\mu\text{L}/\text{min}$ . Samples were collected every 30 min. Separation conditions were the same as reported in Figure 4.14.

#### 4.5 References

1. Allison, L. A.; Shoup, R. E., Dual electrode liquid chromatography detector for thiols and disulfides. *Anal. Chem.* **1983**, *55* (1), 8-12.
2. Bald, E.; Glowacki, R., Analysis of saliva for glutathione and metabolically related thiols by liquid chromatography with ultraviolet detection. *Amino Acids* **2005**, *28* (4), 431-433.
3. Batz, N. G.; Martin, R. S., Selective detection of endogenous thiols using microchip-based flow analysis and mercury/gold amalgam microelectrodes. *Analyst (Cambridge, United Kingdom)* **2009**, *134* (2), 372-379.
4. Causse, E.; Issac, C.; Malatray, P.; Bayle, C.; Valdiguie, P.; Salvayre, R.; Couderc, F., Assays for total homocysteine and other thiols by capillary electrophoresis-laser-induced fluorescence detection. I. Preanalytical condition studies. *Journal of Chromatography, A* **2000**, *895* (1+2), 173-178.
5. Causse, E.; Malatray, P.; Calaf, R.; Charpiot, P.; Candito, M.; Bayle, C.; Valdiguie, P.; Salvayre, R.; Couderc, F., Plasma total homocysteine and other thiols analyzed by capillary electrophoresis/laser-induced fluorescence detection: comparison with two other methods. *Electrophoresis* **2000**, *21* (10), 2074-2079.
6. Causse, E.; Terrier, R.; Champagne, S.; Nertz, M.; Valdiguie, P.; Salvayre, R.; Couderc, F., Quantitation of homocysteine in human plasma by capillary electrophoresis and laser-induced fluorescence detection. *Journal of Chromatography, A* **1998**, *817* (1 + 2), 181-185.
7. Guan, X.; Hoffman, B.; Dwivedi, C.; Matthees, D. P., A simultaneous liquid chromatography/mass spectrometric assay of glutathione, cysteine, homocysteine and their disulfides in biological samples. *J. Pharm. Biomed. Anal.* **2003**, *31* (2), 251-261.
8. Holland, L. A.; Lunte, S. M., Postcolumn Reaction Detection with Dual-Electrode Capillary Electrophoresis-Electrochemistry and Electrogenerated Bromine. *Anal. Chem.* **1999**, *71* (2), 407-412.
9. Hoque, M. E.; Arnett, S. D.; Lunte, C. E., On-column preconcentration of glutathione and glutathione disulfide using pH-mediated base stacking for the analysis of microdialysis samples by capillary electrophoresis. *J. Chromatogr., B Anal. Technol. Biomed. Life Sci.* **2005**, *827* (1), 51-57.
10. Huang, X.; Kok, W. T., Determination of thiols by capillary electrophoresis with electrochemical detection using a palladium field-decoupler and chemically modified electrodes. *J. Chromatogr., A* **1995**, *716* (1 + 2), 347-53.
11. Jones, D. P.; Liang, Y., Measuring the poise of thiol/disulfide couples in vivo. *Free Radical Biology & Medicine* **2009**, *47* (10), 1329-1338.
12. Kang, S. H.; Kim, J.-W.; Chung, D. S., Determination of homocysteine and other thiols in human plasma by capillary electrophoresis. *J. Pharm. Biomed. Anal.* **1997**, *15* (9,10), 1435-1441.
13. Kleinman, W. A.; Richie, J. P., Jr., Determination of thiols and disulfides using high-performance liquid chromatography with electrochemical detection. *Journal of Chromatography, B: Biomedical Applications* **1995**, *672* (1), 73-80.
14. Kubalczyk, P.; Bald, E., Transient pseudo-isotachophoretic stacking in analysis of plasma for homocysteine by capillary zone electrophoresis. *Anal. Bioanal. Chem.* **2006**, *384* (5), 1181-1185.
15. Kusmieriek, K.; Glowacki, R.; Bald, E., Analysis of urine for cysteine, cysteinylglycine, and homocysteine by high-performance liquid chromatography. *Anal. Bioanal. Chem.* **2006**, *385* (5), 855-860.

16. Lada, M. W.; Kennedy, R. T., In vivo monitoring of glutathione and cysteine in rat caudate nucleus using microdialysis online with capillary zone electrophoresis-laser induced fluorescence detection. *J. Neurosci. Methods* **1997**, *72* (2), 153-159.
17. Lakritz, J.; Plopper, C. G.; Buckpitt, A. R., Validated high-performance liquid chromatography-electrochemical method for determination of glutathione and glutathione disulfide in small tissue samples. *Analytical Biochemistry* **1997**, *247* (1), 63-68.
18. Lavigne, V.; Pons, A.; Dubourdieu, D., Assay of glutathione in must and wines using capillary electrophoresis and laser-induced fluorescence detection. *J. Chromatogr., A* **2007**, *1139* (1), 130-135.
19. Lin, B. L.; Colon, L. A.; Zare, R. N., Dual electrochemical detection of cysteine and cystine in capillary zone electrophoresis. *J. Chromatogr., A* **1994**, *680* (1), 263-70.
20. Lunte, S. M.; Kissinger, P. T., Detection of thiols and disulfides in liver samples using liquid chromatography/electrochemistry. *Journal of Liquid Chromatography* **1985**, *8* (4), 691-706.
21. Melnikov, I. O.; Nazimov, I. V.; Stukacheva, E. A.; Glubokov, Y. M., Determination of homocysteine and other low-molecular-weight amino thiols in blood plasma. *Journal of Analytical Chemistry* **2006**, *61* (11), 1093-1099.
22. Nolin, T. D.; McMenamin, M. E.; Himmelfarb, J., Simultaneous determination of total homocysteine, cysteine, cysteinylglycine, and glutathione in human plasma by high-performance liquid chromatography: Application to studies of oxidative stress. *J. Chromatogr., B Anal. Technol. Biomed. Life Sci.* **2007**, *852* (1-2), 554-561.
23. O'Shea, T. J.; Lunte, S. M., Selective detection of free thiols by capillary electrophoresis-electrochemistry using a gold/mercury amalgam microelectrode. *Anal. Chem.* **1993**, *65* (3), 247-50.
24. Pasas, S. A.; Lacher, N. A.; Davies, M. I.; Lunte, S. M., Detection of homocysteine by conventional and microchip capillary electrophoresis/electrochemistry. *Electrophoresis* **2002**, *23* (5), 759-766.
25. Rabenstein, D. L.; Saetre, R., Mercury-based electrochemical detector for liquid chromatography for the detection of glutathione and other sulfur-containing compounds. *Anal. Chem.* **1977**, *49* (7), 1036-9.
26. Shihabi, Z. K.; Hinsdale, M. E.; Cheng, C. P., Analysis of glutathione by capillary electrophoresis based on sample stacking. *Electrophoresis* **2001**, *22* (11), 2351-2353.
27. Stamler, J.; Loscalzo, J. Capillary zone electrophoresis of thiols and their derivatives. 94-US921 9417398, 19940125., 1994.
28. Stenken, J. A.; Puckett, D. L.; Lunte, S. M.; Lunte, C. E., Detection of N-acetylcysteine, cysteine and their disulfides in urine by liquid chromatography with a dual-electrode amperometric detector. *J. Pharm. Biomed. Anal.* **1990**, *8* (1), 85-9.
29. Vandenberg, P. J.; Johnson, D. C., Pulsed electrochemical detection of cysteine, cystine, methionine, and glutathione at gold electrodes following their separation by liquid chromatography. *Anal. Chem.* **1993**, *65* (20), 2713-18.
30. Wang, A.; Zhang, L.; Zhang, S.; Fang, Y., Determination of thiols following their separation by CZE with amperometric detection at a carbon electrode. *J. Pharm. Biomed. Anal.* **2000**, *23* (2-3), 429-436.
31. Wang, W.; Rusin, O.; Xu, X.; Kim, K. K.; Escobedo, J. O.; Fakayode, S. O.; Fletcher, K. A.; Lowry, M.; Schowalter, C. M.; Lawrence, C. M.; Fronczek, F. R.; Warner, I. M.; Strongin, R. M., Detection of Homocysteine and Cysteine. *Journal of the American Chemical Society* **2005**, *127* (45), 15949-15958.
32. Yao, X.; Wang, Y.; Chen, G., Simultaneous determination of aminothiols, ascorbic acid and uric acid in biological samples by capillary electrophoresis with electrochemical detection. *Biomed. Chromatogr.* **2007**, *21* (5), 520-526.

33. Zhou, J.; O'Shea, T. J.; Lunte, S. M., Simultaneous detection of thiols and disulfides by capillary electrophoresis-electrochemical detection using a mixed-valence ruthenium cyanide-modified microelectrode. *J. Chromatogr., A* **1994**, *680* (1), 271-7.
34. Houk, J.; Whitesides, G. M., Structure-reactivity relations for thiol-disulfide interchange. *J. Am. Chem. Soc.* **1987**, *109* (22), 6825-36.
35. Stamler, J. S.; Slivka, A., Biological chemistry of thiols in the vasculature and in vascular-related disease. *Nutrition reviews* **1996**, *54* (1 Pt 1), 1-30.
36. Bayle, C.; Causse, E.; Couderc, F., Determination of aminothiols in body fluids, cells, and tissues by capillary electrophoresis. *Electrophoresis* **2004**, *25* (10-11), 1457-1472.
37. Metayer, S.; Seiliez, I.; Collin, A.; Duchene, S.; Mercier, Y.; Geraert, P.-A.; Tesseraud, S., Mechanisms through which sulfur amino acids control protein metabolism and oxidative status. *Journal of Nutritional Biochemistry* **2008**, *19* (4), 207-215.
38. Liang, L.-P.; Patel, M., Seizure-induced changes in mitochondrial redox status. *Free Radical Biology & Medicine* **2006**, *40* (2), 316-322.
39. Reid, M.; Jahoor, F., Glutathione in disease. *Current Opinion in Clinical Nutrition and Metabolic Care* **2001**, *4* (1), 65-71.
40. Bouligand, J.; Deroussent, A.; Paci, A.; Morizet, J.; Vassal, G., Liquid chromatography-tandem mass spectrometry assay of reduced and oxidized glutathione and main precursors in mice liver. *J. Chromatogr., B Anal. Technol. Biomed. Life Sci.* **2006**, *832* (1), 67-74.
41. Kissinger, P. T.; Refshauge, C.; Dreiling, R.; Adams, R. N., Electrochemical detector for liquid chromatography with picogram sensitivity. *Analytical Letters* **1973**, *6* (5), 465-77.
42. Russell, J.; Rabenstein, D. L., Speciation and quantitation of underivatized and Ellman's derivatized biological thiols and disulfides by capillary electrophoresis. *Analytical Biochemistry* **1996**, *242* (1), 136-144.
43. Lochman, P.; Adam, T.; Friedecky, D.; Hlidkova, E.; Skopkova, Z., High-throughput capillary electrophoretic method for determination of total aminothiols in plasma and urine. *Electrophoresis* **2003**, *24* (7-8), 1200-1207.
44. Chen, D.-c.; Chang, S.-S.; Chen, C.-h., Parallel-Opposed Dual-Electrode Detector with Recycling Amperometric Enhancement for Capillary Electrophoresis. *Anal. Chem.* **1999**, *71* (15), 3200-3205.
45. Chen, G.; Zhang, L.; Wang, J., Miniaturized capillary electrophoresis system with a carbon nanotube microelectrode for rapid separation and detection of thiols. *Talanta* **2004**, *64* (4), 1018-1023.
46. Holland, L. A.; Lunte, S. M., Capillary electrophoresis coupled to electrochemical detection: a review of recent advances. *Analytical Communications* **1998**, *35* (2), 1H-4H.
47. Owens, G. S.; LaCourse, W. R., Pulsed electrochemical detection of thiols and disulfides following capillary electrophoresis. *Journal of Chromatography, B: Biomedical Sciences and Applications* **1997**, *695* (1), 15-25.
48. Zhong, M.; Lunte, S. M., Tubular-Wire Dual Electrode for Detection of Thiols and Disulfides by Capillary Electrophoresis/Electrochemistry. *Anal. Chem.* **1999**, *71* (1), 251-255.
49. Powell, P. R.; Woods, L. A.; Ewing, A. G., Characterization of etched electrochemical detection for electrophoresis in micron inner diameter capillaries. *Journal of Separation Science* **2005**, *28* (18), 2540-2545.
50. Price, K. E.; Larive, C. K.; Lunte, C. E., Tissue-targeted metabonomics: biological considerations and application to doxorubicin-induced hepatic oxidative stress. *Metabolomics* **2009**, *5* (2), 219-228.
51. Talt, R. J.; Thompson, D.O.; Stella, V.J.; Stobaugh, J.F., Sulfo Ether beta-cyclodextrin as a Chiral Discriminator for Use with Capillary Electrophoresis. *Analytical Chemistry* **1994**, *66*, 4013-4018.

52. Zhang, Y.; Ping, G.; Zhu, B.; Kaji, N.; Tokeshi, M.; Baba, Y., Enhanced electrophoretic resolution of monosulfate glycosaminoglycan disaccharide isomers on poly(methyl methacrylate) chips. *Electrophoresis* **2007**, *28* (3), 414-421.
53. Arnett, S. D.; Osbourn, D. M.; Moore, K. D.; Vandaveer, S. S.; Lunte, C. E., Determination of 8-oxoguanine and 8-hydroxy-2'-deoxyguanosine in the rat cerebral cortex using microdialysis sampling and capillary electrophoresis with electrochemical detection. *J. Chromatogr., B Anal. Technol. Biomed. Life Sci.* **2005**, *827* (1), 16-25.
54. Griffith, O. W.; Meister, A., Origin and turnover of mitochondrial glutathione. *Proceedings of the National Academy of Sciences of the United States of America* **1985**, *82* (14), 4668-72.

## Chapter 5: Conclusions and Future Directions

### 5.1 Conclusions

#### 5.1.1 Chapter 2

An LCEC method was developed for the simultaneous detection of ubiquinone-10 and ubiquinol-10. The method was an improvement over previously published works in that it had reduced retention times and was capable of detecting both reduced and oxidized ubiquinone-10 simultaneously and without any additional sample pretreatment. It was demonstrated that both the series and parallel electrode configurations could be used to elicit different information. For example, in the series configuration voltammetry could be used to verify that the starting material, ubiquinone-10, was unchanged when the Jones Reductor was used to reduce it to ubiquinol-10. That is to say no side products were formed during the reduction. More importantly, using the parallel electrode configuration simultaneous detection of ubiquinone-10 and ubiquinol-10 was possible. Furthermore, this configuration allowed for greater selectivity as each electrode could be held at a reduction or oxidation voltage specific for the oxidation or reduction of the quinone moiety. As a result more accurate determination of endogenous redox states was possible. This was demonstrated through the analysis of pooled human plasma. Ubiquinone-10 and ubiquinol-10 were extracted from plasma and reconstituted in the sample matrix used for the standards. Standard additions were performed at three different concentrations to confirm the extraction efficiencies of the two analytes from plasma. Both analytes were extracted with  $\geq 90\%$  efficiency demonstrating that redox concentrations could be reported accurately within a complex sample using the established method. The use of this cell geometry provides a superior means by which these compounds can be detected over the previously published electrochemical detection schemes. This method provides an efficient and effective means by which electroactive lipophilic or fat soluble

vitamins redox status can be determined in blood. Furthermore, this method could also be applied for analysis of these compounds in harvested tissues.

### 5.1.2 Chapter 3

Several dual electrode detection schemes had been reported previously in the literature; however, most of these dual electrodes were used in the series configuration. Most of the dual electrodes developed for CE were for the detection select thiols and disulfides, in which the upstream electrode was held at roughly -1.0 V. This voltage was sufficient to reduce disulfides. The detection electrode was then placed downstream either on-capillary or off-capillary. By placing the electrodes in a parallel-opposed configuration it was shown that redox cycling occurred. A 2-fold increase at the oxidation electrode was observed with the same increase in sensitivity when compared to using only the single electrode. The proposed mechanism for the observed redox cycling with the parallel dual electrode is shown below:

The observed redox cycling could only be achieved with both electrodes on and the effect was diminished with increasing distance between the electrodes. The utility of this electrode was demonstrated further by using the electrodes in dual potential mode. In this mode the electrodes were held at two different oxidation potentials generating a two point voltammogram. The ratio of the responses was used to confirm migration based peak identification. It was shown that although migration times in the whiskey analysis corresponded with migration times of the standards the voltammetry did not corresponded with all assignments made based on migration times alone. By using the dual electrode in dual potential mode proper peak assignments could be made. Furthermore, the redox cycling mode was also used to clarify migration based peak assignments by assessing the chemical

reversibility of peaks of interest. These two configurations demonstrate the utility of this parallel dual electrode over currently published dual electrodes for CE<sup>1-7</sup>. This dual electrode could be used to investigate other electrochemically active compounds with biological relevance. Specifically, this dual electrode would be useful for distinguishing non-reversible, semi-reversible and reversible compounds in complex matrices where co-migration could occur between structurally similar compounds.

### 5.1.3 Chapter 4

The parallel dual-electrode developed in Chapter 3 demonstrated that redox cycling and as a result signal enhancement. In addition, the ability to use the developed dual-electrode in both redox cycling mode and dual-potential mode offered two additional means to verify migration based peak identification for CE. These characteristics made application of this dual-electrode for the analysis of biologically relevant compounds advantageous. The redox chemistry involving thiols and disulfides, in particular GSH and GSSG, have long been of great interest due to their ability to scavenge free radicals and maintain tissue homeostasis. Several modes of analysis have been used to detect these thiols and disulfides including, fluorescence, UV and EC. CE with EC is an ideal technique due to its ability to handle small sample volumes while providing superior efficiencies compared to traditional LC systems. Furthermore, EC detection with Au/Hg electrodes offers a direct and selective means to detect thiols and disulfides when compared to spectroscopic techniques. Therefore, a dual Au/Hg electrode was developed for the analysis of both thiols and disulfides based off of the design in Chapter 3. A signal enhancement of 1% or less was observed for Cys and Hcy, while no signal enhancement was observed for GSH. This demonstrated that the mechanism of action for the dual Au/Hg electrode was the same as that observed for the conventional series mode.

Although the initial goal of this chapter was to develop a method to separate and three thiols (GSH, Hcy, Cys) and their corresponding disulfides using CE with the developed dual Au/Hg electrode it was found

through investigation in both normal polarity and reverse polarity modes that resolution of all six analytes could not be achieved. Even though not all of the analytes could be resolved chromatographically, the dual electrode detector was used to resolve the analytes based on their respective electrochemistries. By using the dual electrode in this fashion the redox chemistry of these analytes was analyzed *in vivo*. The demonstration of the utility of this dual electrode detector for analysis *in vivo* was carried out in the liver. A linear probe was implanted into the midline region of the liver. During collection of basal dialysate the concentration of GSH was significantly higher than GSSG. A similar observation was seen for Cys and Cys<sub>ox</sub>, indicating that oxidative damage was not occurring. By dosing doxorubicin through the probe for one hour, reduced thiol levels were decreased with increased levels of disulfides. The presence of disulfides would indicate free radical scavenging resulting from oxidative damage. Once the perfusion of doxorubicin was stopped and replaced with aCSF reduced thiol concentrations began to increase, but did not return to initial basal concentrations. The observed redox chemistry *in vivo* demonstrates the ability of the developed dual Au/Hg electrode to determine changes in redox status as a result of oxidative damage.

The developed dual Au/Hg electrode demonstrated a direct means by which thiol redox chemistry can be monitored *in vivo*. However, the system currently utilizes end column detection, which does not effectively shield all the electrophoretic current required for the separation. Consequently, detection limits are worse and efficiencies are low. A detection limit of 1.0  $\mu\text{M}$  was observed for GSH, while no response was observed for the other analytes of interest below 3.0  $\mu\text{M}$ . These detection limits compared well with those reported previously, but did not improve upon systems where series configurations were used. In addition, the electrochemical mechanism for the dual Au/Hg electrode was not the same as that proposed for the parallel dual carbon fiber electrode developed in Chapter 3. In order to obtain redox cycling direct oxidation or reduction of a compound must occur at the electrode

surface. Indirect detection which occurs with modified electrode surfaces will not result in signal enhancement.

## 5.2 Future Directions

### 5.2.1 Mitigation of Oxidative Stress in Neurodegenerative Diseases via Antioxidant Therapies

#### 5.2.1.2 Dietary Co-enzyme Q<sub>10</sub>

Dietary Co-Q<sub>10</sub> has been of significant interest over the last decade due to potential role in maintaining aiding in the maintenance of tissue redox status as a result of oxidative insult. As mentioned in Chapter 2, Co-Q<sub>10</sub> has several roles endogenously, as shown in Figure 5.1. First maintaining the proton gradient within the mitochondrial respiratory chain and second maintaining other endogenous antioxidants systems through free radical scavenging. It was hypothesized that dietary intake of Co-Q<sub>10</sub> in patients who were considered at risk for heart attacks could be an effective way to diminish tissue damage associated with oxidative stress. The results from several studies conducted mainly with rats or rabbits each reported different outcomes<sup>8-12</sup>.

No immediate effect was observed for animals sacrificed directly after dosing, in reference to maintained tissue redox status as measured by the ratio of reduced to oxidized GSH/GSSG<sup>9-11</sup>. Maintained tissue redox status was only observed in animals that received dietary Co-Q<sub>10</sub> for two weeks prior to sacrifice<sup>9</sup>. As one of the main focuses of our lab is to investigate the role of seizures relating to oxidative stress, it would be interesting to investigate the effect of dietary Co-Q<sub>10</sub> on maintained redox status after chemically inducing seizures.

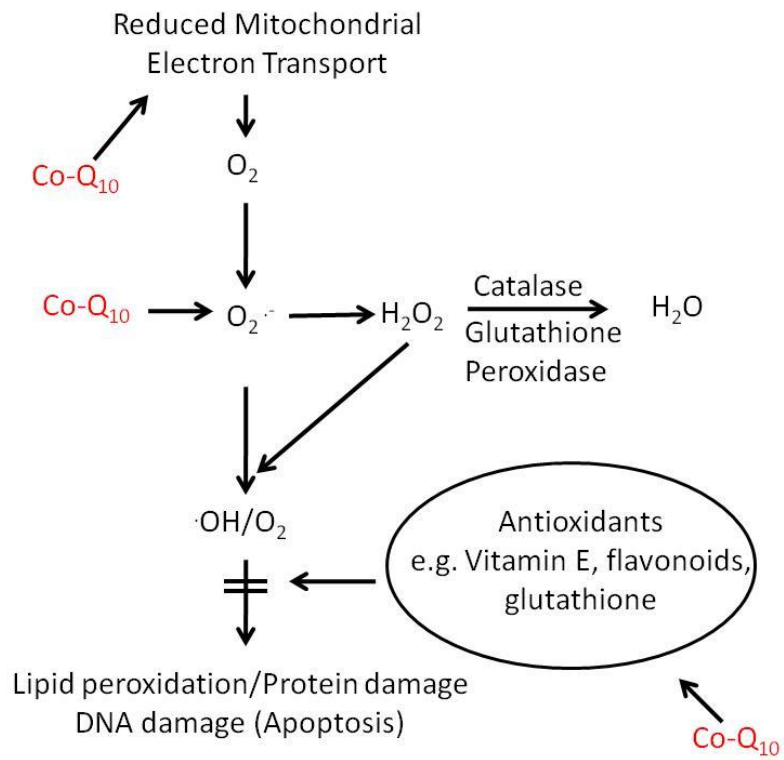


Figure 5.1: Potential mechanisms of action for dietary Co-Q<sub>10</sub> in oxidative stress.

A minimum dosing period of two weeks should be imposed prior to chemical inducing seizures, as previously published works did not observe effect prior to this time point. As Co-Q<sub>10</sub> is quite large (FW 863 g/mol) and contains a long hydrophobic chain it is unlikely that it would cross the membrane of a microdialysis probe. Therefore, its affect could be monitored indirectly by assessing the ratio of thiols to disulfides as a means to gauge tissue redox homeostasis.

#### 5.2.1.3 Application for Dual Carbon Fiber Electrode

Various phenolic acids have been shown to evoke different biological responses. Interestingly, not all cinnamic acid derivatives possess the same action *in vivo* even if their chemical reactivity is the same (i.e. 3,4-dihydroxybenzoic acid and gentisic acid are both benzoic acid derivatives, but may have very different functions *in vivo*). This would lead one to believe that structure would then play a larger role in therapeutic benefit. Table 5.1 shows several benzoic acid and cinnamic acid derivatives functionalities *in vivo*<sup>13-22</sup>. Although, the results of dosing these compounds *in vitro* or *in vivo* have shown biological implications the mechanisms of action are not well understood.

Structural Classes	Quantity in Spirited Beverages (mg/mL)	Molecular Action
<b>Benzoic Acids</b>		
4-hydroxybenzoic acid	$\leq 1.1^a$	unknown
protocatechuic acid	$\leq 0.3^a$	RS <sup>1</sup>
vanillic acid	$\leq 3.6^a, \leq 0.64^c$	unknown
syringic acid	$\leq 0.5^a, \leq 2.06^c$	RS <sup>1</sup>
gallic acid	$\leq 0.2^a, \leq 1.29^c$	RS <sup>1</sup> , VR <sup>5,6</sup>
gentisic acid	-	APE <sup>10,11</sup>
<b>Cinammic Acids</b>		
p-coumaric acid	$\leq 0.9^a, \leq 5.7^b$	APE <sup>10,11</sup>
caffeic acid	$\leq 0.3^a, \leq 13^b, \leq 75^d$	RS <sup>1</sup> , VR <sup>5,6</sup> , IE <sup>8</sup> , AHR <sup>8</sup> , IGT <sup>8</sup> , SROS <sup>8,13</sup> , IADH <sup>9</sup> , APE <sup>10,11</sup> , PRD <sup>12,13</sup>
ferulic acid	$\leq 6.5^a, \leq 0.5^b$	RS <sup>1</sup> , PA <sup>3,4</sup> , LRG <sup>7</sup> , IE <sup>8</sup> , AHR <sup>8</sup> , SROS <sup>8</sup> , APE <sup>10,11</sup>
sinapic acid	$\leq 0.25^a, \leq 0.5^b$	RS <sup>1</sup> , PA <sup>3,4</sup>

<sup>a</sup>: beer, <sup>b</sup>: wine, <sup>c</sup>: whiskey, <sup>d</sup>: coffee

Table 5.1: Compilation from literature of therapeutic benefit of phenolic acids. RS (radical scavenger), VR (vascular relaxation), IE (inhibition of enzymes), AHR (anti HIV replication), PA (decreased platelet aggregation), LRG (lowered blood glucose), IGT (inhibited tumor growth), SROS (signal reactive oxygen species), IADH (inhibition of alcohol dehydrogenase), APE (activation of phase II enzymes), PRD (prooxidant DNA breakage).

The most straight forward therapeutic effect is likely the ability of several of these phenolic acids to aid in radical scavenging. The ability of these compounds to undergo oxidation-reduction reactions makes interaction with molecular oxygen or even nitrogen species quite plausible. However, mechanisms involving minimization of HIV replication or tumor growth suppression are not well understood<sup>23</sup>. It was hypothesized in *in vitro* studies conducted using cancer cell lines, that dosing with caffeic acid inhibited nuclear factor- $\kappa$ B, resulting in suppression of tumor growth<sup>23</sup>. Two other roles for several phenolic acids were 1) the involvement in action or transcription of phase II enzyme systems and 2) reaction with biologically relevant metals acting as pro-oxidants in DNA breakage. Both of these modes of action are of interest, because of their roles in mitigating oxidative stress and maintaining homeostasis. Similar studies proposed in the previous section could be used to study the dietary effects of phenolic acids in relation to oxidative stress as a result of seizures. Several of these compounds including caffeic acid could easily be dosed directly through the probe to look at the effect on mitigating oxidative stress locally or they could also be dosed orally in order to assess the effects of long term dosing. It would also be interesting to dose some of these compounds in conjunction with medications currently used to control epilepsy.

#### 5.2.1.4 Thiols and Disulfides

The dual Au/Hg electrode developed in Chapter 4 offers a selective, sensitive and direct way to measure redox status of thiols *in vivo*. This was demonstrated with analysis several thiols and disulfides in liver dialysate as reported in Chapter 4. Establishing the initial parameters of this system (e.g. electrochemical mechanism, linear range, LOD) were important steps in reaching the ultimate goal of this project, analysis of thiol redox chemistry in brain dialysate. Currently, there are several methods established in the lab to investigate mechanisms of oxidative stress, with the express intent of using

these methods to establish the role of seizures in causing oxidative stress. It is well known that the GSH/GSSG ratio plays a key role in maintaining tissue redox hemostasis in the brain (refs). These compounds are present in relatively high concentrations ( $\leq 1.0 \mu\text{M}$ ) in the brain, making analysis by most detection schemes (UV, fluorescence, EC, MS) feasible. However, each of these detection schemes, excluding EC, requires derivatization of thiols to achieve greater selectivity (refs). EC detection offers a direct and selective means by which these analytes can be detected without additional sample pretreatment. Currently the LOD's obtained with the dual Au/Hg electrode, reported in Chapter 4, are not adequate to determine redox status in brain dialysate.

Osbourn and Lunte previously published work on the development of a cellulose acetate decoupler for CEEC<sup>24</sup>. The use of an electrical decoupler enables the current produced from the separation to be shielded completely from the detector. This decreases the noise at your detector, effectively improving your detection limits. While the design presented by Osbourn and Lunte was initially used with only a single electrode, it would be relatively easy to integrate the dual Au/Hg electrode developed in Chapter 4 by exposing the capillary to HF acid increasing the inner diameter of the capillary. In addition, because the separation voltage would be shielded from the detector separation conditions would not be restricted as they are with end column detection. This would likely result in baseline resolution between all six analytes of interest.

### 5.3 Development of a Robust Decoupler for CEEC

As mentioned in Chapter 1 several approaches have been reported in the literature for on-capillary electrochemical detection for capillary electrophoresis. Many of these designs involve complex fabrication that compromises the integrity of the capillary, leaving the structure quite fragile. As indicated previously, electrochemistry is a powerful detection technique and coupling it with capillary electrophoresis is ideal due to the fact that electrochemical detection can be easily miniaturized without

a loss in sensitivity. The combination of these techniques has not been widely applied to industry due to the lack of robustness in the design.

In order to come up with a more robust design collaborators from South Korea design a decoupler in which a Plexiglas frame housed a T-junction. As shown in Figure 5.2, the T-junction incorporated the outlet end of the capillary aligned with a packed bed of Nafion, which could be wetted with buffer solution and provided a ground for the separation voltage. A single electrode was then inserted into the capillary, with the outlet reservoir placed downstream containing the reference and auxiliary electrodes. Theoretically, this design provided a more robust structure by which the separation voltage could be decoupled. It was determined however that the packed Nafion was too dense and the surface of the Nafion was not adequate to decouple the separation voltage from the detector. Two positive aspects from this design were 1) the design was quite robust in the sense that the integrity of the capillary was not compromised by fracturing or ablation and once the issues involving density and surface area were optimized further the decoupler could essentially be used for a prolonged period of time and 2) because the decoupler was separated from the capillary, if method development was being carried out or if the capillary was being subjected to several biological samples it could easily be changed out without to fabricate the decoupler simultaneously.

Microchips have been considered a more robust approach, in some instances, to coupling CE with electrochemical detection. This is namely through the use of material (e.g. PDMS, PMMA) not necessarily the process of fabrication. In order to fabricate a more robust decoupler design, a microchip could be used as a platform to couple conventional CE with electrochemical detection, as shown in Figure 5.3.

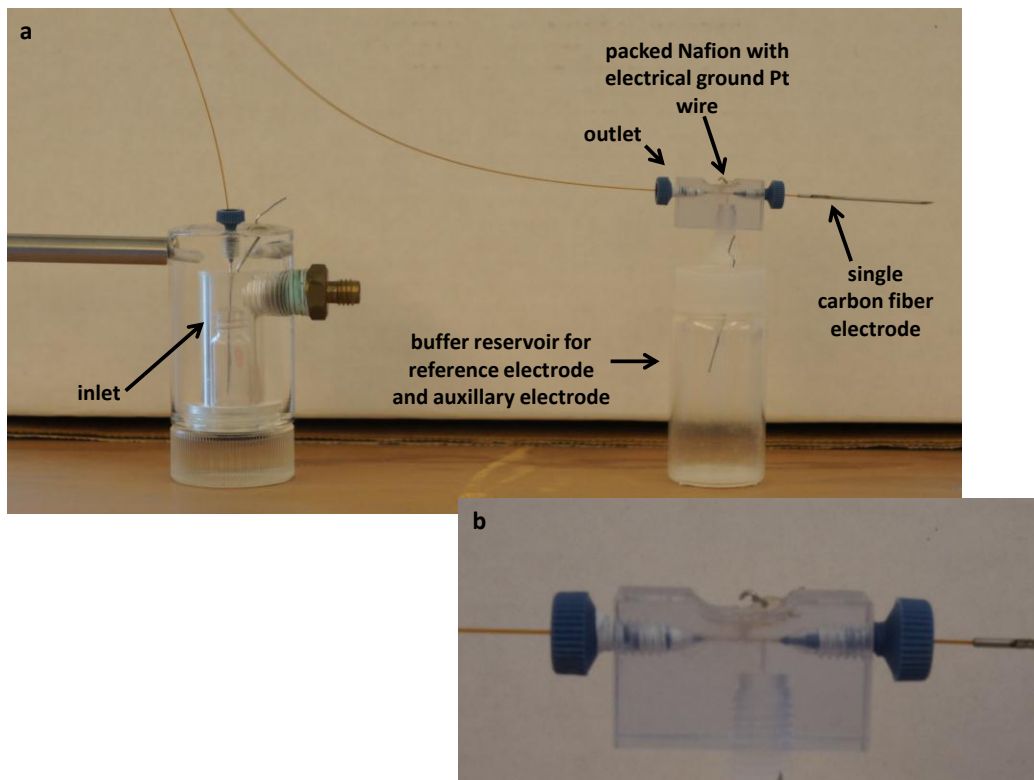


Figure 5.2: Packed Nafion decoupler. a) image of inlet and outlet portions of the design. b) zoomed image of Nafion decoupler T-junction.

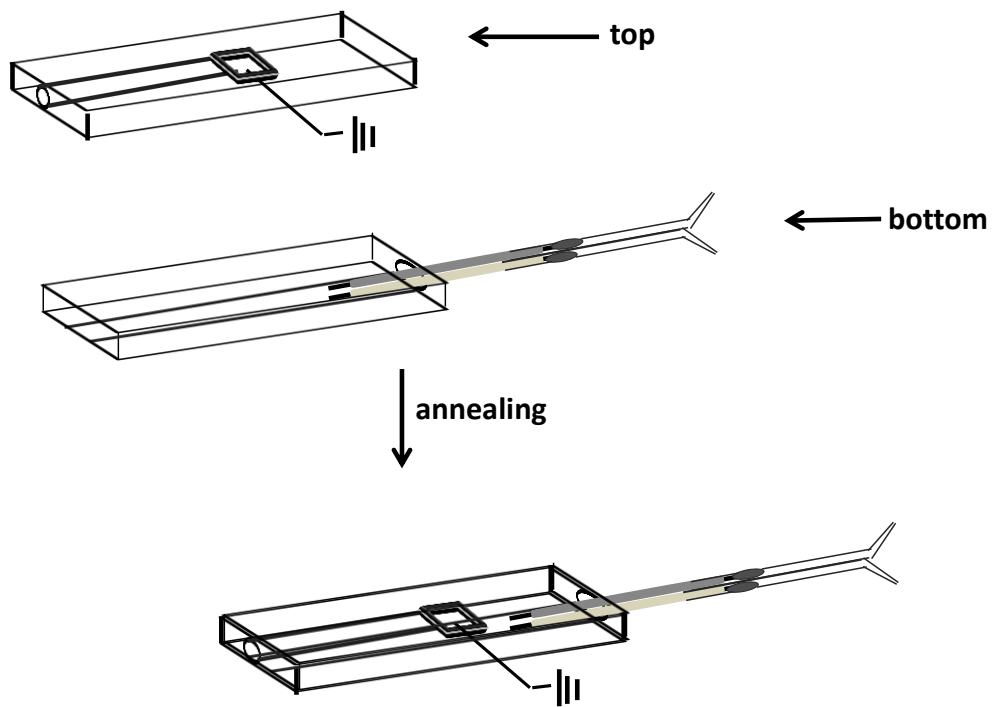


Figure 5.3: Design for microchip decoupler platform for coupling with conventional CE.

The idea of this design would be to go back to the simplest decoupler design, a fracture. A small section of the microchip platform would be subjected to HF acid to create a fracture in the material. The surface area and time of HF etching would need to be optimized. An important feature of the design would be the ease of which each component could be replaced. For example, the capillary could be easily replaced without having to fabricate the decoupler, similarly if the electrode(s) needed to be changed out that could be achieved without impacting the capillary or the decoupler. This like the Nafion design, aims to maintain the efficiencies obtained with conventional CE, while taking advantage of the robust nature of microchip platforms.

#### 5.4 References

1. Castano-Alvarez, M.; Fernandez-Abedul, M. T.; Costa-Garcia, A., Amperometric detector designs for capillary electrophoresis microchips. *Journal of Chromatography, A* **2006**, *1109* (2), 291-299.
2. Chen, D.-c.; Chang, S.-S.; Chen, C.-h., Parallel-Opposed Dual-Electrode Detector with Recycling Amperometric Enhancement for Capillary Electrophoresis. *Analytical Chemistry* **1999**, *71* (15), 3200-3205.
3. Du, F.; Fung, Y. S., Development of CE-dual opposite carbon-fiber micro-disk electrode detection for peak purity assessment of polyphenols in red wine. *Electrophoresis* **2010**, *31* (13), 2192-2199.
4. Holland, L. A.; Lunte, S. M., Postcolumn Reaction Detection with Dual-Electrode Capillary Electrophoresis-Electrochemistry and Electrogenerated Bromine. *Analytical Chemistry* **1999**, *71* (2), 407-412.
5. Lai, C.-C. J.; Chen, C.-h.; Ko, F.-H., In-channel dual-electrode amperometric detection in electrophoretic chips with a palladium film decoupler. *Journal of Chromatography, A* **2004**, *1023* (1), 143-150.
6. Lin, B. L.; Colon, L. A.; Zare, R. N., Dual electrochemical detection of cysteine and cystine in capillary zone electrophoresis. *Journal of Chromatography, A* **1994**, *680* (1), 263-70.
7. Zhong, M.; Lunte, S. M., Tubular-Wire Dual Electrode for Detection of Thiols and Disulfides by Capillary Electrophoresis/Electrochemistry. *Analytical Chemistry* **1999**, *71* (1), 251-255.
8. Dhanasekaran, M.; Ren, J., The emerging role of coenzyme Q-10 in aging, neurodegeneration, cardiovascular disease, cancer and diabetes mellitus. *Current Neurovascular Research* **2005**, *2* (5), 447-459.
9. Kalenikova, E. I.; Gorodetskaya, E. A.; Kolokolchikova, E. G.; Shashurin, D. A.; Medvedev, O. S., Chronic administration of coenzyme Q10 limits postinfarct myocardial remodeling in rats. *Biochemistry (Moscow)* **2007**, *72* (3), 332-338.
10. Lakomkin, V. L.; Konovalova, G. G.; Kalenikova, E. I.; Zabbarova, I. V.; Kaminnyi, A. I.; Tikhaze, A. K.; Lankin, V. Z.; Ruuge, E. K.; Kapelko, V. I., Changes in antioxidant status of myocardium during oxidative stress under the influence of coenzyme Q10. *Biochemistry (Moscow)* **2005**, *70* (1), 79-84.
11. Lakomkin, V. L.; Konovalova, G. G.; Kalenikova, E. I.; Zabbarova, I. V.; Tikhaze, A. K.; Tsyplenkova, V. G.; Lankin, V. Z.; Ruuge, E. K.; Kapelko, V. I., Protection of Rat Myocardium by Coenzyme Q during Oxidative Stress Induced by Hydrogen Peroxide. *Biochemistry (Moscow, Russian Federation)(Translation of Biokhimiya (Moscow, Russian Federation))* **2004**, *69* (5), 520-526.
12. Whitman, G. J. R.; Niibori, K.; Yokoyama, H.; Crestanello, J. A.; Lingle, D. M.; Momeni, R., The mechanisms of coenzyme Q10 as therapy for myocardial ischemia reperfusion injury. *Molecular Aspects of Medicine* **1997**, *18* (Suppl.), s195-s203.
13. Bhat, S. H.; Azmi, A. S.; Hadi, S. M., Prooxidant DNA breakage induced by caffeic acid in human peripheral lymphocytes: Involvement of endogenous copper and a putative mechanism for anticancer properties. *Toxicology and Applied Pharmacology* **2007**, *218* (3), 249-255.
14. Clifford, M. N., Chlorogenic acids and other cinnamates - nature, occurrence and dietary burden. *Journal of the Science of Food and Agriculture* **1999**, *79* (3), 362-372.
15. Freedman, J. E.; Parker, C., III; Li, L.; Perlman, J. A.; Frei, B.; Ivanov, V.; Deak, L. R.; Iafrafi, M. D.; Folts, J. D., Select flavonoids and whole juice from purple grapes inhibit platelet function and enhance nitric oxide release. *Circulation* **2001**, *103* (23), 2792-2798.
16. Gerhauser, C., Beer constituents as potential cancer chemopreventive agents. *European journal of cancer (Oxford, England : 1990)* **2005**, *41* (13), 1941-54.

17. Leifert, W. R.; Abeywardena, M. Y., Grape seed and red wine polyphenol extracts inhibit cellular cholesterol uptake, cell proliferation, and 5-lipoxygenase activity. *Nutrition Research (New York, NY, United States)* **2008**, *28* (11), 729-737.
18. Nichenametla, S. N.; Taruscio, T. G.; Barney, D. L.; Exon, J. H., A review of the effects and mechanisms of polyphenolics in cancer. *Critical Reviews in Food Science and Nutrition* **2006**, *46* (2), 161-183.
19. Stoclet, J.-C.; Chataigneau, T.; Ndiaye, M.; Oak, M.-H.; El Bedoui, J.; Chataigneau, M.; Schini-Kerth, V. B., Vascular protection by dietary polyphenols. *European Journal of Pharmacology* **2004**, *500* (1-3), 299-313.
20. Taubert, D.; Berkels, R.; Klaus, W.; Roesen, R., Nitric oxide formation and corresponding relaxation of porcine coronary arteries induced by plant phenols: Essential structural features. *Journal of Cardiovascular Pharmacology* **2002**, *40* (5), 701-713.
21. Vicente, S. J. V.; Ishimoto, E. Y.; Cruz, R. J.; Pereira, C. D. S.; Torres, E. A. F. D. S., Increase of the Activity of Phase II Antioxidant Enzymes in Rats after a Single Dose of Coffee. *Journal of Agricultural and Food Chemistry* **2011**, *59* (20), 10887-10892.
22. Yeh, C.-T.; Yen, G.-C., Induction of hepatic antioxidant enzymes by phenolic acids in rats is accompanied by increased levels of multidrug resistance-associated protein 3 mRNA expression. *Journal of Nutrition* **2006**, *136* (1), 11-15.
23. Lee, Y. S., Role of NADPH oxidase-mediated generation of reactive oxygen species in the mechanism of apoptosis induced by phenolic acids in HepG2 human hepatoma cells. *Archives of Pharmacal Research* **2005**, *28* (10), 1183-1189.
24. Osbourn, D. M.; Lunte, C. E., Cellulose Acetate Decoupler for On-Column Electrochemical Detection in Capillary Electrophoresis. *Analytical Chemistry* **2001**, *73* (24), 5961-5964.